ABSTRACT

Title of dissertation: MECHANISMS FOR AXIAL BAND FORMATION IN A ROTATING DRUM OF GRANULAR MATERIAL

Michael K. Newey, Doctor of Philosophy, 2006

Dissertation directed by: Professor Wolfgang Losert
Department of Physics

We study granular particles, like sand or glass beads, that are mixed in a partially filled, horizontal, cylindrical drum. When the drum is rotated, it is observed that there is a flowing layer of grains on the free surface of the granular medium. In addition, if the particles have different sizes, spatial segregation of the particles by size is obsurved. This segregation occurs in two phases. During the first phase, called radial segregation, the smaller particles form a radial core. In the second, called axial segregation, particles segregate into alternating bands along the axis of the drum.

We perform a detailed study of the characteristics of the flow to determine the physical mechanisms driving axial segregation. We characterize the top surface of the flowing layer by tracking particles using a high speed camera. We then extract average quantities such as velocity and diffusion. The average velocities show surprising behavior: Particles in small particle bands have a higher downhill flow velocity than particles in large particle bands. We also observe that there is a pattern of sideways velocity as a function of position down the flow. Particles flow

into small particle bands in the middle of the flow but flow out of small particle bands at the bottom.

We present the framework for a new model based on our experimentally observed results. We explain the axial band formation in terms of the observed surface flow patterns. We show how two physical processes could contribute to the band formation: A.) Accelerating granular material does not necessarily collide while decelerating granular material requires collisions. B.) Different size particles flow at different velocities. Our framework connects differences in flow velocities on the surface of the drum with the radial segregation in the bulk of the drum.

We compare these results to current models, including models by Savage, Zik, Aranson, and Elperin. We test the general model assumption that the particles always flow in the direction of steepest descent by measuring the surface height of the banded state with a laser line. We find that although there is some indication that particles flow in the direction of steepest descent, there is strong flow that is not in the direction of steepest descent, contrary to the given models.

Finally, we study oscillating patterns in mixtures of three sizes of glass beads. Ternary mixtures of particles form bands within bands of the different particle sizes. For certain experimental conditions we observe traveling and oscillating patterns. We analyze these patterns in light of the different models for granular band formation.

MECHANISMS FOR AXIAL BAND FORMATION IN A ROTATING DRUM OF GRANULAR MATERIAL

by

Michael K. Newey

Dissertation submitted to the Faculty of the Graduate School of the
University of Maryland, College Park, in partial fulfillment
of the requirements for the degree of
Doctor of Philosophy
2006

Advisory Committee:
Professor Wolfgang Losert, Chair/Advisor
Professor Mikhail Anisimov, Deans Representative
Professor Edward Ott
Professor Rajarshi Roy
Professor Steven Anlage

ACKNOWLEDGMENTS

I am grateful to everyone who made my graduate experience enjoyable and edifying and who made the thesis possible.

First of all, I would like to thank my advisor, Professor Wolfgang Losert, for his constant support and encouragement and for all his advice. He provided me the opportunity to work on interesting and applicable projects. Throughout my years as a graduate student, he provided the vital guidance and advice needed to accomplish this research. I am especially grateful for his unselfishness in providing opportunities for me to learn to grow and for listening to and encouraging my own opinions and ideas.

I would also like to thank Professor Julio Friedman, Professor Edward Ott, and Professor Jack Douglas for their advice and input into this thesis. I am appreciative as well to Professor Anisimov, Professor Anlage and Professor Roy for serving on my thesis committee and for their input.

I am grateful as well to those I worked with here at Maryland as well as elsewhere: Sander Van Der Meer for starting this project and observing the initial results; Masahiro Toiya for providing a constant source of advice and insight; And Nicolas Taberlet for providing me with his simulation code to run on my experiments. I am also appreciative for the undergraduates who worked with me on many experiments: Ken Desmond, Wally, and Andrew Porter. I am grateful as well for everyone else in our research group: Queyong Lee, Justin Stambaugh, Cory Poole,

Andrew Pomerance, Erin Rericha, and Steve Slotterback.

I would also like to thank Donald and Mathew Martin for doing much of the work in designing and building my experiments. I am appreciative of the staff here at IREAP: computer hardware support and snack vending from Edward Condon and purchasing help from Nancy Boone. The timely completion of this thesis would have been impossible without the help of Jane Hessing who repeatedly performed miracles to allow my defense to happen on schedule.

I am deeply appreciative for my friends and family that encouraged and helped me during this time. I am grateful to my mother and father for their advice and insight. I am thankful for Tara Brundick and for her support and concern. Finally I express gratitude for all others who helped me during the last five years, I needed every insight and every smile.

I am also appreciative of NASA, NSA, and the Cosmos Club for providing the financial support for this research.

TABLE OF CONTENTS

LIST OF FIGURES

Chapter 1

INTRODUCTION

1.1 Sand and Granular Physics

Granular materials are common to our everyday experience. We played with them in the sandbox and at the beach as children. We empty them out of our shoes, and try to keep them out of our carpets. They make up much of our food and fill our pharmaceutical pills. We pile them up and we make walls out of them (especially if you live in Massachusetts). Granular materials is a general term that refers to a large class of systems that interact only through direct particle-to-particle contact forces and no, or very limited, attractive forces. Common granular materials include sand and rocks, powders and mixtures of glass and steel balls and various foodstuffs like nuts and corn.

Granular materials appear to be very simple in nature, yet exhibit a variety of strange and unexpected behavior. From simple sandpiles to powerful avalanches, we can observe rich and complex dynamics. Granular materials cluster and segregate when you try to mix them [1, 2]. They 'remember' the forces that have been applied to them [3]. Sometimes they flow like fluids and other times they support weight like solids [1, 4].

The physics of granular materials turns out to be very complex and hard to model. Granular materials are constantly dissipating energy and techniques of

statistical mechanics that require conservation of energy, or that assume a minimization of energy or entropy, often do not work [5]. Because there are so few particles compared to a fluid, granular flows cannot always be described by standard fluid dynamics. Because there are so many, it is impossible to solve the physics of each particle. While granular systems can be simulated, we do not know what must be included to model their basic interactions. This in between state of granular materials can be very frustrating, yet it makes for beautiful physics.

The simple, yet rich and complex, world of granular materials has become an active area of research in physics in only the last 20 or so years. Many successful attempts have been made to model granular dynamics [2, 1, 6, 7], and yet each specific system often requires a new model and new physics. We are still far from, and may never achieve, anything resembling a universal model of granular materials. Although difficult to understand, granular physics provides fascinating and beautiful phenomena to study. It may be the difficult nature of the field that makes it so intriguing to so many physicists [1, 3, 4].

1.2 Force Chains

A simple pile of sand effectively illustrates some of the complexities of granular physics. In figure 1.1, we see two seemingly identical piles of sand. The only difference between them is the way in which they were prepared. One of the piles was prepared by pouring the sand onto a small area at the center of the sample, while the other was prepared by evenly raining the sand onto the entire sample area,

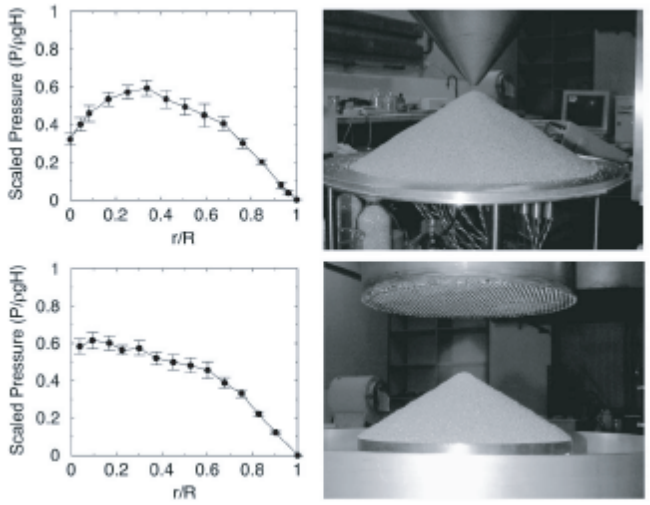

Figure 1.1: Pressure versus radial distance in two piles of sand. The only difference between the two piles is the method of preparation: The top pile was prepared by pouring the sand out of a funnel directly into the center of the preparation area and allowing the pile to build up around the center. The bottom pile was prepared by pouring the sand evenly out on the whole area, allowing the excess to avalanche off, until a pile was formed [3].

namely a finite diameter circle, and letting the extra fall off. Although in both cases the final state is an identical pile of sand, there is a distinct difference in the way the pressure is distributed in each pile. The pile that was poured into the center has a distinct dip in pressure at the center of the sample. The pile that was evenly rained out has no dip in pressure. Seemingly identical, these sandpiles somehow 'remember' how they have been prepared.

This granular memory can be explained by looking at how the weight of a sandpile is supported. It turns out that weight in a granular material is not evenly distributed but is instead carried only by some of the particles, along granular 'force chains'. Bob Behringer's group at Duke University measures the force chains in

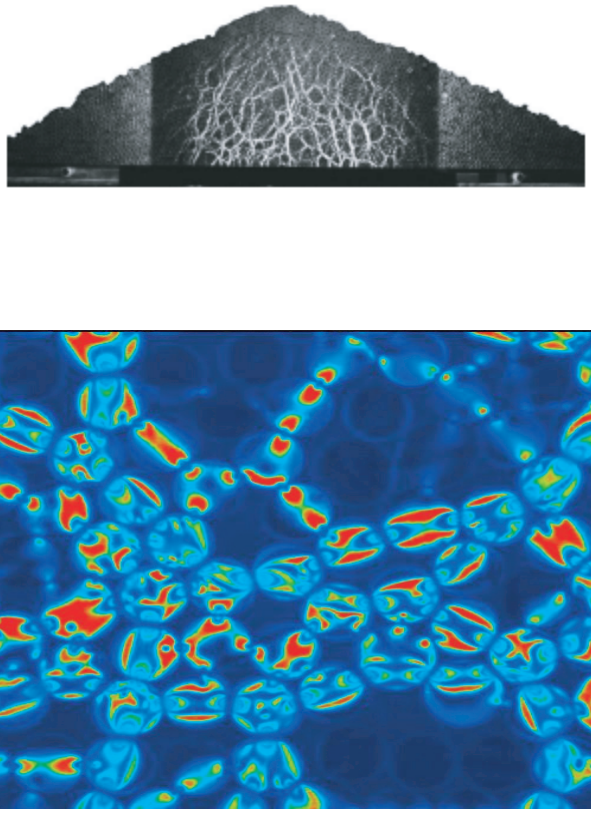

Figure 1.2: Top: The force chains in a pile of photo elastic discs. Bottom: A close-up of force chains in a typical system of photo elastic disks [3].

granular systems using photo elastic disks [3]. Light from Photo elastic disks can be seen through cross polarizers when stress is applied to the disk. In figure 1.2 there is a picture of typical force chains. The top picture shows a pile of photo elastic disks, similar to a pile of sand and the bottom shows a typical close-up of the force chains for a densely packed system. We can see from the picture that the force chains completely bypass whole areas of particles. Which particles carry the forces and how the force chains are distributed is dependent on the history of the material. In the two sandpiles, the differences in preparation method causes subtle difference

in the force chain distributions, giving rise to the pressure difference between the two systems as shown in figure 1.1.

In sheared systems, the force chains have been shown to depend on the direction of shear [8]. Couette cell (see figure 1.6b) shearing experiments are done by putting a granular material between 2 concentric cylinders and then rotating one or both of them. Toiya et al. [8] observed that, like the sand piles, the flow profiles of these mixtures were history dependent. When the cell was sheared in one direction for a long period of time and then the direction of shear was reversed, the initial flow profile was distinctly different. This was again shown [9] to be due to the force chains: the force chains carrying the shearing force from the moving walls line up in the direction of shear.

This has direct application to many areas of geology and industry. Through force chains, a granular material can remember what has happened to it. A hillside might look the same to the naked eye, but based on its history it might be ready to fail. Friedmann et al. found that there is a correlation between the direction of prior shear and the likelihood of avalanche events [10]. Specifically that a catastrophic rock avalanche was more probable if the direction of prior shear was the same as the landslides eventual path.

1.3 Driven Granular Systems

It is a commonly experienced fact that the smallest bits in a cereal box, or in a box of nuts, always end up in the bottom. When mixtures of different size particles

Figure 1.3: A picture of a mixture of nuts where the large Brazil Nuts have risen to the top. This picture is from the University of Texas chaos website (chaos.ph.utexas.edu/s̃chroeter/images/mixed.jpg).

are perturbed (usually by vertical shaking) the larger particles tend to rise to the top [11] and even if only a single large particle is mixed in with a sample of smaller particles, then that large particle will rise to the top. This is called the Brazil Nut effect, because it can be observed in a container of nuts that the larger Brazil nuts always rise to the top of the container over time (see figure 1.3).

For a long time it was thought that this was caused by the smaller particles filling the voids below the large particle(similar to the small particles in a cereal box falling through the cracks of the larger particles) [11]. Recently, though, it has been shown that convection rolls exist in vertically shaken containers and that this may cause the segregation of large particles at the top [12, 13]. The mixture of particles convects up and then back down again, and the large particles follow the convective

Figure 1.4: Localized excitations, called oscillons, in a driven bed of granular material [14]. Image from the University of Texas (cns.utexas.edu).

flow up but once the large particles are brought to the top, they can no longer go back down into the mixture because of their size. Even though this is a very simple experiment, it is still unclear which description is correct, or if both effects happen at the same time. For some conditions, the first might be the most accurate, while for others the second effect might dominate.

Many of the avalanches and other large scale phenomena are caused by the violent shaking of the earth during an earthquake. In figure 1.4, we see a stunning display of the effect of shaking on one granular system. As the granular particles are shaken vertically, localized excitations appear–strong distinct features that oscillate between a peak and a valley that are called oscillons. These oscillons were observed by Harry Swinney et al. [14]. Hexagonal, square and mazelike patterns have also

Figure 1.5: A snow avalanche [17].

been observed depending on system parameters. Other oscillated granular materials include rods and magnetic beads, and these each form distinct patterns [15, 16].

1.4 Granular Flows

We now look at the characteristics of flowing granular material. The most obvious form of this in nature is an avalanche of dry grains (snow or dry rocks and dirt). Avalanches happen when a portion of the hill or mountainside can no longer support the weight above it. The material then breaks and flows down the mountain until it reaches a flatter area. An avalanche can be very destructive and dangerous to anything in its path (see figure 1.5). Although an avalanche flows down an incline like a fluid, as soon as it reaches the bottom it stops and forms a pile with a distinct

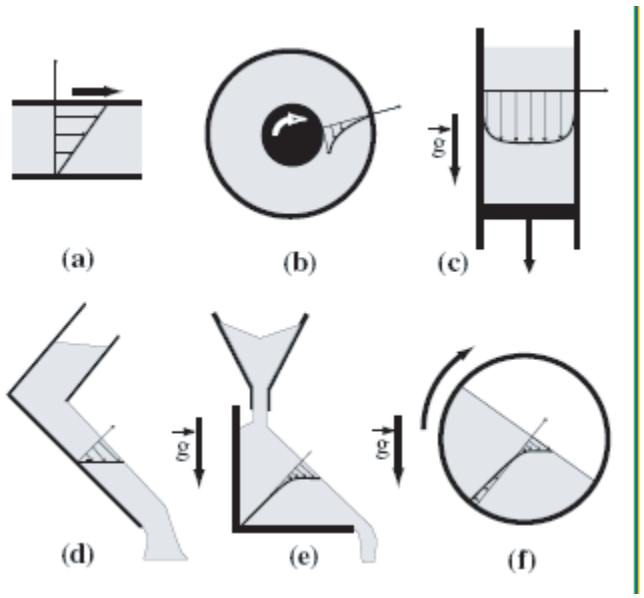

Figure 1.6: Methods of studying granular flow. (a-b): Moving wall shear flows. (c-f): Gravity driven shear flows. Figure from reference [21].

angle called the angle of repose. There are a few unexplained exceptions, called long run-out avalanches, that fluidize and flow up to 10 times longer than expected for a dry granular material [18, 19, 20].

Some of the methods of studying granular flow in the lab are shown in figure 1.6 and include shear flows studied with moving walls in straight geometries (figure 1.6a) and cylindrical Couette geometries (figure 1.6b), a variety of gravity driven sand flows figure 1.6(c,d,e), and continuous avalanching flows in a rotating tumbler (figure 1.6f).

All of these flows exhibit segregation phenomena. Makse et al. reported on granular stratification in an article on avalanche flow in Nature in 1997 [2]. When mixtures of different kinds of materials are poured onto a flat surface (similar

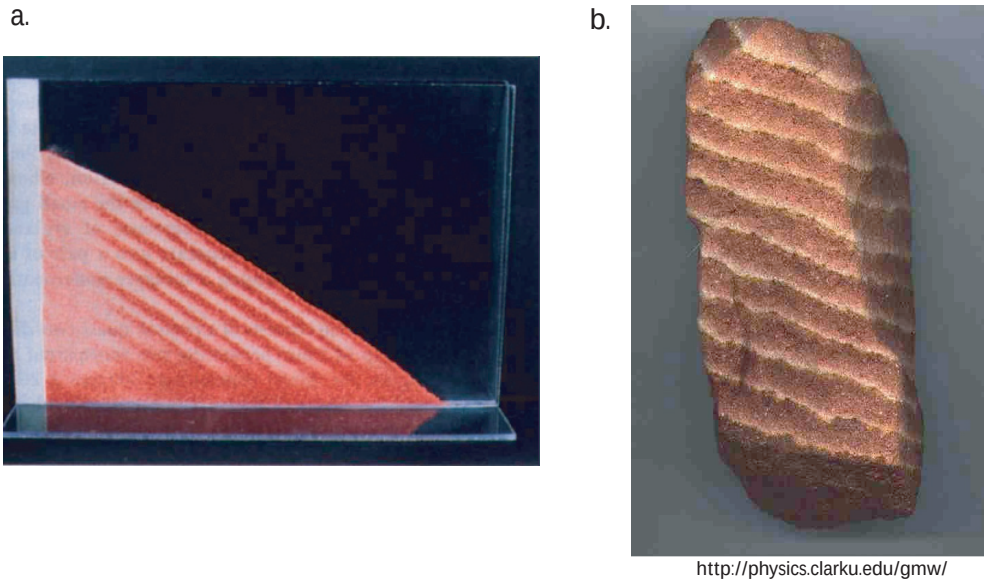

Figure 1.7: Stratification in granular experiments [2] (left) and in a solid rock (right). The rock is an Aeolian sandstone from Petra in Jordan. The dark layers are coarse grain material while the white layers consist of finer grained material. The picture of this rock was taken on March 31, 1997 by H. A. Makse and H. Hlalat [22].

to figure 1.6(e)) interesting segregation patterns develop. For a mixture of two different sizes of particles, the particles spontaneously separate into stratified layers. In figure 1.7a we can clearly see this distinct layering in an experimental setup [22].

Often, when we look at exposed rock surfaces, we see similar patterns. In figure 1.7b we see a picture of an exposed rock surface that shows a pattern very similar to those seen in experiments. Clear stratification patterns of coarse red material and fine white material can be seen in the exposed rock face.

1.5 Rotating Drum

In this thesis we examine pattern formation in a rotating drum (systems similar to figure 1.6(e)). A long transparent cylinder is partially filled with granular material, placed on its side to be horizontal with respect to gravity, and then rotated around its axis. Rotating drums in the continuous avalanche regime have many applications. They are used in a variety of situations in industry, including rotary kilns and mixers of all sorts. They are used for mixing, humidifying, cooling and heating, and in calcining processes [23]. They also provide an interesting example of a continuous avalanche, applicable to studies of geological and granular flows [7, 24, 25, 26].

1.6 Outline of Thesis

The focus of this thesis is on the segregation of different kinds of particles in a rotating drum. In mixtures of two or more particles sizes, two types of segregation have been observed: radial and axial segregation. During radial segregation, the small particles percolate to the bottom of the flowing layer. This happens immediately upon rotation and extends throughout the drum, forming a radial core of small particles. During axial segregation, the particles separate into alternating bands according to size horizontally across the drum. Axial segregation takes longer–a few hundred rotations–to become observable. The mechanism for the axial segregation process is less well understood and is the focus of this thesis.

In this thesis we investigate the axial banding pattern, and in particular at-

tempt to answer the question: why do axial bands form? We address this question by directly studying the properties of the top surface flow of granular material with a high speed camera. The high speed camera allows us to track thousands of individual particles. We can then extract and study averages of these particles, such as velocities and concentrations. We focus on the role of the velocity differences in the axial banding process. We also look at the effect of acceleration and deceleration on mixtures of flowing granular material. We incorporate the entire 3-D nature of the flow into our analysis.

We begin with an exhaustive background of the literature on rotating drum experiments in Chapter 2. We review the basic physics specific to granular flow in a rotating drum. The literature provides extensive scaling experiments that give insight into the important dynamics. Many of these experiments and arguments have been extended to bidisperse mixtures in the radially segregated state. We give an overview of axial band formation and the theories describing this process. We then present two processes that have not been considered in models to date.

A driving parameter in many models for axial segregation is the difference in the flowing angle and surface height of the different particle types. Flow in the direction of steepest descent is usually assumed as the driving force for segregation, and this is related to the angle at which the surface flows. In chapter 3, we review the literature on flowing angle, and present results for the flowing angles of the particles we use in our experiments. We also look at the flowing angle across the banded state.

In chapter 4, we present novel results on high speed tracking of particles in

the top surface flow for mixtures in the banded state. High speed tracking of the particles has not been done for the banded state in the rotating drum and we observe fascinating flow patterns. We measure the downhill velocities and find that particles in a small particle band flow significantly faster than particles in a large particle band. We look at the velocities in the direction transverse to the flow and we find an interesting in and out flow pattern around a small particle band. We then compare the measured surface flow properties to theory.

When we mix three different size particles in a drum we see fascinating patterns of oscillating bands. We discuss these beautiful results as well as analysis in chapter 5. These results show good qualitative in terms of current theory as the three particle sizes allow two coupled concentration equations.

Chapter 2

BACKGROUND AND THEORY

A large volume of work has been done on mixtures in a rotating drum. Studies have been carried out on mixtures in drums with a large range of shapes: in 2-D drums, in long 3-D drums, in tilted drums, rotating spheres, and even in helical drums. Monodisperse, bidisperse, tridisperse, and continuously varying mixtures have all been studied. Mixtures of particles of different size, density, and shape have also been investigated. We now review much of this work, focusing on binary and more polydisperse mixtures of different particle sizes in long 3-D drums. We also look at monodisperse systems as well as 2-D systems to understand and characterize the basics of the drum flow. As they are applicable, we will mention other more obscure systems as well.

2.1 Basic Drum Flow

Depending on the speed of rotation of the drum, many different kinds of motion can be observed. The different regimes of motion are called, in order of increasing rotation rate: avalanching, rolling, cataracting, and centrifuging [27]. At very low rotation rates, the material flows in separate distinct avalanches [28, 29]. The drum rotates the mass of particles until the surface reaches a critical angle, called the angle of marginal stability [27], at which point the material avalanches down to the angle

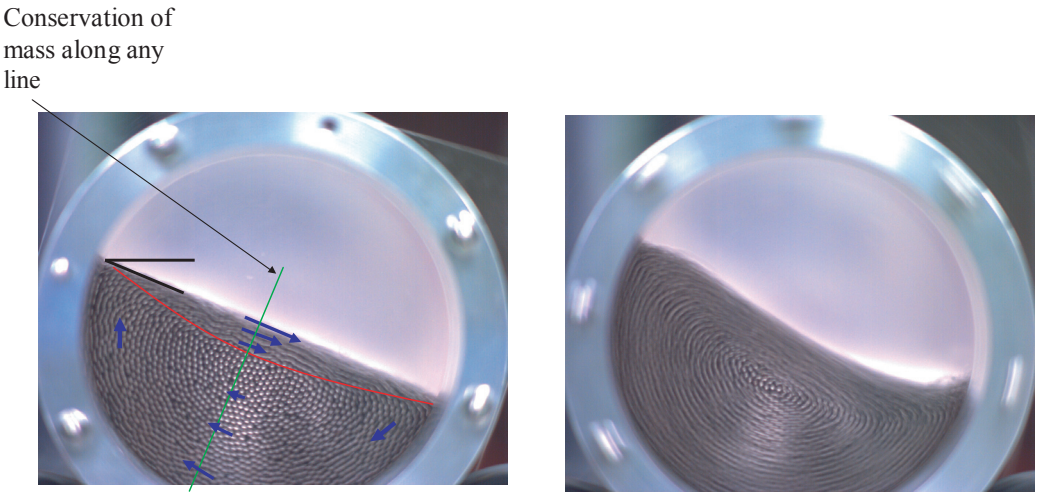

Figure 2.1: Left: A picture through transparent endplates of the flow of granular material in a rotating drum at 7 RPM. The arrows indicate the direction of flow: particles flow down the surface in the area marked by the red line and then rotating back around in the bulk. Right: A similar flow but at much higher rotation speeds (28.5 RPM). This flowing surface has a distinct 'S' shape.

of repose. The angle of repose is the steepest angle at which a material is stable and is the angle at which materials naturally relax to when an avalanche stops. It is commonly used in the geosciences. Both angles depend on the material type.

The cataracting and centrifuging regime are seen at very high rotation rates. In the cataracting regime, the particles are thrown into the air and free fall down to the bottom. In the centrifuging regime, the rotation rate is so high that centrifical forces take over and the particles stick to the outside of the drum. The rolling regime is seen at intermediate rotation rates, and is the focus of this work.

The rolling regime is also sometimes called the continuous avalanching regime because the material flows down the free surface continuously as shown in figure 2.1. The particles flow at an angle referred to as the dynamic angle of repose. The

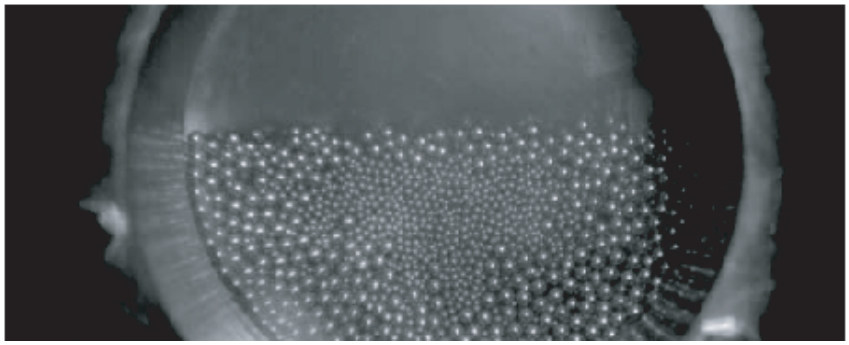

Figure 2.2: The radially segregated state in a mixture of 1/16"' and 1/8"' steel ball bearings in a rotating drum. The small particles drop to the bottom of the flowing layer and form a radial 'core'. Note that though the drum is rotating, the camera is tilted to the dynamic angle of repose to obtain this and many of the other images of the side of the drum.

dynamic angle of repose depends on the rotation rate and the drum diameter, as well as the particle type and size.

The particles flow down the surface as shown in figure 2.1 and are rotated back around in the bulk. The downhill flow extends below the free surface of the drum and has a lenticular shape: the flow is deeper at the center of the drum as the deeper particles follow a much shorter path, rotating around in a small half circle and then avalanching only a short distance down. At low rotation rates, the free surface is nearly flat. At higher rotation rates, the surface develops an s-like shape as seen on the right in figure 2.1.

2.2 Radial Segregation

Looking at the drum from the side as in figure 2.2, it is observed that after only a few rotations the small particles segregate to the bottom of the flowing layer. After segregation, the small particles are advected through a shorter path in the bulk and form a radial core, surrounded by large particles. Radial segregation is most likely caused by the smaller particles percolating down through the mixture during the flow as well as by the observed tendency of large particles to flow more easily farther down a free surface [1, 30].

There is a well defined but continuous transition from large to small particles as one looks deeper into the flowing layer [31]. Some small particles are still found near the top surface of the flowing layer and some large particles are found near the bottom of the flowing layer. G.H. Ristow [27] measured the strength of the radial segregation numerically and found that the concentration of small particles was about 20% by volume near the top of the flowing layer as opposed to 80-100% in the radially segregated core. Invasive probing [32] and magnetic resonance imaging (MRI) [33] studies have also shown that this radial segregation extends throughout the whole drum in long 3-D drums.

Segregation similar to radial segregation is seen in many different geometries with surface flow, including inclined chute flow. Hirshfeld and Rapaport [34] used molecular dynamics simulation to study a few large particles mixed with a large number of small particles flowing down an inclined plane. Over time, as with the brazil nut experiments shown in chapter 1 [11], the large particles rose to the top.

Radial segregation has also been seen in mixtures of similarly sized but different density particles [30]. In that case, the heavier particles generally tend to the bottom of the flowing layer, though it can be complicated by the tendency of the heavier particles to roll farther down the flow.

Cantelaube and Bideu [35] studied the statistics of trapping of the small particles in radial segregation and found that the strength of the segregation increased with time as $1 - e^{-t/\tau}$, τ being a time constant depending on system parameters.

Using ternary mixtures of 1 mm, 1.5 mm and 2 mm steel beads rotated at .33 rotations per minute (RPM) Clement et al. [36] studied the concentration as a function of position in the radially segregated state. They found that the strength of the radially segregated core of the smallest particles, c, followed an exponential decay with respect to the distance from the center of the drum, r,

$$c = e^{\alpha * r} \tag{2.1}$$

They found that α for the largest (2 mm) particles was 0.1 and for the smallest (1 mm) particles was -0.06 (exponential decay with increasing radius). At higher rotation speeds, for glass beads, Khakhar et al. [31], found similar decays, although at the highest rotation speed (18 RPM), the decay looked more linear than exponential.

In some binary mixtures in a rotating drum, chaotic bulges have been seen to form in the radially segregated state [31, 37]. The radial core is not identical around the z axis but instead has extending bulges of small particles (see figure 2.3) forming a star looking pattern. This is mainly seen at very low rotation rate, in the

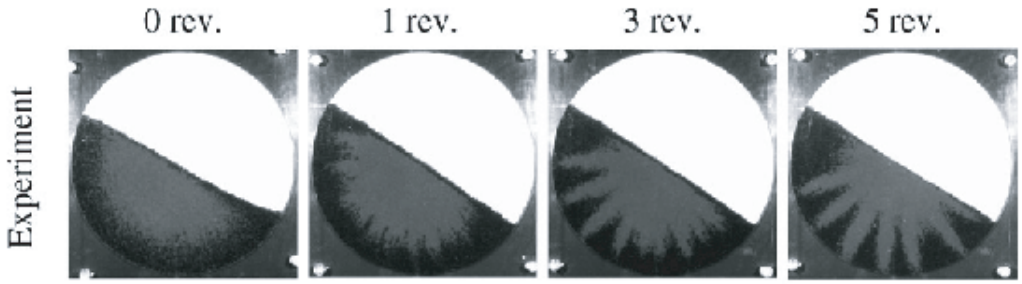

Figure 2.3: Image sequence showing bulge formation in the radially segregated state. This mixture is a 5% volume mixture of 3 mm (dark) and 1 mm (light) glass beads rotated at 0.75 RPM. Courtesy of Khakhar et al. [31].

avalanche regime, where the flowing surface experiences distinct avalanches, but can also be seen in some mixtures in the continuous regime. These are similar to streak formation seen with monodisperse systems of particles differing only in color [1].

2.3 Axial Segregation

In figure 2.4, we see a simple example of axial segregation. Here we have 2 different sizes and shapes of particles, rice and split peas, that have separated into alternating bands. This segregation is fascinating in that it happens in the direction perpendicular to the flow and to gravity, unlike most other granular segregation processes. For example, stratification bands look similar to the bands in the rotating drum, but are actually more like radial segregation than axial segregation. It is a very slow, statistically driven, process. The mechanisms for axial banding are a

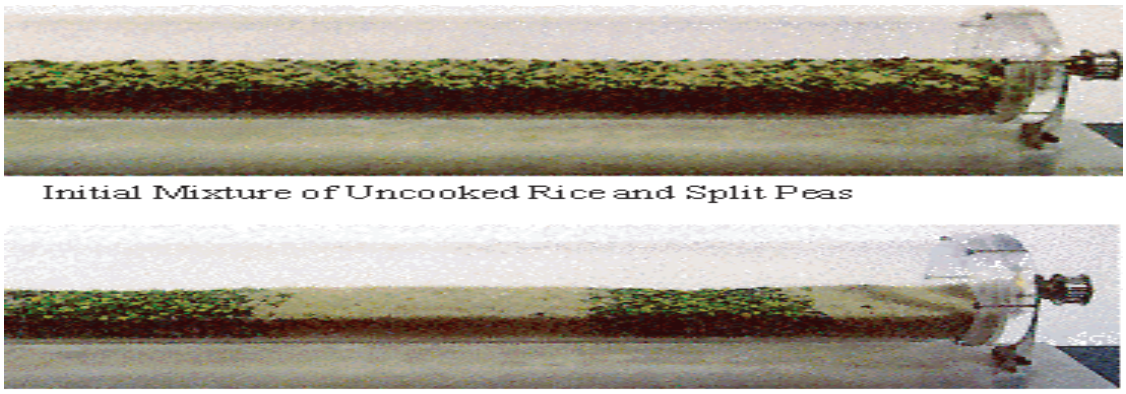

Picture from web page of K.M. Hill and J. Kakalios

Figure 2.4: A mixture of rice and split peas in a rotating drum. The rice and split peas have completely separated into alternate bands. Picture from web page of K.M. Hill and J. Kakalios [38].

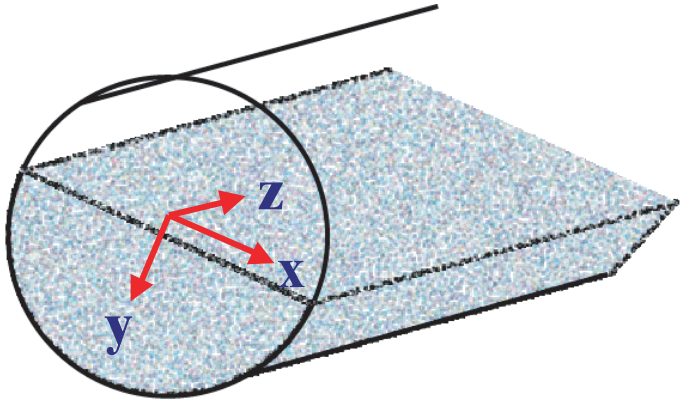

Figure 2.5: Schematic for the drum with labeled coordinate system.

subject of great interest and debate.

For reference, we have plotted a schematic of the 3-D drum with the coordinated system that we will use throughout this paper (see figure 2.5). The drum is rotated around the $\hat{z}$ axis such that the flow is in the direction of $\hat{x}$. The $\hat{y}$ axis is positive down into the flow. The axis is turned such that the free surface is aligned with the x axis. We will refer to the drum diameter and radius in capital letters (D and R respectively), while we will refer to the particle diameter as little d.

Axial segregation was first observed in a rotating drum by Oyama in 1939 [39, 40]. Axial segregation was subsequently studied in depth experimentally, computationally, and theoretically. It was observed in many of the experiments that often, bands formed first near the endwalls and then additional small bands form from one end of the drum to the other.

The connection between the subsurface and surface flow and between radial and axial segregation was made by Rogers and Clements [32] using invasive sampling and by Hill et al [33] using MRI. They were able to show that bands of small particles form in conjunction with an instability of the concentration of small particles in the inner core. A local increase in thickness of the inner core (indicating locally more small particles) generally grows and eventually penetrates the surface. A radial core of small particles often persists in the large particle bands [32, 33], and some robust scaling relations can be found for radial and axial segregation (these are discussed in section 2.4) [24].

We plotted the MRI results along with a schematic demonstrating the band formation in figure 2.6. Images from the MRI experiment are plotted on the left.

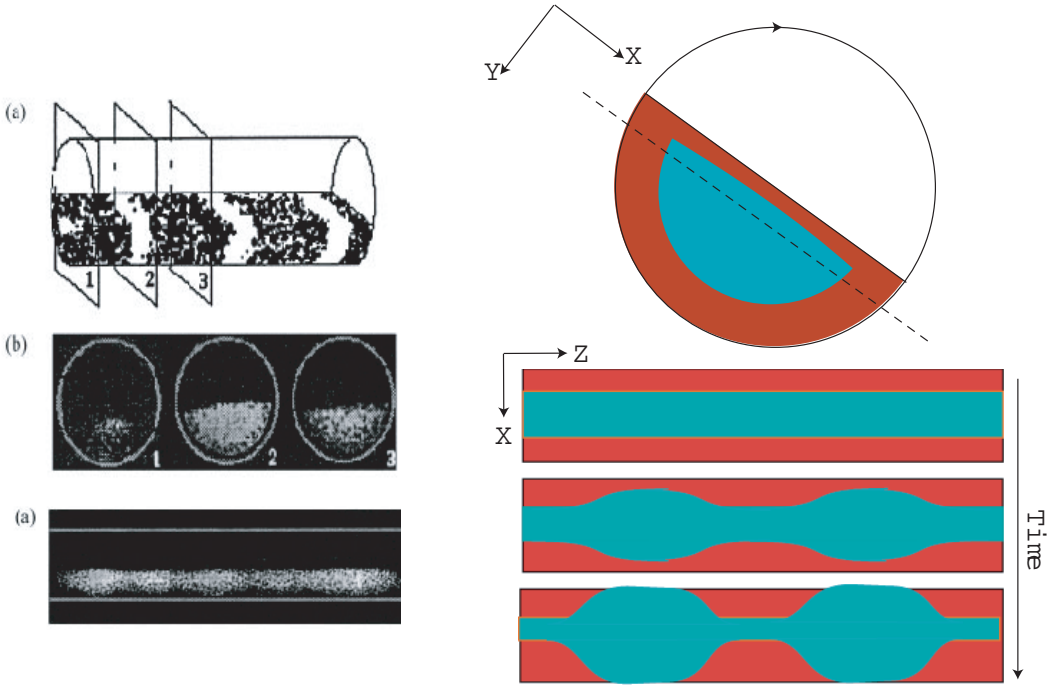

Figure 2.6: Connection of the radial core to axial band formation: On the left, MRI images from Hill et al. [33] show the radial segregation in the banded state. The areas of small particles are white while the large particles mix with the background and are black. On the right, a schematic representation of the band formation as an instability in the radial core. Here the top figure shows the Elkview of the initial radially segregated state and the figures represent the time evolution of a slice taken along the dotted line.

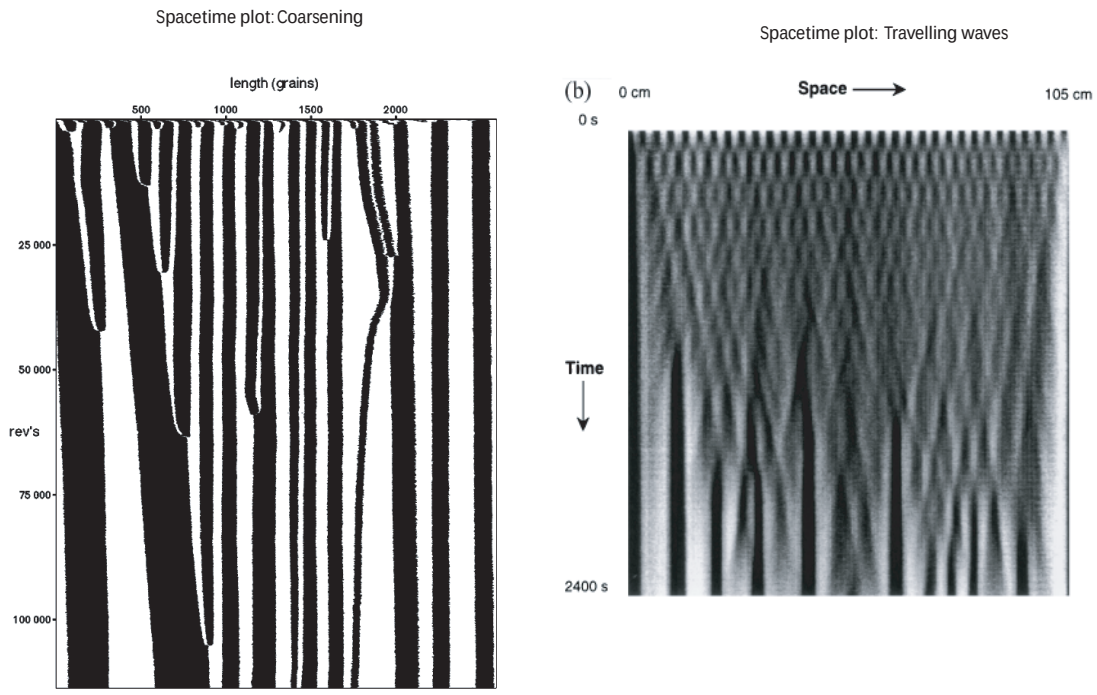

Figure 2.7: Left: A spacetime plot of the long-time dynamics of axial bands in a rotating drum. Each horizontal pixel line represents the banding state at one instant in time and time progresses downward. The bands coarsen over time to form fewer and larger bands. Picture taken form the work of Boris Levitan [41]. Right: A spacetime plot of a traveling/standing wave pattern in a mixture of sand and salt. Picture from the group of Steve Morris [25].

They show a view of the entire drum, a view through cross sections at different places in the drum and a view through the center of the drum showing the axial evolution of the radial core. We can clearly see that the axial core exists inside the large particle bands. Slice number 3 even shows the presence of a subsurface band, an increased thickness of the radial core that does not reach to the outside of the drum. On the right in figure 2.6, we show a schematic representation of the time evolution of the radial core as the bands form.

After the initial array of bands has formed, the bands combine (coarsen) over

time to create wider but fewer bands (see figure 2.7). Levitan [41] and Stavans [42] found that the number of bands decreases exponentially. Because this coarsening process is so slow, it is hard to be certain of the final state. In some experiments, the final state has been observed to be either a small number of stationary bands [42] or two completely separated bands [43], depending on experimental conditions. It may well be that all rotating drum mixtures will eventually segregate completely, but it takes far too long to be reasonably checked in all experiments. It is also possible that other factors such as slight tilts in the experimental setup or slight differences in the drum diameter may drive such slow processes.

A possible connection was made with the formation of a final state (end of coarsening) and the radial core by Taberlet et al. [44]. They observed in molecular dynamics simulations that the coarsening appeared to end, after some coarsening, when the radial core did not extend throughout the entire drum anymore. The radial core did not extend all the way through the large particle bands, but 'pinched off' instead, separating the small particle bands. This stopped further segregation, or at least strongly increased the timescale for any further segregation process.

In 1997, Morris et al. [25] observed the fascinating pattern evolution shown on the right in figure 2.7. The pictures shown are spacetime plots of the evolution of the banding pattern. An average slice is taken from each image in the sequence so that each new horizontal line of pixels represents the banding pattern at a given time. Morris et al. found that for certain mixtures of sand and salt and at certain filling heights, the bands traveled to the left or right. If the drum was perfectly balanced, particles of one type traveled in one direction and particles of the other type traveled

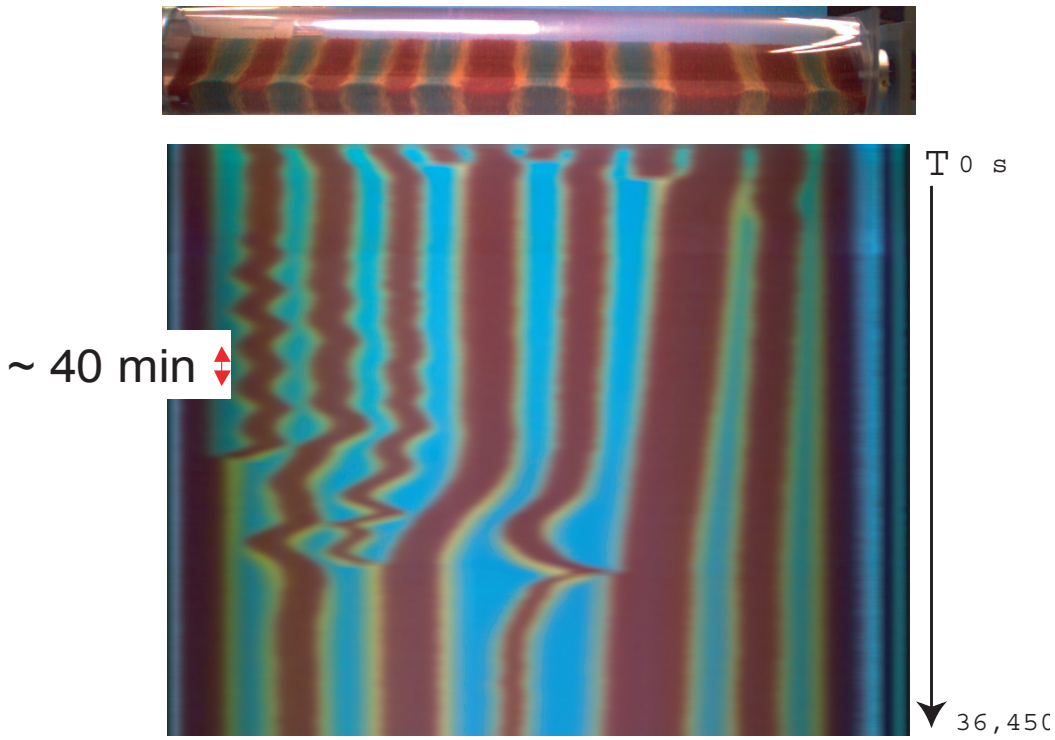

Figure 2.8: Spacetime plot of oscillations in a mixture of 0.5 mm (green/blue), 1.0 mm (yellow), and 2.0 mm (red) glass beads rotated at around 30 RPM.

in the opposite direction. This created a stunning standing wave pattern. Note that this experiment had presegregated initial conditions: The drum was seeded with alternating bands and no radial core before rotation.

Morris et al. [45] and others [42, 46] also observed other strange and interesting patterns, including a fountain wave pattern, satellite traveling waves, and more. In a Europhysics letter, Newey et al. [47] reported on the pattern of oscillating bands for mixtures of three particle sizes shown in figure 2.8.

The size and number of bands generally do not scale with the rotation rate [48, 49]. The Morris group [50] carried out an as-of-yet-unpublished work on how the

band pattern scales with particle to drum diameter ratio. They found that the average wavelength of the bands increased linearly with drum to particle diameter ratio. i.e.

$$\lambda \propto \frac{1}{d/D} \tag{2.2}$$

where d/D is the particle to drum diameter ratio. They used the average particle diameter of the two particle types for d in this calculation. They also noticed that there was a maximum particle to drum diameter at which bands would form. Above $d/D = 0.025$, no bands formed.

S. Das Gupta [51] observed ternary banding for mixtures of three particle sizes and Masami Nakagawa [49] observed banding in mixtures with a continuous size distribution. Nakagawa recorded the number of bands initially formed at different rotation rates, but found that the number of bands did not show a strong dependence on the rotation rate.

Patterns similar to axial banding can be observed with fluids. Krasnopol'skaya et al. [52] observed band formation in rotating drums of mixtures of fluids of different viscosities. The fluid formed alternating bands of vortices of one type of the fluid. A detailed comparison was made between this and granular band formation in rotating drum experiments. Tirumkudulu et al. [53] observed that neutrally buoyant particles mixed with a single fluid in a rotating cylinder (in this case a Couette geometry) also clustered and formed bands. Comparison can also be made with two phase fluid/gas flow in a pipe. Here fluids with different velocities flowing in an confined

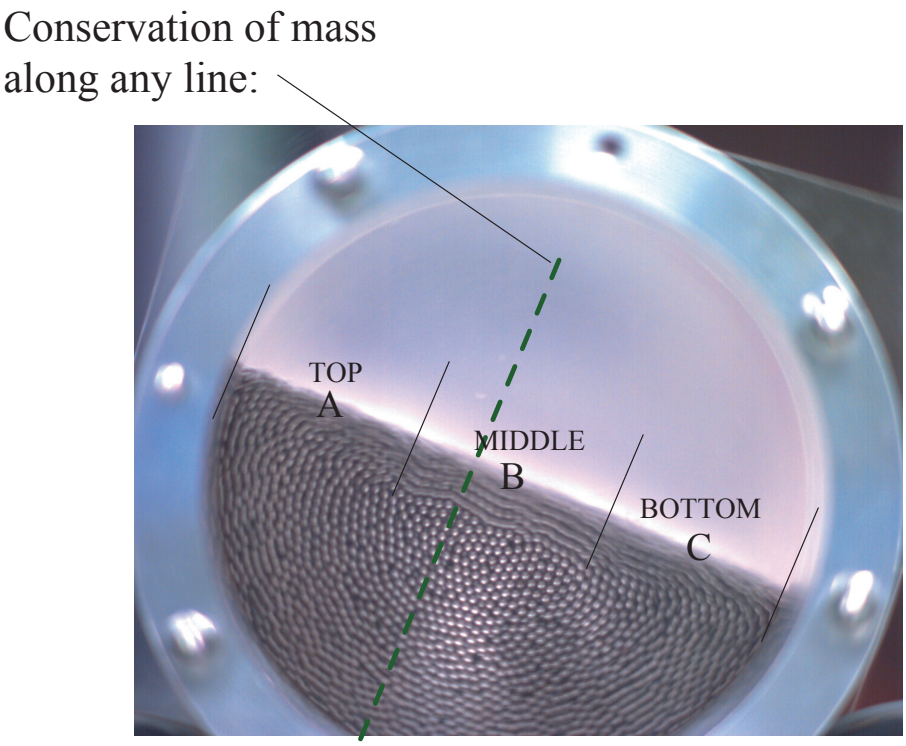

Figure 2.9: View of the drum through the transparent endplates showing the different sections of the downhill flow. At the top of the flow, particles are accelerating. In the middle, they are flowing at a high velocity and mixing. At the bottom, particles are decelerating.

space tend to segregate and break up [54].

2.4 In Depth Flow Studies

It is constructive to look at the basic physics of particles in a rotated drum in detail. We mark point A as the beginning of the flowing layer (see figure 2.9) for reference. Here the particles are accelerating downhill in the x direction. In 2-D, conservation of mass necessitates that either the surface layer of particles must be getting less dense or particles must be added to the surface flow from the layers

beneath (or both). A slight y velocity component will be expected in the upper half of the drum (due to bulk rotation) and this could contribute to particles being added to the free surface. In the middle of the flowing layer, the flowing layer must either be less dense, or be composed of a mixture of particles from deeper in the flowing layer, or both. This middle area of high speed flow is where much of the mixing between particles should occur (the particles have the most energy here). At the bottom of the flowing layer, the particles will collide and decelerate. Here the density must increase again and the particles will be pulled down into the bulk rotation of the drum.

We must also take into account the granular nature of the flow. Granular particles are discrete and interact only through repulsive forces and friction. There is no attractive force between the particles and no tensile stress to oppose separation of particles. There is no long distance interaction (except through chains of other particles). This creates an asymmetry in the flow: particles can separate indefinitely during acceleration (top region), but during deceleration (bottom region), contact forces will keep particles a distance d apart-resulting in jamming.

The velocity and density profiles of the flowing layer have been studied in detail for a large number of different experimental parameters [24, 55, 56, 57]. For all experimental parameters, the velocity profile as a function of depth in the flowing layer (y) is similar: The velocities decrease linearly from the top of the flowing layer. Assuming conservation of mass, the velocity of the particles has a direct relation to the depth of the flowing layer. Assuming that the number density of particles in the flowing layer is the same as in the bulk, and that the depth of the flowing layer at

the middle of the drum, δ_0, is small compared to the radius of the drum, R, then $\overline{v}_x = \omega R^2/(2\delta_0)$.

A scaling argument based on this relationship can be created. Ottino et al. [24] plotted y/δ vs $v_x\delta_0/(\omega R^2)$ at the middle of the downhill flow for 1 mm, 2 mm, and 3 mm glass beads at different rotation rates. They found that the data then collapsed to 2 possible curves. The reason they gave for the lack of universality in the collapse was the distinct "s" shape for the smaller beads at high rotation rates. They extended the scaling to apply to any position in the drum: $\overline{v}_x = \frac{\omega R^2}{2\delta}\left[1-(x/R)^2-(\delta/R)^2\right]$, where δ is the depth of the flowing layer at downhill position x. For 1 mm beads at different locations of the drum, they found this scaling accurately collapsed the data onto a single curve. If the thickness of the flowing layer increasing with the square root of the rotation rate, as seen by Nakagawa [55], then the velocity will also increase as the square root of the rotation rate.

Khakhar et al. [56] studied the velocity profiles as a function of the Froude number, $\omega^2 R/g$, and the size ratio of the particle diameter to the drum radius, d/R, for glass and steel balls and for sand particles. He found that the scaled layer thickness, δ_0/R increased with increasing Froude number and increasing particle diameter to drum radius. He found that the Froude number provided good scaling for the velocity profiles. Both of the previous two experiments found that the thickness of the flowing layer, and therefore the average and top surface velocity, increase with increasing particle size as the square root of the particle diameter (or the ratio of particle to drum diameter).

Alexander et al. [57] did the most in depth study of the scaling of the velocity

profile versus rotation rate, particle size, and drum diameter. They found a scaling of the downhill velocity with changing drum diameters and rotation rates to be $v_x = kD\omega^{2/3}(g/d)^{1/6}$, where g is the constant of gravity, and k is an arbitrary constant. For identical particles rotated at 10 RPM, the velocities in a drum diameter of 6.3 cm peaks at around 13 cm/s while the velocity for a drum diameter of 24.8 cm peaks at around 58 cm/s. This is a ratio of d1/d2 of 3.9 and of v1/v2 of 4.46, reasonably consistent with his prediction that the velocity scales linearly with R. While this scaling appears to work for changing R, it goes against that seen above for changing d (and d/D). It gives a different scaling for d/D and shows that d/D does not provide complete scaling, but the value of d alone needs to be taken into account as well (not just the ratio d/R). This indicates that there may be different scaling depending on the parameters of the experiment (rotation rate, particle type, etc.) for how v will depend on d or R. Our results generally fall in the regime given in the previous paragraph and therefore will show increasing velocity with the square root of the ration of particle to drum diameter.

Another important parameter is the velocity fluctuations of the flowing particles. This can be related to the diffusion, and is often referred to as the effective granular temperature [58, 59]. The granular temperature is $T_g \propto \langle v^2 \rangle - \langle v \rangle^2$. This is simply the standard deviation (of the velocity) squared. The velocity fluctuations have been observed to decrease with increasing depth in the flowing layer [24]. When scaled by the velocity of the particles, the fluctuations actually increase with increasing particle size, but no clear relationship between particle size and fluctuations can be seen on an absolute scale.

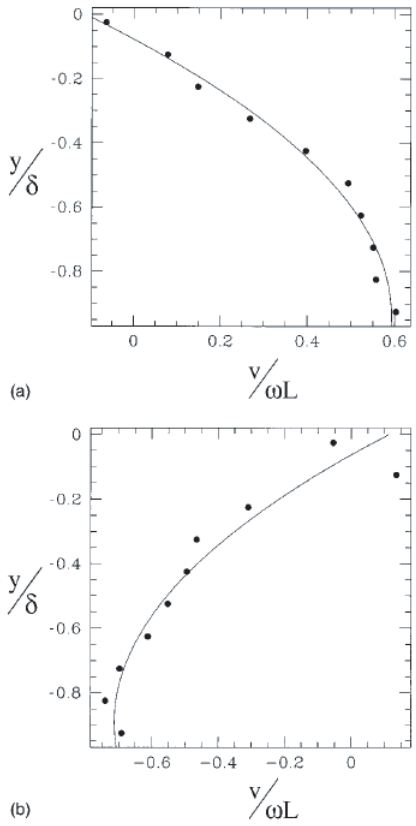

Figure 2.10: v_y for 1 mm beads rotated at 1.6 RPM at two positions offset from the flowing layer. The top curve is a vertical slice at the downhill position x=-0.57R (upstream of the flow middle) and the bottom curve is at x = 0.70R (downstream). Figure from Ottino et al. [24].

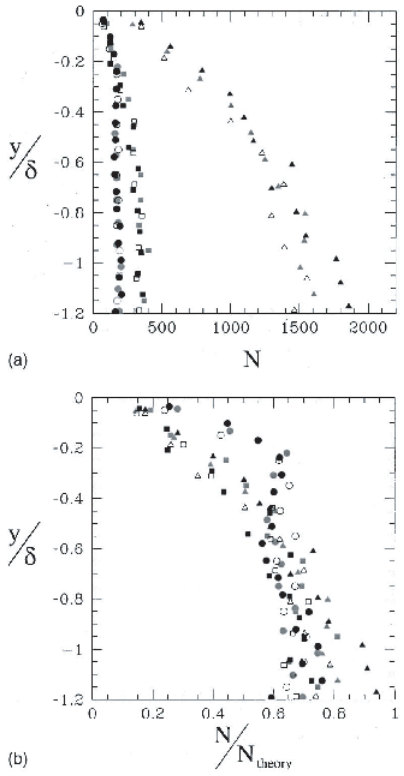

Figure 2.11: Total number of beads versus y. The triangles are 1 mm beads, squares are 2 mm beads, and circles are 3 mm beads. The top plot is the absolute number of beads, and the bottom plot is scaled by the number of beads that can fit in an area d^2. Figure from Ottino et al. [24].

Ottino et al. [24] also measured the $\hat{y}$ velocity profile (the direction perpendicular to the flow–see figure 2.10). They found that particles offset from the center had $\hat{y}$ velocities equal to that imparted by the drum, and that the velocities fell off near the surface of the flow. In Ottino's experiment, v_y fell to about 50% of the tangential bulk velocity around 50% into the flowing layer.

The number density of particles in monodisperse samples has been studied in less detail and in only a few works. Qualitatively, Nakagawa [55] observed the

number density of particles to decrease at the surface ($y = 0$) of the flowing layer. Ottino et al. [24] measured the number density as a function of depth (y) for 1mm, 2mm, and 3 mm glass beads (see figure 2.11). They scaled the plots onto 1 figure by multiplying by d^2, and plotting y/δ. The plots come close to collapsing, except that with careful inspection one can see that the curves do not in fact have the same shape, and for larger particles, the number density begins to decrease much later. Rajchenbach et al. [60] also observed a decrease in the particle number near the surface in experimental studies of 1.5 mm steel beads and Ristow [61] observed a similar decrease in simulations. Bonamy et al. [62] also observed similar dynamics and defined the area of decreased density as the free surface of the flow as particles are less confined there.

Taking Rajchenbach's entirely 2-D experiment as a test case we can analyze the particle number densities and the velocities with respect to conservation of mass. The radius of the drum is 10 cm (we start our analysis at 9 cm inside the drum) and for the fastest curve the rotation rate is not explicitly given in the paper, but we assume it is around the maximum given for these experiments, 20 RPM. From his plots we find the relationship between the x velocity and y, v_x = 550 mm/s +25 1/s y. The initial speed is taken to be the speed at which old particles are replaced by new, or the speed of rotation near the outside of the drum ($v = \omega r$). This gives v_0 = .053 rad/s $\times$.09 m = 4.77 mm/s. Conservation of mass says that in one dimension, ρv is constant: $\rho v = C_1$, where $C_1 = \rho_0 v_0$. Taking ρ_0 to be about 0.7, $C1$ can be calculated: $C1 = 0.8\rho_{steel} \times 4.66$ mm/s = 3.728 ρ_{steel} mm/s . Now solving for ρ versus y, v_x: $\rho = 3.728/v_x = 3.738/(550 - 25y)$ ρ_{steel}. At the maximum

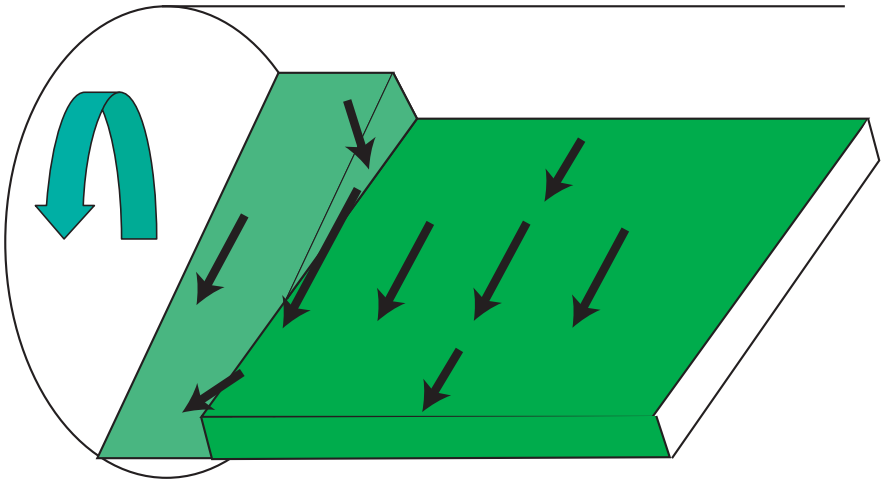

Figure 2.12: Schematic of the flow near the endwalls. The endwalls pull the flow up to a higher angle. This causes a flow away from the endwalls at the top and towards the endwalls at the bottom. This creates an area of higher velocity just out from the endwalls although friction with the endwalls slows particles immediately adjacent down.

velocity, $v = 500$ mm/s, this gives a density of 0.007456 ρ_{steel}, far lower than the average near the surface of the drum. These curves give number density curves much steeper and lower than the true observed curves. Particles must be added to the mixture from below.

When extending the study to three dimensional monodisperse samples in long drums, we must also take into account the fluctuation in the axial, or z direction and the effects of the wall on the flow. Unfortunately, studies have not been done on the $\hat{z}$ fluctuations and little work has been done on scaling of flows in fully 3-D drums. Pohlman at al. [63] studied the effect of the walls on the flow of granular materials in a drum. They found that (as also observed by Donald and Roseman [48]), the particles flow away from the wall at the top and towards the wall at the bottom.

They also observed that the velocity was often greater just out from the endwalls. A schematic of the effect of the endwalls on the flow is given in figure 2.12. The endwalls also cause an increase in the dynamic angle which we will discuss later in greater detail.

The velocity profiles of the radial segregated state of particles have also been studied in depth. Ding et al. [64] used PEPT (Positron emission particle tracking) to track particles in 3-D and Ottino et al. studied the radial segregation velocities through transparent endplates [65]. All experiments on radial segregated velocity profiles find that the flow velocities in a binary mixture showed a linear profile with depth under the flowing layer with little or no kink at the particle type interface (similar to that seen for monodisperse particles). This means that the flow profile under the layer can be predicted from surface measurements only.

Donald and Roseman [66] studied the radial mixing in a long rotating cylinder of two sizes of particles. They found that mixing increased with increasing ratio of one particle size to another. The explanation for this is that the voids between larger particles will appear relatively larger to the small particles for bigger size ratios. Increasing the drum speed increased the rate of radial mixing. An equal mixture (by total particle weight) of large and small particles showed the greatest mixing, and the mixing dropped off as the concentrations were increased or decreased from there.

The radial and axial mixing of different sized particles is related by the radial core. We would expect the axial mixing in a bidisperse mixture to increase for greater ratio in d between the large and small particles. We expect that bands

will not form for high ratios between large and small particles as the radial mixing (which leads to radial segregation) and axial mixing will be too strong.

2.5 Theories of Axial Band Formation

Many different mechanisms may be behind band formation, depending on the experimental conditions. We now provide an overview of the mechanism of band formation in the literature, conceptual and mathematical. It is worth noting that many of the models of granular segregation are engineering models, which aim to provide guidance in design, but not new fundamental principles. We refer again to figures 2.5, 2.9, and 2.12 in the following discussion.

When Oyama first observed band formation, he noticed that the bands formed first near the endwalls and therefore attributed the band formation to endwall effects. The fact that the particles flow at a steeper angle near the endwalls [67], lends support to this idea. Donald and Roseman [48] also observed that the bands formed first near the endwalls and claimed that band formation was caused by differences of the static angle of friction [68] of the different particles as well as by endwall effects. They argued that the small particles, which generally have a higher angle of flow, would tend to flow faster. Velocity gradients created by the endwalls would create areas of higher velocity near the walls and the faster small particles would be attracted to these areas and bands would form. This was confirmed (see above) experimentally by Pohlman et al. [63]

Bridgewater et al. [69] suggested that the large particles, being on the top of

the flowing layer, would be more mobile. They noted that they would then flow to the lowest points in the bed at the bottom of the flow. Because of the increase in angle of repose at the endwalls, the lowest point would be the bottom of the flow right next to the endwalls. This would drive the band formation of large particles right next to the endwalls and therefore push small particles from the endwalls, consistent with most experimental observations.

Zik et al. [70] and Nakagawa [49] saw band formation that could not be explained simply by endwall effects. In a very long drum, the bands formed spontaneously near the middle of the drum–too early to be driven by endwall effects propagating outward from band to band.

In 1990, Das Gupta et al. [51], tested some of the ideas of the preceding researchers. They noted that the different particle types had different flow angles (dynamic angle of repose) and that the difference was dependent on rotation speed. Their mixtures did not band at all rotation rates, but only at rotation rates for which there was a significant difference in the dynamic angles of repose between the particle types in the mixture (as measured in monodisperse samples, of course). They also observed undulations in the shape of the free surface of the material. The surface of the small particle bands was slightly higher than the surface of the large particle bands.

Non-endwall driven mathematical models were created based on differences in flow angle and shape for the different size particles and initiated by statistical fluctuations in the concentration. According to these models, the difference in shapes and angle cause particles to flow axially in the direction of steepest descent. In order

for mass to be conserved there must be backflow for both particle types. Differences in mobility of the two particle types then gives band formation.

Simple models for axial segregation are often constructed from mass conservation:

$$\partial_t c = -\partial_z j \tag{2.3}$$

where c is the local concentration of a given particle type, and j is the mass flow current (generally we are here looking at the surface currents, because that is what we can measure). The axial current, j_z, is often assumed to have the form

$$j_z = (\beta - D)\partial_z c \tag{2.4}$$

where D is the usual diffusion coefficient ($D > 0$) and β is a coefficient describing the strength of the segregation. The first term drives segregation, while the second term is diffusive and opposes segregation. If β is greater than D, then this equation is effectively a diffusion equation with a negative diffusion coefficient, and particles tend to concentrate instead of dispersing.

In models that describe the segregation as axial surface flux due to differences in surface height and dynamic angles of repose [71], axial current is assumed to be proportional to the gradient in height of the free surface:

$$j_z \propto \partial_z y \tag{2.5}$$

The surface height is proportional to the dynamic angle of repose and the current can be written as

$$j_z = \beta \partial_z \theta \tag{2.6}$$

θ is then proportional to the concentration and β is also related to the concentration of the mixture. Adding this current to a current due to diffusive mixing gives an equation like the one above with the first term being 2.6.

Under the assumption that β is note dependent on the concentration, we can combine these equations with conservation of mass to get the final equation for the concentration of particles of a given type:

$$\partial_t c = -D\partial_z^2 c + \beta\partial_z^2 c \tag{2.7}$$

Although β may be dependent on the concentration, this gives us the basic idea of the form of the segregation equations often used. A noise term can be added to this equation to account for coarsening, but because these models are first order in time, they cannot describe traveling waves and other oscillatory behavior. Aranson et al. [7] created a model by distinguishing the concentration from the dynamic angle of repose. This gives two coupled equations, which can describe traveling waves if the concentration and the dynamic angle of repose are out of phase. The first equation,

$$\partial_t c = \partial_z(-D(c)\partial_z c + g(c)\partial_z\theta) \tag{2.8}$$

is similar to equation 2.4 above, where g(c) is in the place of β, and the dynamic angle of repose no longer proportional to concentration of a particle type in the mixture. The second equation is:

$$\partial_t\theta = \alpha[\omega - \theta + f(c)] + D_\theta\partial_{zz}\theta + \gamma\partial_{zz}c \tag{2.9}$$

where α is a constant determining the time scale of segregation and $f(c)$ is the static angle of repose of a mixture of the given concentration. The first term on the right

describes the local dynamics of the angle of repose, the second describes normal diffusion, and the third is a concentration based term.

Aranson assumes no radial segregation, a thin flowing layer, and an axial flow in the rotated bulk–none of which are physically accurate. Despite this, his model provides interesting insight, as the coupled equations provide a model that predicts the traveling waves seen in the experiments (see figure 2.8). It is interesting to consider the concentration term in the second equation as the size of the radial core. Then more correct physical assumptions might be made. Even though this gives oscillations, it still requires that the concentration (radial core) be out of phase with the dynamic angle of repose, and this has been contradicted by experiments which showed the radial core and particle concentration in phase with the angle of repose during oscillations [72].

Another problem with this and the other simple diffusion related models is that Khan et al. [73] showed that the particles in a drum do not obey regular diffusion equations, but instead are sub diffusive. Khan et al. measured the spreading of a pulse of grains, and found that both pulses of different size grains and similar sized grains spread as $t^{1/3}$ instead of $t^{1/2}$. This suggests that although the grains mix, they mix through a process slower than normal diffusion and the mixing term in the above equations would need to be replaced with a sub diffusive term.

All of the models discussed above assume that the segregation happens at the 2-D surface of the flowing layer. Except for the Aranson model, they cannot account for the 3D nature of the flowing layer. Most of the continuum models based on surface flow assume a difference in the mobility of the two particle types. At

the same point in the flow, one particle type moves faster (laterally) than the other particle type. This allows for segregation while simplifying the system to 1-D by averaging over both x and y. Most models also assume that there is a reverse flow that is equal for both particle types to conserves mass. It is usually assumed that the axial flow is caused by a difference in flow surface angle, shape, or height, and that the backflow happens in the bulk.

In another model, Elperin and Vikhandsky [74] again assume that the particles flow in the direction of steepest descent, but also work radial segregation into the model. The radial core was modeled by small particles occupying entirely the center of the flowing layer (this is unphysical–large particles do just skip over the middle of the flow). Large particles flow out of small particle bands (or areas of increased small particle concentration) at the top and back in at the bottom because of the steeper angle of the small particles. An asymmetry in this out and in flow would allow segregation to occur. For example, a greater flow at the top (out) than at the bottom (in) would mean that large particles are flowing out of the small particle band (assuming equal backflow for both particle types).

Unfortunately, as we shall show later, the specifics of this model are incomplete. We will create our own mechanism based on a similar principle, taking into account the entire dynamics of the flow and of the radially segregated core as observed experimentally in numerous works and outlined above.

2.6 Framework for a New Model

There are many different conditions and particle properties under which band formation has been observed. They include difference in particle size, difference in particle density, and difference in particle shape. Band formation is very generic and is recreated by the simplest of simulations: in computer simulations and simple models we have shown that bands can form even in a mixture where only the friction coefficient is different [47, 44]. Although segregation by itself is very generic, real experiments are far more complex, and may sometimes be driven by far more complicated forces.

In order to understand and predict the band formation, these factors must be taken into account. Two important factors are the connection between the radial and axial segregation and the effect of the difference of the velocities of the two particle types. We first investigate the connection between the radial core and the axial banding and answer the question: what causes the instability of the radial core?

We present the framework for a model based on the idea that axial flows and concentrations can vary with downhill position (x). This work is being prepared for publication in a paper by M. Newey and W. Losert [75]. Similar to the model by Elperin and Vikhasky [74], we postulate that the free surface in the middle of the flow is composed of a higher concentration of small particles than the free surface at the top or the bottom (the top, middle, and bottom are defined in figure 2.9). The reason for this is simple conservation of mass, because the particles in the

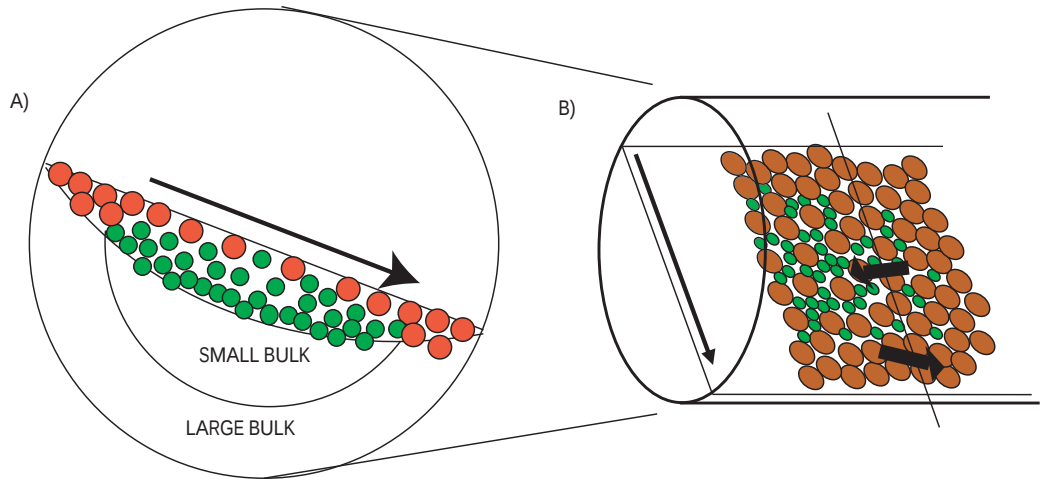

Figure 2.13: A.) A schematic of the radially segregated state demonstrating the increased number of small particles in the middle of the top flowing layer. B.) A schematic of the flowing surface, as seen from above, demonstrating the axial flow with this distribution of particles.

flowing layer are flowing faster, the flowing layer will have to be thinner and less dense (see above). The particles deeper in the bulk will now be closer to the surface and will be more free to move axially (see figure 2.13a). One model, developed by Chakraborty [76] for radial segregation, predicted this–that the concentration of small grains would increase in the middle (middle of x) of the free surface flow (we see this in our experimental results in chapter 4).

For axial segregation to occur due to free surface flows with this concentration distribution, the particles at the free surface in the middle of the flowing layer would need to flow axially toward areas of a larger radial core of small particles (figure 2.13b). The particles at the free surface at the top or bottom of the flow would have to flow outward away from areas with a larger radial core of small particles. This would give a net drift of particles into like particle bands. This net

segregating flux would be opposed by diffusive (or sub diffusive–see above) mixing. This would happen until the core surrounding the band was small enough that mixing balanced the segregating flux.

We relate the strength of the axial flow to both the gradient in the velocity of the particles (although it could just as easily be related to the gradient in the dynamic angle of repose) and assume that it is dependent on the gradient in the concentration. We will provide motivation for this assumption at the end of this section. The total current of a given particle type will be the integral with respect to x of the axial current times the concentration:

$$J_{tot} = \frac{1}{2R} \int j_z(x) c(x) dx \tag{2.10}$$

Where J_{tot} is the total z current of particle type i integrated down the free surface and $j_z(x)$ is the axial current of particles as a function of x. We can simplify this substantially by assuming: No axial flow at the top, $j_{top} = 0$; A constant axial flow, j_{mid}, and concentration, C_{mid}, in the middle third; A constant axial flow, j_{bot}, and concentration, C_{bot}, in the lower third. These assumptions are clearly not exact, but will suffice for a general picture of the dynamics. We also make the assumption that the axial flow happens in a 2-D layer (in the x-z plane), containing approximately the same amount of mass all the way down the flow. If $j_{mid} + j_{bot} = 0$ then:

$$J_{tot} = J_{mid}(C_{mid} - C_{bot}) \tag{2.11}$$

and if we assume that $|J_{mid}|$ is proportional to the difference of flow angle or downhill velocity and therefore the gradient in particle concentration, and we introduce a

mixing term then:

$$J_{tot} = -D\partial c_z + \beta_2 \partial c_z (C_{mid} - C_{bot}) \tag{2.12}$$

Here, like earlier models, we have a diffusion equation that can have a negative effective diffusion coefficient. This is equivalent to using equation 2.4 with $\beta = \beta_2(C_{mid} - C_{bot})$ where β_2 determines the proportionality of the axial flow to the concentration. This equation will lead to segregation if $\beta_2(C_{mid} - C_{bot})$ is greater than D.

The term $C_{mid} - C_{bot}$ represents the size of the radial core and $\partial_z c_z$ represents the strength of the axial flow. The term $C_{mid} - C_{bot}$ will be a complicated function of the total concentration over a given x-y slice, $c(z)$. If we assume that the radial core can be represented by an area of constant concentration with an exponential decay, then a couple of observations can be made. First, when the radial core is too small, then $C_{mid} - C_{bot}$ will be small, and segregation will be balanced by mixing. $C_{mid} - C_{bot}$ will be dependent on the velocity and on the size of the radial core (which both should be proportional to the overall concentration c(z)). This term should grow slowly with increasing concentration of small particles.

Motivations are as follows:

- Assuming the velocity fluctuations are the same for the large and small particle bands, then the lower density of the faster flowing small particles might cause an inflow of particle in the high speed middle of the flow.

- Conservation of mass arguments might lead one to expect axial flow towards areas of higher acceleration and flow away from areas of higher deceleration.

The asymmetry in the flow, due to the granular nature of the particles, (see above) will favor an outflow at the bottom, particularly if there has been an inflow in the middle.

In other words, either one needs a variation in the axial flux between large and small particles or a varying axial flux as a function of x and a varying concentration of particles in the x-y plane. Radial segregation gives us the varying concentration in the x-y plane. The middle of the free surface effectively samples deeper into the flowing layer. This means that for the radially segregated state, there is a higher concentration of small particles in the middle of the flow than at the start or finish.

Particles flow towards higher concentrations of small particles in the middle of the flow, and they flow away at the top and bottom of the flow. Taking into account the higher number of small particles in the middle of the flow, this can lead to a net flow of small particles to areas of higher concentration of small particles, and large particles to areas of higher concentration of large particles. If this effect is large enough to overcome mixing, then segregation results.

In the following chapters, we will measure the surface flow properties of the banded state. We will experimentally test and compare each model in the following chapters (see outline of chapters in chapter 2).

Chapter 3

DYNAMIC ANGLE OF REPOSE

Most of the models use a concentration dependent dynamic angle of repose as a driving force for segregation. The dynamic angle of repose has been measured extensively in experiments and simulation, and differences between angles of repose of different particle types have often been linked to band formation. In order to compare our experiment with other experiments and these models, we present results from the literature on the measured dynamic angles of repose as well as our own measurements on the dynamic angle of repose for the systems used in our experiments.

3.1 Background

The most important question is how the dynamic angle varies with particle parameters. The dynamic angle of repose of a flowing material is related to the static angle of repose for that material at rest. The static angle of repose has been measured for different particle sizes and shapes. It was observed that the static angle of repose decreases with increasing particle size and increases with increasing particle non-sphericity for 10/16 and 22/30 sieved powder [77]. For small glass spheres, sizes ranging from 75 to 600 μm, the static angle was observed to also decrease with increasing particle size [78].

The dynamic angle of repose has been measured for a variety of experimental conditions. It is generally measured in quasi 2-D drums through transparent end-walls or by using magnetic resonance imaging. The height of the surface is extracted and is fit to a line. For high rotation rates where the free surface is not flat but has a characteristic s-shape, either an average is taken of the entire flow, the angle is measured at the mid-point, or at the steepest point of the flow. Often the steepest point of the flow is very near the mid-point of the flow. Using the angle at the midpoint of the flow tends to give a higher answer for s-shaped flow, but both give qualitatively similar results.

The dynamic angle of repose has been measured for a variety of particle types and for a variety of drum systems. It has been observed to increase with increasing particle roughness [32, 56]. Sand (high roughness) particles have much higher dynamic angles of repose than glass beads, and glass beads have slightly higher angles than steel. The variation of the dynamic angle with size in the literature can be confusing and sometimes gives conflicting results. We provide an experiment by experiment overview of the pertinent results:

- Ristow et al. [67] used glass balls (beads) of size 1.5 mm and 3.0 mm in an acrylic 7 cm diameter drum. They observed decreasing dynamic angle with increasing particle size above 15 RPM but identical angle below.

- Ristow et al. [67] used mustard seeds of diameter 2.5 mm and 1.7 mm in an acrylic 7 cm diameter drum. In this case, they saw increasing dynamic angles of repose with increasing bead size below 20 RPM and identical angles above

20 RPM.

- Hill et al. [26] used 2.85 mm and 0.5 mm glass beads in a 13 cm diameter Plexiglas drum. They observed decreasing angle of repose for increasing particle size above 5 RPM and identical angles below.

- Khakhar et al. [56] used glass and steel balls of similar size and varied the drum diameter between 4 and 16 cm. They saw a decrease in angle of repose with decreasing drum diameter or increasing particle to drum diameter. This is similar but not the quite the same as seeing a decrease in dynamic angle with increasing particle size.

- The Morris group [25, 73] used 75-212 μm and 300-710 μm sand in a 2.7 cm diameter drum. They saw a decrease in the angle of repose with increasing particle size.

- Rogers and Clements [32] used glass beads of size 0.65 mm and 0.50 mm. They found a 0.5 degree difference in the angle between the two sizes of glass beads.

- Hill et al. [79] used a mixture 2 mm and 4 mm fluid filled spheres in a 7.5 diameter acrylic drum. When rotated at 15 RPM, the dynamic angle decreased with increasing concentration of large particles. When rotated at 30 RPM, the dynamic angle did not change with concentration of large particles

For most experimental conditions, the angle of repose has been seen to increase with decreasing particle size, although the opposite is seen in some cases [67]. Often the dependence on particle size depends on the rotation rate: the particles have

similar angles at some rotation rates, but the angles diverge as the rotation rates increase (or decrease). In many cases this divergence has been linked to the start of band formation [26, 67].

The reason for the differences in the dependence of observed angles on particle size is not completely clear, but the details of the flow are affected by a variety of factors. The type of material that the drum is made out of might play a role, as rougher walls would tend to pull the particles to a higher starting point before avalanching. The absolute diameter of the drum might also be important as the ratio of particle diameter over drum diameter does not always provide good scaling in these experiments. The different methods of measuring these angles could also play a significant role.

The scaling dynamic of angle of repose has been studied as a function of rotation rate. Rajchenbach [28], observed that the dynamic angle of repose increased with R^2 for low rotation speeds, whereas Dury et al. [67] and Yamane et al. [80] observed a linear increase with rotation speed for a range of particles. Orpe and Khakhar [56] also found a near linear increase of dynamic angle with rotation rate. Khosropour et al. [81] considered a wider range of rotational speeds and obtained a slower than linear increase in b with rotational speed.

In experiments and simulations of 3-D drums, Dury et al. found that the dynamic angle of repose at the endplates was 4-5 degrees higher than in the rest of the drum [67]. The angle decayed exponentially with the distance from the endwalls. Dury et al. determined a characteristic length for the decay of the angle away from the endwalls and found that it scaled with cylinder radius.

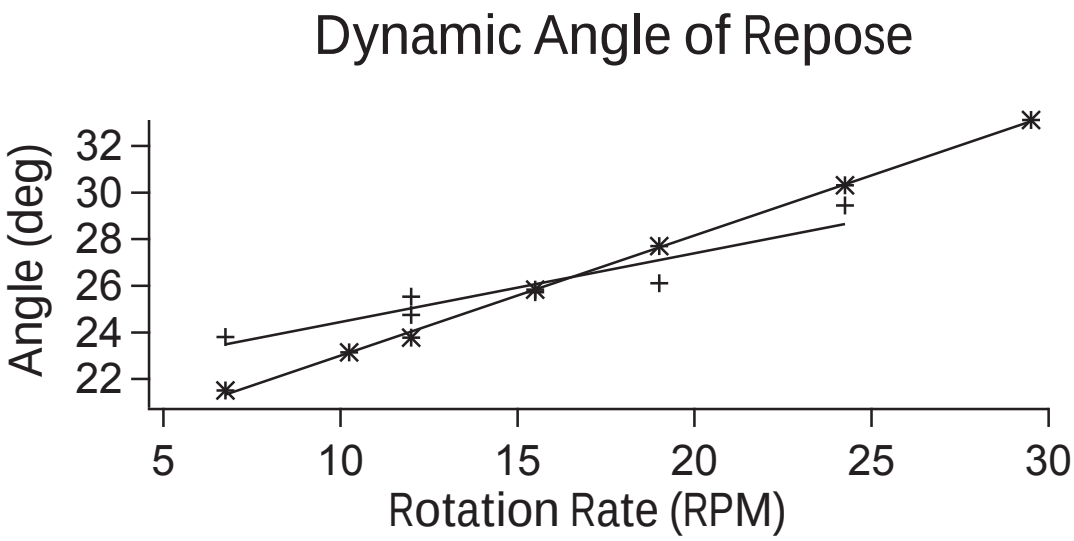

Figure 3.1: Dynamic angles of repose plotted against rotation rate for 1/16" (stars) and 1/8" (crosses) steel balls in a 10 cm diameter drum. The solid lines are linear fits to each curve. Unfortunately, error bars are unavailable for this plot.

3.2 Dynamic Angle vs. Rotation Rate

We were able to measure the dynamic angle of repose through the transparent endplates of our drum by imaging the side flow with a color camera. We extracted the free surface by eye and fit to a line. Because the angle is greater right next to the wall, the free surface away from the wall was higher and showed up in our imaging. This made it unclear how to extract the free surface on the lower half of the flow and we only used the top half of the flow in our fit. In figure 3.1 we plotted the dynamic angles of repose for 1/16" and 1/8" spherical steel balls as a function of rotation rate. A linear fit has been applied to the angle versus rotation rate for each particle size. The sensitivity of the angle fit to the error is significant, and there is a high likelihood of systematic error due to methods of finding the free surface

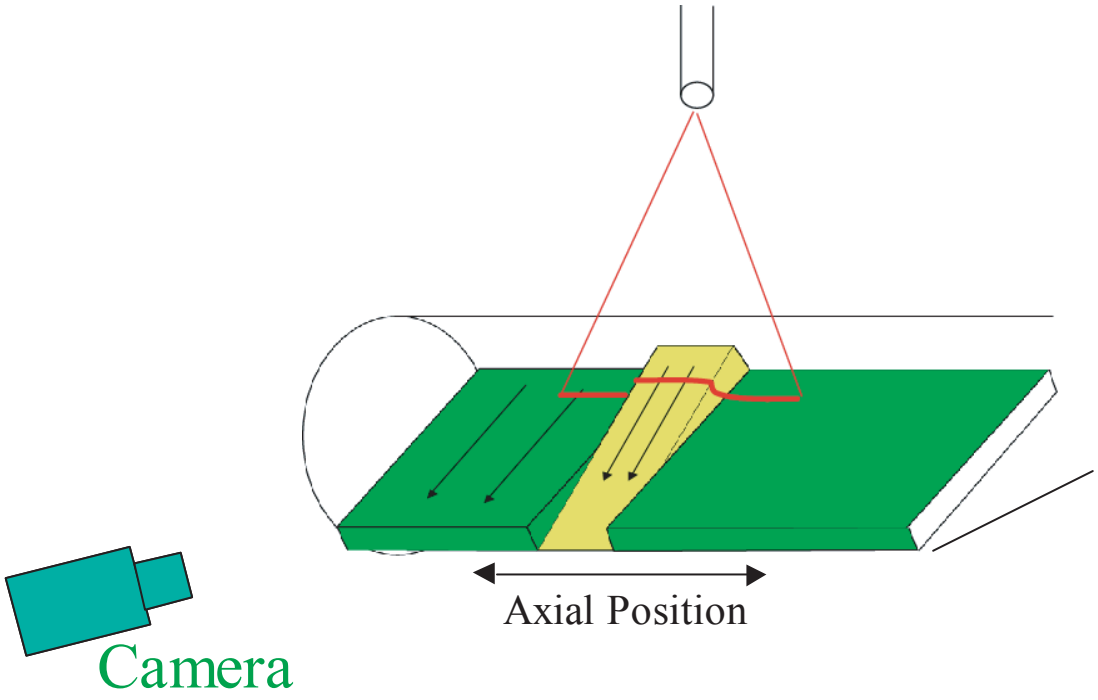

Figure 3.2: Experimental setup for measuring the free surface with a laser line.

(probably ± 0.5 degrees), but qualitative comparisons can be made. It is immediately noticeable that for low rotation rates, the smaller particles actually have a lower angle of repose than the large particles. At around 16 RPM, the dynamic angles for the two particle types cross and above that rotation rate, the smaller particles have a larger angle of repose. A little below 7 RPM, the lowest rotation rate plotted, the flow is no longer continuous and flows in discrete avalanches.

3.3 Laser Line Measurements

In order to directly measure the surface height and surface angle of the granular mixture in the banded state away from the endwalls, we used a laser line. This

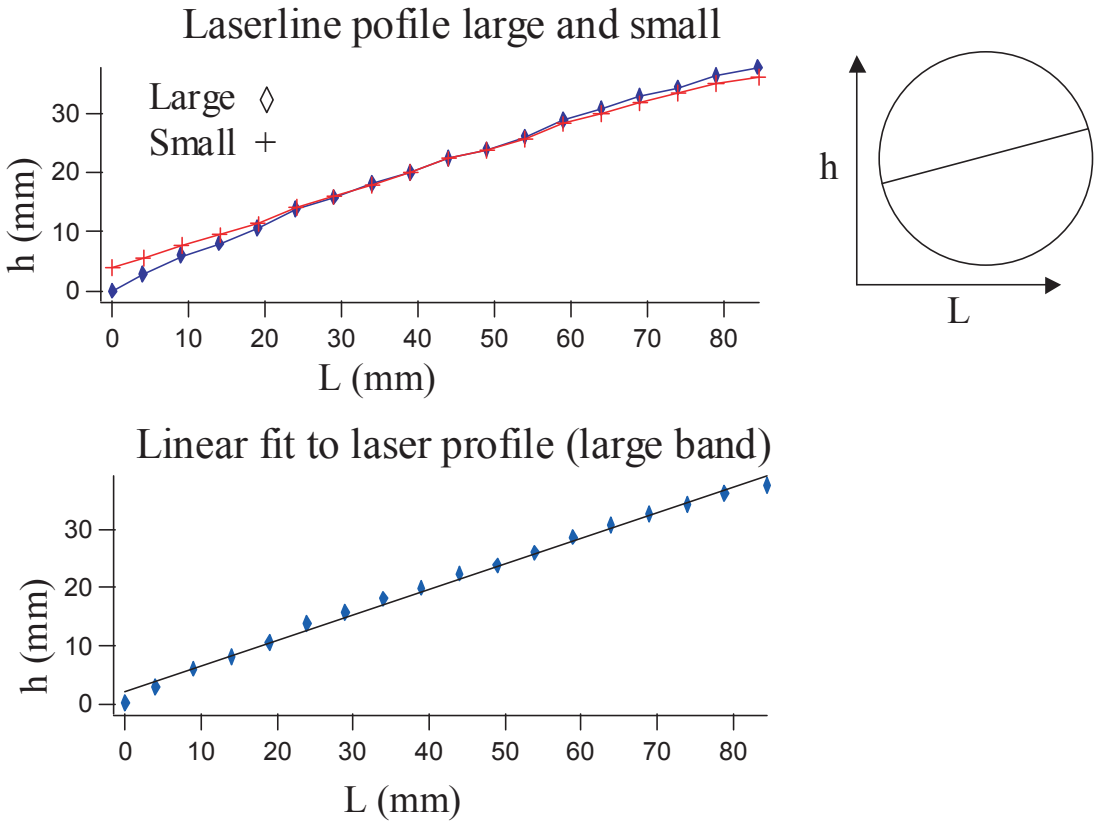

Figure 3.3: Height profile of the flowing surface as measured by a laser line for steel beads rotated at 12 RPM. The top plot shows a comparison of the profile for 1/8" (crosses) and 1/16" (diamonds) steel beads. The bottom plot shows a sample linear fit to the profile for the large particles. Although it was extremely difficult to accurately determine exact error bars in this experiment, they were generally on the order of the symbol size.

method has been used before in a rotating drum by Khan et al. [73] and in avalanche experiments by Losert et al.

We illuminated the sample from above with a laser line (see figure 3.2), and took images with a high resolution color camera that was level horizontally with the drum. Observed from the side, height differences can be detected as vertical deflections of the laser line. Normally painted particles could be used, but reflective steel spheres gave the best results.

A 90 degree difference in orientation between the laser line and the camera gave the best possible resolution of the surface height differences. Multiple images were taken for each position of the laser line and the average center was calculated using image analysis. We slowly scanned in the x direction to obtain the profile down the flowing layer. For one measurement, the scanning took about 5 minutes, and so our technique is only accurate if the system does not change significantly in that time.

Knowing the complete geometry of our setup, we can create a 3-D picture of the free surface. The dynamic angle of repose is extracted by fitting the entire flow to a line and taking the arctangent of the slope. Figure 3.3 shows the laser line profiles for 1/16" and 1/8" steel balls in the banded state (we will discuss these in detail below). We fit the profiles to a line (figure 3.3) and for the low rotation speeds we are considering here, the flow profile showed only slight deviations from linearity.

To characterize our samples, we first measured the dynamic angle of repose for monodisperse samples of 1/8" and 1/16" steel beads. We measured these from

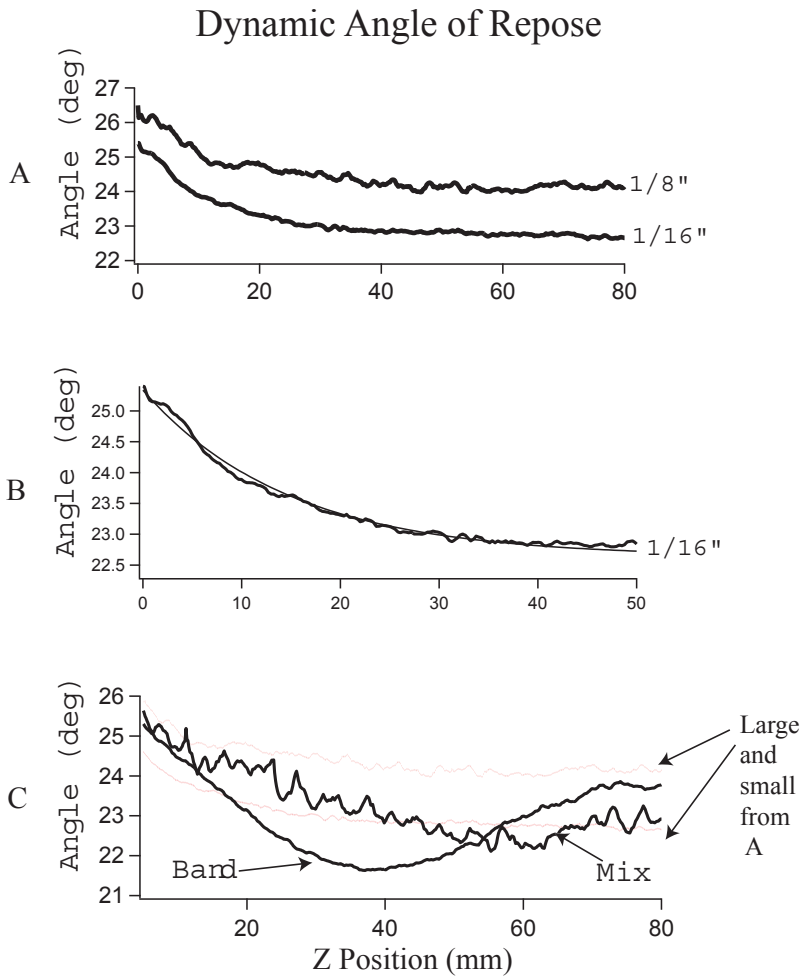

Figure 3.4: Dynamic angles of repose at 12 RPM from the sidewalls and inward. The top plot (A) gives the dynamic angle of repose for 1/16" (lower solid line) and 1/8" (higher solid line) steel balls. The middle plot (B) shows an exponential fit to the 1/16" steel balls. The lower plot (C) compares the monodisperse angles with the angles of a mixture of the two particle types, in the initial mixed state and in the banded state.

the left side wall to about 8 cm into the drum. This gave both the wall effects and the monodisperse steady state dynamic angle far from the wall. We can see from fig. 3.4a that the large particles have a dynamic angle of repose about 1.5 degrees higher than the small particles. The angle near the wall is a little over 2 degrees higher than the angle away from the wall, as opposed to the 4-5 degree difference seen in simulations and experiments by Dury et al [67]. When we compare our dynamic angles of repose with our measured angles from the side we find good agreement.

In figure 3.4c, we plot the angles near the wall for binary mixtures of 50% 1/16" and 50% 1/8" steel beads in the initial mixed and in the banded states. Because a single scan of the laser line down the entire flow took around 4-5 minutes, it represents an average of the state of the drum during that time. The initial mixed state therefore represents the radially segregated state during the first 5 minutes of rotation. Fortunately, mixtures of steel beads at these rotation rates took a long time to form bands and the state of the sample did not change significantly over the 5 minutes of the laser scan.

We notice some interesting properties of the initial mixed state and the banded state near the endwalls. First, the initial mixed state angle starts out at the angle of the large particles near the wall and goes slowly to the angle of the small particles far from the wall. It is possible that this is a result of the long time it took the angle to be measured and represents the beginnings of segregation–of increasing concentration of large particles right next to the wall. Second, the banded state near the endwalls starts out with a high angle (large particle band) near the endwall. It then drops

below the angle for monodisperse small particles (small particle band) and goes back close to the angle for large particles. It is interesting that the small particle band has a dynamic angle lower than the dynamic angle for the monodisperse mixture.

In figure 3.5, we have plotted the angle of flow across a band of small particles in the center of the mixture. Similar to a band near the wall, the angle of flow is lower by about 2 degrees across the band of small particles. Our fitting method has a distinct effect on the resulting difference in angles: If instead of fitting the entire surface, we find the angle by fitting only the middle of the flowing layer, then the difference is somewhat lower, around 1-1.5 degrees. The dynamic angle of repose around a small particle band is what would be expected from the monodisperse measurements. The angle is lower over the band of small particles. The dynamic angle does not immediately go to the angle for the large particle at the edge of the small particle band. Instead, it slowly transitions from one angle to the other, with the lower angle of small particles extending into the band of large particles. This is an indicator that the concentration of small particles does not immediately drop to zero at the edge of the band, but that the core of small particles extends into the large particle band.

The most prominent feature in the axial velocity is the in and out axial flow at the edges of the band of small particles. If we look at the left edge of the band, we see a small positive (right-hand) velocity at the start of the flow, a larger positive velocity in the mid range x positions, and a very large negative (left-hand) velocity at the end of the flow. The opposite is seen at the other edge of the band so that there is an axial velocity into the band at the middle of the surface flow and a large

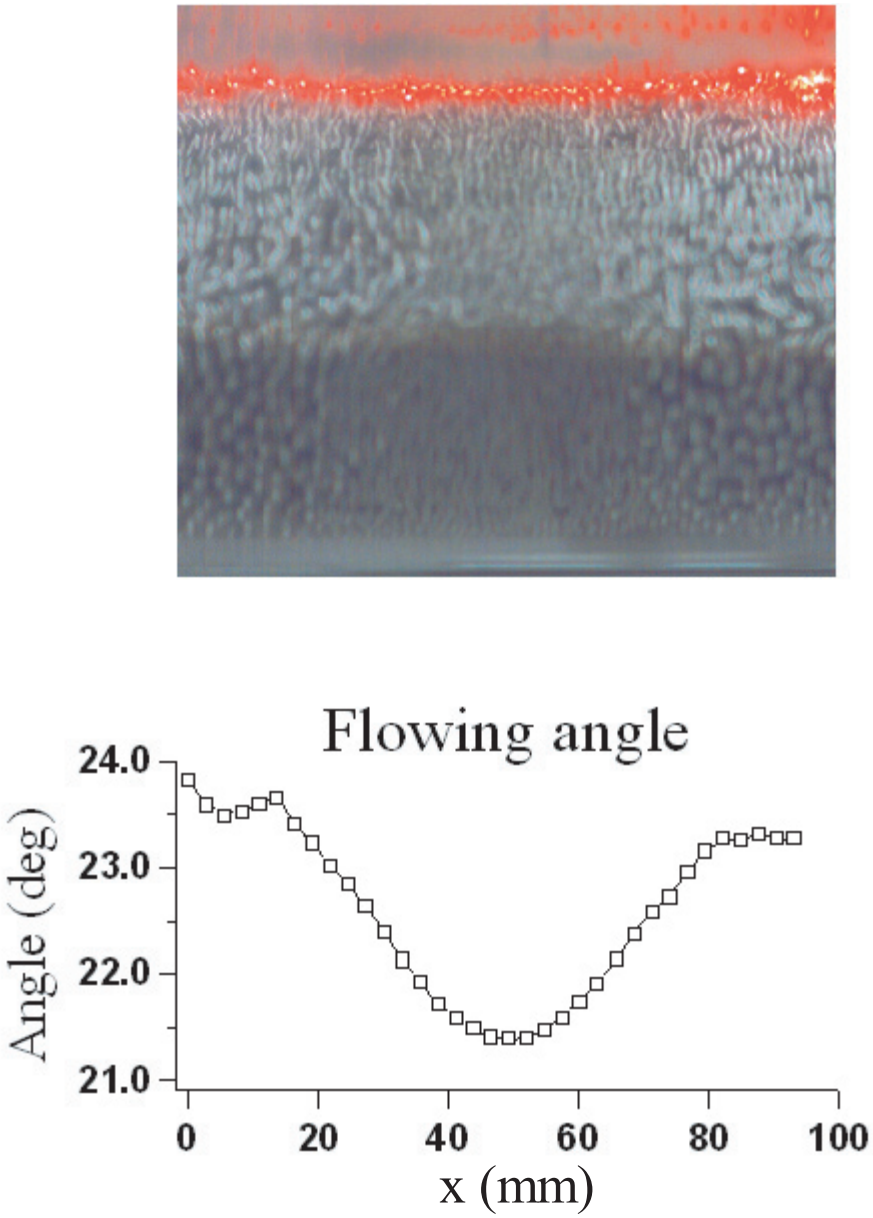

Figure 3.5: Top: An image from the laser line scan of the banded state. Bottom: The dynamic angle of repose of the flowing particles as a function of position in the banded state. The top and bottom figures are aligned so that their x axis are equivalent.

axial velocity out of the band at the very bottom. At the top of the flow, there is a slight axial flow of particles into the small particle band, but this is small compared to the axial flows at the middle and bottom.

Chapter 4

HIGH SPEED IMAGING

4.1 High Speed Imaging

The physical explanations for axial band formation revolve around the flow of the free surface of the granular materials. Each model has a different description of a flow at the free surface that drives band formation. Because of contradictions in the different models, many physical questions remain unanswered: How do the particles move axially to allow pattern formation? Do the small and large particles have different mobilities or do they flow homogeneously? Does the flow go in the direction of steepest descent and does this cause band formation? Do velocity gradients play a role in band formation? We now attempt to answer these questions by directly measuring the free surface flow of particles in the banded state of a rotating drum.

We analyze individual particle motion and compute average velocities using direct imaging. We imaged the top surface of the flow with a high speed high resolution CCD camera. We imaged the radial flow from the side through the transparent endplates. We took images at 1000 frames per second, with a resolution of 1280 by 512. The system was illuminated by a single bright light so that each particle reflected a single bright spot. After some image analysis these spots were identified and tracked and particle positions and velocities were extracted by tracking using particle tracking software originally developed by Grier and Crocker in IDL

(Interactive Data Language).

Only the surface can be imaged by our camera. In these experiments, the camera has a depth of field on the order of centimeters. Because it images only reflected spots, the camera cannot distinguish between particles right at focal point from particles a few particle diameters above or below from the focal point. When the density of the particles is lower, the camera will pick up particles in the top layer as well as particles deeper in the flow. We find that experimentally, for monodisperse samples, the image always contains the same number of particles, no matter what the actual density of the mixture in the area being imaged by the camera.

Because we cannot tell from the images what the density of the sample is, we define the free surface of the mixture as the area that is seen by the camera. When appropriate we will also include areas directly beneath this free surface in our discussion of the results, though we cannot image particles motion in such subsurface layers.

We will present data taken for steel balls of diameters 1.59 mm (1/16") and 3.18 mm (1/8"), since steel beads are more spherical and monodisperse, and can be more accurately tracked in images. We have published or are preparing to publish much of this data [75, 47, 82, 83]. Some of the main results were also verified for glass beads of size 0.5 mm and 1.0 mm for comparison to our earlier works described in chapter 5 and other published results. By measuring the spot intensity of each particle we can distinguish small and large particles on the surface of the granular flow. The accuracy of distinguishing particles is decent, with misclassification of $3-5\%$: meaning that $3-5\%$ of large particles are tracked as small particles and

$3-5\%$ of small particles are tracked as large particles. The misclassification here will cause any differences found by comparing particle motion for the two particle sizes to be underestimated by about 10% for a mixture with $30-70\%$ small particles [84]. The error caused by misclassification will be much greater as the relative percentage of one type of particle goes down (40% underestimation if we only have 10% of one particle type in the image). Thus we focus particle size dependent results on regions where both particle types are present in comparable quantities.

The correct scale on images for each experiment was found by measuring the distance in pixels from the bottom of the drum to the top of the drum in a single image. Because we know the inside diameter of the drum to be 10 cm, this gave the scaling of pixels per millimeter. In experiments where this was not possible because the camera area was zoomed in too far to see the entire drum, either a ruler was placed in the image on the outside of the drum or individual particle diameters were measured and compared. The last tended to underestimate the pix/mm and was only used as a last result.

Depending on the experiment (and the camera zoom) the scale was usually between 3 and 5 pixels/mm. The camera lens and the lens shaped plastic top of the drum provide some distortion in the resulting image, and though these were not corrected for, the distortions are minimal compared to the patterns we observe. Because we use multiple particle sizes, and it is not yet known how various properties scale with particle size and rotation rate, we will present our results in dimensional units (as opposed to non-dimensionalizing our plots).

4.2 Downhill Flow Velocities

We measured the downhill flow velocities for binary mixtures of 1/16" and 1/8" steel beads using the particle tracking methods as described above. To first compare particle motion in our mixture to past work, we imaged the drum from the side in the radially segregated state. The camera was aligned as well as possible so that the horizontal was parallel to the flowing surface of the drum (as shown in figure 2.2 in chapter 2). These particular experiments were done at 7 and 24.5 rotations per minute (RPM). At 7 RPM, the surface was flat and so alignment of the camera with the drum was simple. At 24.5 RPM, the surface had a distinct "s" shape (figure 2.1 in chapter 2) and so alignment was done by eye to be as close as possible to straight on average. All of the flowing layer from left (ie. top or start of the flowing layer) to right (ie. bottom or end of the flowing layer) was included in the image as well as most of the way down into the bulk rotation.

The scale on the experiments viewed through the transparent endplates was 7.9 pixels/mm. To get good spatial resolution over the thin flowing layer we divided the image into sections 5 pixels by 5 pixels (0.63 mm by 0.63 mm) and averaged our particle tracking velocities in each of these. We then averaged these over the middle (in x) third of the drum to get good statistics. In figure 4.1, we plot the downhill velocities versus the depth below the surface (y). The results agree with the results found the literature [64, 65] and we see a linear decrease in velocity in the flowing layer with increasing depth and an exponential transition to bulk rotation with the drum. The slope is constant from small to large particles, with little or no kink in

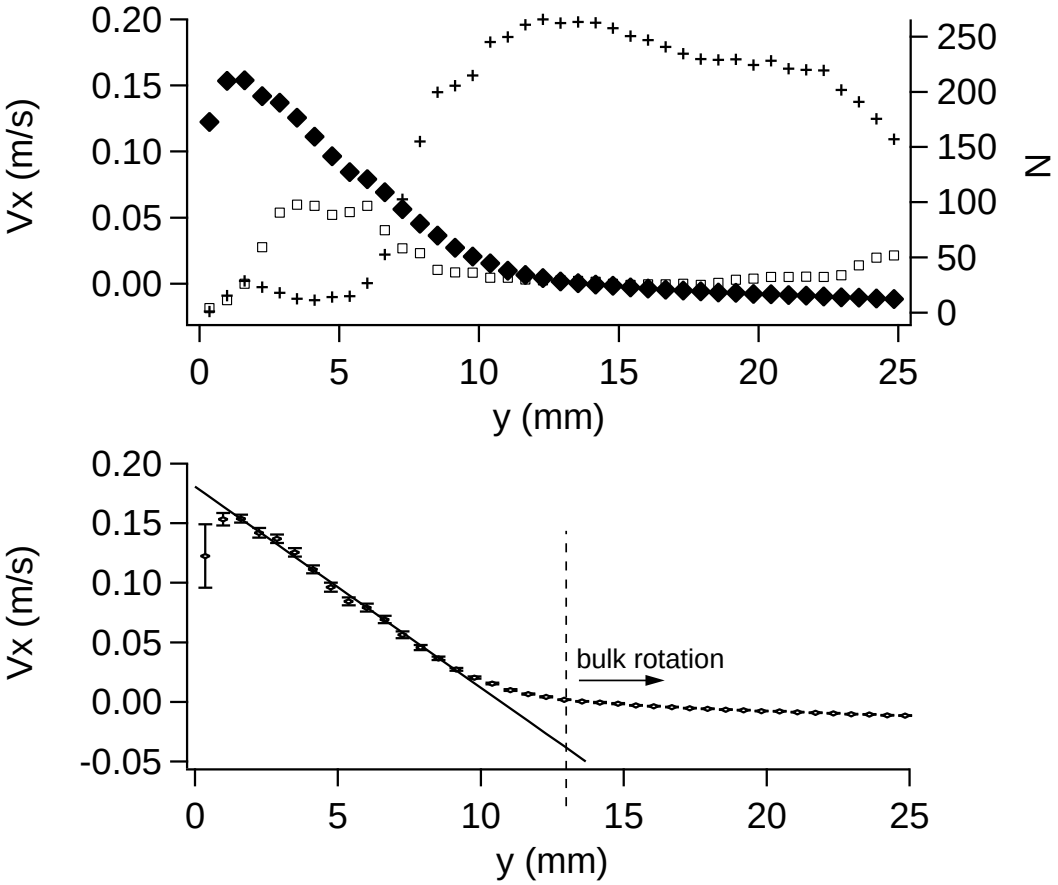

Figure 4.1: Downhill velocity, v_x, as a function of depth in the flowing layer, y, as viewed through the transparent endplates. This was a binary mixture of 1/16" and 1/8" steel beads in the radially segregated state rotated at 7 RPM. This is the same mixture as that shown in figure 2.2. The top plot shows v_x (diamonds) plotted with the number of small (crosses) and large (triangles) particles. The arrows indicate which vertical axis the data corresponds to. The bottom plot shows a linear fit to v_x.

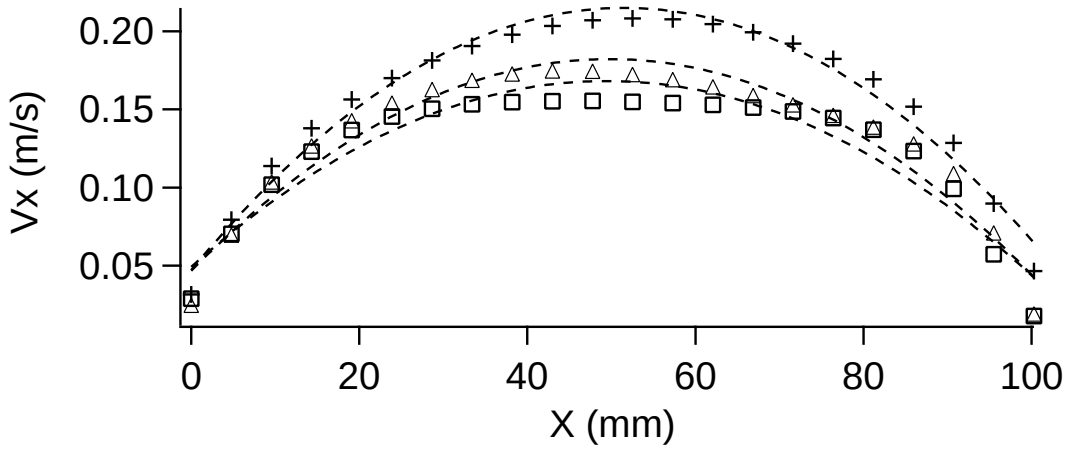

Figure 4.2: Downhill velocities, v_x, as a function of x, for a binary mixture of 1/16" and 1/8" steel beads rotated at 12 RPM. Average velocities are plotted for particles in a small particle band (crosses), particles in large particle bands (squares), and the initial radially segregated state (diamonds). Dashed lines represent polynomial fits to each curve. Error bars for this data are smaller than the symbol size in the graph.

the velocity profile. We fit the slope to a line (solid line in figure 4.1), which gave a slope of -0.0169 1/ms and an intercept of 0.54 m/s.

In order to study the flow properties of particles during band formation we imaged the drum from the top, through the cylindrical walls. We aligned the camera with the cylinder so that the horizontal camera axis was aligned with the cylinder z axis and the particles flowed in the positive x direction. To compare with the laser line measurements, the drum was rotated at 12 RPM. The surface at this rotation rate is reasonably straight.

We followed the evolution of the banding pattern, including the initial transient, by taking image sequences every 2 minutes for about an hour. The first image sequence was taken after only 5 seconds of rotation (1 rotation). When necessary,

we stopped the drum while the data was being saved. Each time the drum is started a transient occurs where particles are brought to an angle higher than the normal dynamic angle of repose before flowing down and stabilizing at the dynamic angle of repose. To mitigate the effect of this we allowed the drum to rotate for a minute before and after taking images (of course, the stopping and starting of the drum could still have affected the band formation). Later on in the experiment, we increased the time between sequence acquisition, and we allowed the flow to run uninterrupted between image sequences.

In many of our plots, we plot data for the small particle band and for large particle bands. The small particle band refers to averages over the right-hand small particle band in figure 4.3 from its left edge to its right edge. The large particle band refers to the area from 60 pixels (14.3 mm–about 9 small particle diameters) in from the right side of the left small particle band to 60 pixels before the left side of the right small particle band as well as the area of large particles just to right of the small particle band.

We divided the image and particle tracking results into sections 20 pixels by 20 pixels (4.77 mm–about 3 small particle diameters). We plot the downhill velocities, v_x, for the initial mixed state (triangles), for a small particle band (crosses), and for a large particle band (squares) in figure 4.2. The initial mixed state was averaged over 5 runs from $t = 5s$ to $t = 480s$ to get good statistics, and radial segregation will have already happened. The large and small particle banded velocities were averaged over 7 runs from $t = 2760s$ to $t = 4765s$. During this time, the large and small particles banded state was stable over several hundred drum rotations,

though further coarsening would have occurred on longer timescales. The error in these averages is much lower than the size of the symbols in the figure.

The scaling given in chapter 2 [85, 24] predicts a polynomial dependence of the velocity on x and we fit polynomials to the velocity curves (dashed line). The smaller particle's velocity fits nicely with its peak slightly later in the flow. At the z center of the small particle band, the peak in v_x is even sharper. The large particle's velocity does not fit as well as it tends to plateau, with a long, flat peak. The small particles flow at significantly higher speeds than the large particles at all points down the flow. The velocity profile of the mixed state flow velocity is in between the magnitude of the small and large particle band flow velocities, indicating that the initial mixed state has higher velocity gradients than large particle bands.

In this run, the band we are looking at formed very slowly, taking 3500 seconds (about 1 hour) to form a steady state band. In figure 4.3 we have plotted a time sequence of the x velocity versus axial z position. Corresponding images from some of the data sets are shown for reference and visualization purposes. The velocities are averaged over the middle third of x to get good statistics on the peak flow velocity while still averaging over an area of somewhat constant v_x. Almost at the very start, we see a slight increase in the velocity in the area where a band is forming, indicating the presence of an increased concentration of small particles, and a large radial core. At this point there is also a slight increase in the number of small particles on the surface, but it is barely visible.

In this figure (figure 4.3) we can also see the long tales of the particle velocities. The increase in velocity extends beyond the edges of the visible small particle band,

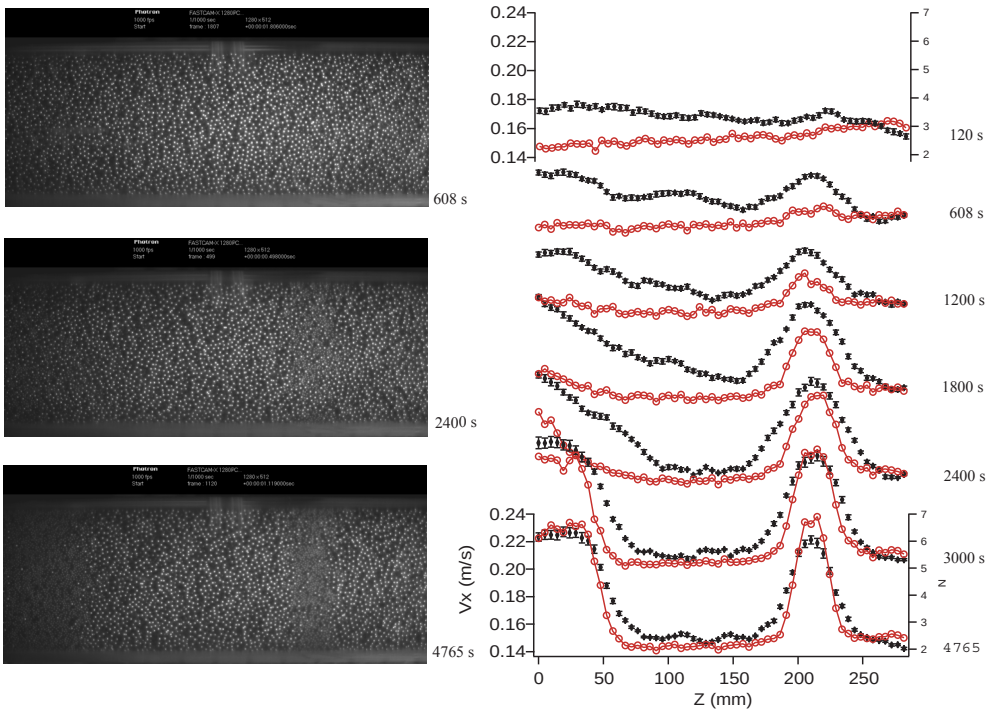

Figure 4.3: v_x as a function of z as it evolves in time during the band formation. The images on the left are frames from the camera corresponding to 10 min., 40 min., and 1 hour 19 min. The velocities are plotted in black with error bars and the lighter (red) connected circles are the number of particles. Although error bars are shown only for velocities, they are approximately the same size for the number of particles.

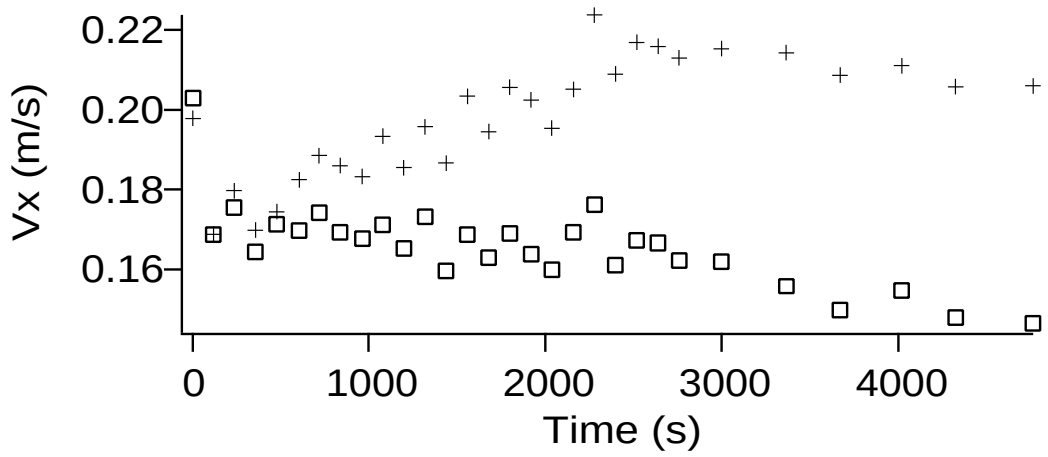

Figure 4.4: v_x of particles in a small particle band (crosses) and in a large particle band (squares) as a function of time. The actual error bars here are less than the size of the symbols, but there is significant systematic error from run to run possibly having to do with periodicity in the width of the band as the drum rotates.

indicating the extent of the radial core. The laser line measurements earlier showed that the dynamic angles of repose show similar tails. The left hand band of small particles is much wider. Around 1800 seconds into the run, this band influences the velocities 75 mm (about 25 large particle diameters) from where it will later form.

The velocity peaks tend to get tighter (thinner) and higher as time increases and the bands become more distinct. We measured the area under the banded state and found that it was roughly constant, although the area for the right-hand bands increases with time with a maximum area at around 3000 s.

In figure 4.2, the ratio in peak velocities between large and small particles graphs was approximately 1.35. Because the velocities reach a maximum generally in the center of a band, and we averaged over the entire band, the ratio in maximum small band velocity and minimum large band velocity will generally be larger. In

figure 4.3 the ratio of maximum small velocity to minimum large velocity in the final banded state is 1.467. Both of these numbers are close to 1.41 which is the particle size scaling expected by experiments on monodisperse samples [56]: $\sqrt{d_l/d_s}$ where $d_{l,s}$ is the diameters of the large and small particles respectively.

We also plot the velocity in the large and small particle band as a function of time in figure 4.4. The error over a single measurement is low, but there is significant error from run to run. This error may be caused by the starting and stopping of the flow or more likely by high frequency oscillations in the band width. These that can clearly be seen by eye following the band through a few rotations and are similar to those seen in simulations in the literature [44, 86]. They have a oscillation period on the order of one rotation of the drum.

The velocities for the small particle (large particle) bands appear to increase (decrease) linearly as a function of time. If the velocities are proportional to the concentration of small particles, then the concentration increases linearly over time as well. Note, that this is the concentration of particles over a constant z, from z_{left} to z_{right}, the left and right sides of the *final* small particle band. The velocity increases from about 0.175 to about .21 in about 2000 s giving an approximate slope of $1.75 \times 10^{-5} m/s^2$.

We studied the effect of varying the rotation rate on the properties of the already formed stable band. We stopped the motor in between changing the rotation rate and allowed the mixture to run for 1 minute at the new rotation rate before and after taking an image sequence. This has the advantage that the same banded state can be compared for different rotation rates. On the other hand, granular materials

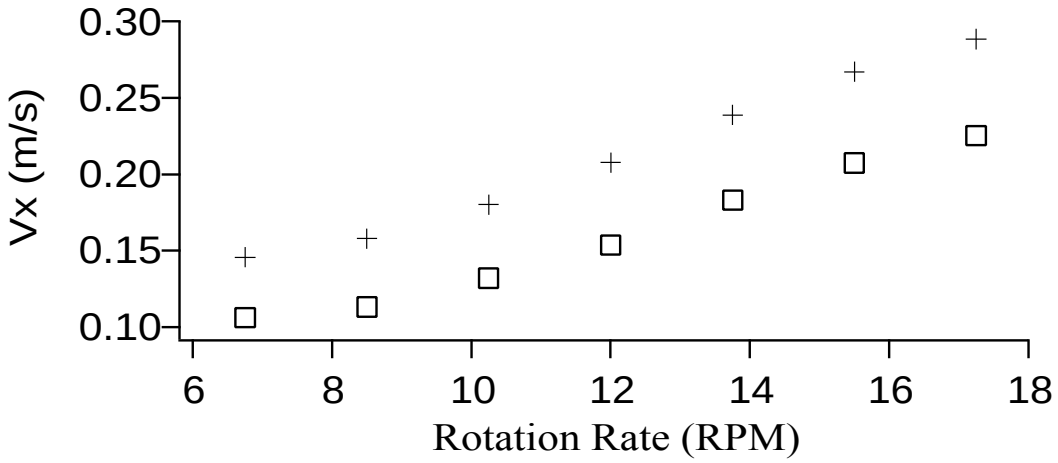

Figure 4.5: v_x versus rotation rate for particles in a small particle band (crosses) and particles in a large particle band (squares). The error bars are smaller than the size of the symbols.

often exhibit memory effects and the dynamics of the flow might have been different–even for a similar looking band–if we had started the drum at another rotation rate. We do not know if this banded state is stable at the other rotation rates.

The variation of the x velocity versus rotation rate for particles in small and large bands is plotted in figure 4.5. Above about 10 RPM, the velocities increase linearly with rotation rate, as expected by the scaling results of Ottino [24] et al. (see discussion in chapter 2).

We plot the derivative of the velocity with respect to x and t in figure 4.6. Alexander et al. [57] found the acceleration to be an important parameter in their scaling arguments. Our accelerations ($\partial_t v_x$) show symmetric acceleration profiles, with the larger particles have a longer area of low acceleration (flattened velocity peak–see figure 4.2). Comparing to Muzzio et al.'s data, increasing the size of our particles compares to decreasing the rotation rate of theirs. This suggests a scaling

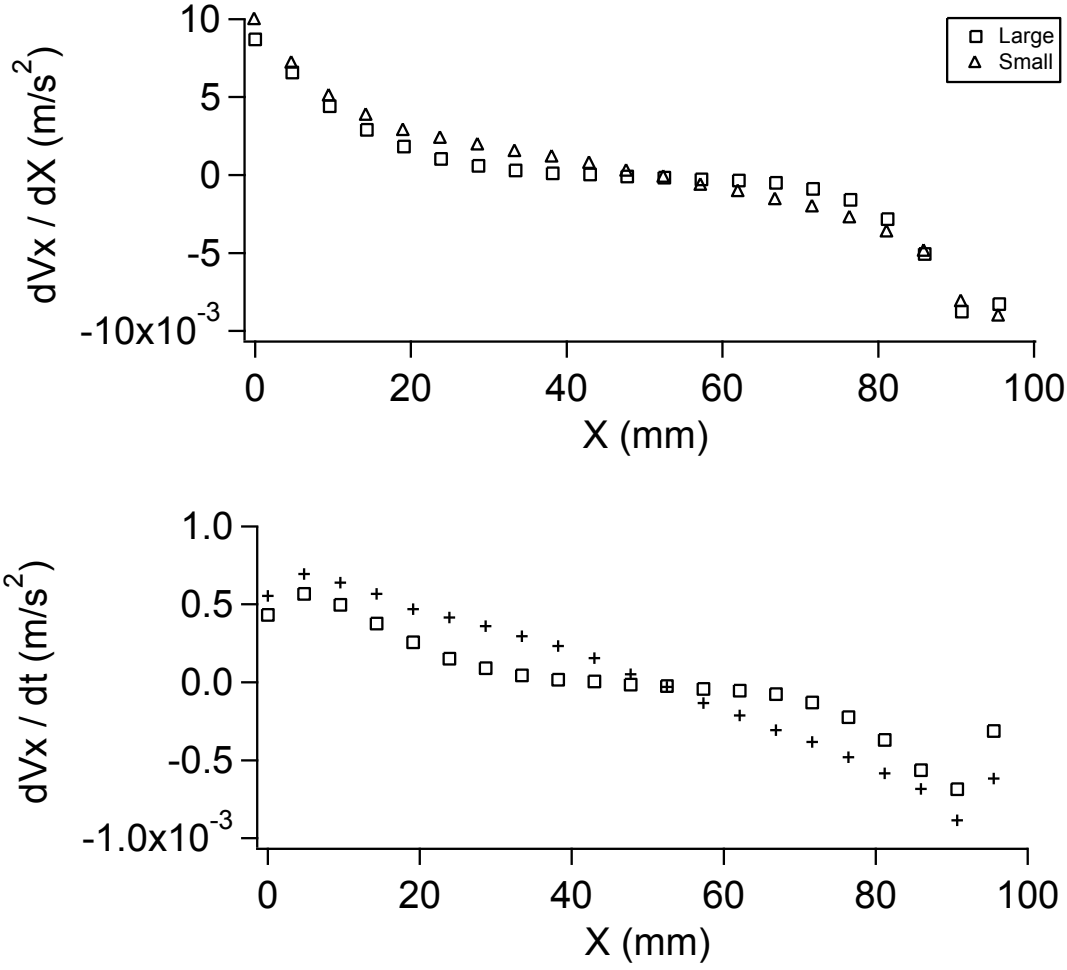

Figure 4.6: Top: $\partial_x v_x$ as a function of x. Bottom: The acceleration, $\partial_t v_x$, as a function of x. Once again, the error bars are in general on the order of the symbol size.

parameter of the size of the particles that could be introduced. The derivative of v_x with respect to x, or $(\partial_t v_x)v_x$, relates nicely to the effective stretching or thinning $(\partial_x \rho)$ of the flowing granular layer. Thinning or the effective decrease in density (assuming 1-d flow) can be calculated from $\Delta_x \rho = -\frac{C_1}{v_x^2 \Delta_x v_x}$, where C_1 is a constant. The differences in the magnitude of (dv_x/dx) for the small particles and large particles are the largest at around x=25 mm and x=75 mm (in figure 4.2, this is where the velocities begin to diverge significantly).

4.3 Axial Velocities

All of the models for axial segregation assume that the important dynamics happen in the top surface of the flowing material. This intuitively makes sense because the particles are less dense near the top surface and are not held down by particles above them. They are more free to move and they are moving faster downhill. In experiments in the x-y plane, the y velocity fluctuations have been seen to be higher near the surface of the flowing layer [24] (ie. near y=0).

Using this assumption, segregation requires an axial (z) flow of particles on this top surface. The differences between each model are sometimes subtle, but always involve this axial flow. Many of the models predict axial flow in the direction of steepest descent and differences in axial mobility of the different particle types. We now compare our surface measurements to those and other model assumptions.

Because of the errors in distinguishing large and small particles, it is difficult to separately measure the large and small particle drift. Calculations for one type of

particle in the band of another type are very unreliable. The only way to distinguish between the large and small particle band would be right at the edge of the band, and the number of particles that would apply here would be few, as the band edges are pretty distinct. In the transient, when the band is only partly formed, the velocity is too small compared to the error to distinguish particles. The concentrations depend on position and the finite size of our averaging sections also complicates the issue and so we choose not to attempt to distinguish between particles for the z velocity.

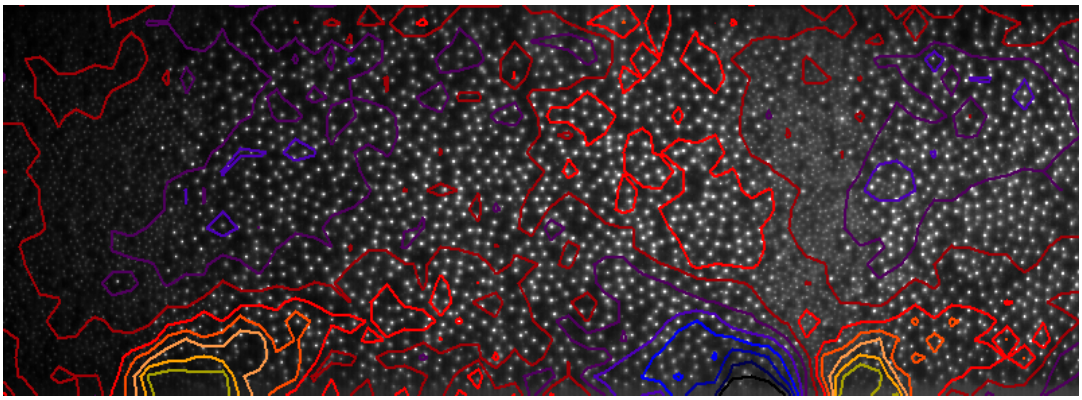

Figure 4.7: Contour plot of v_z in the banded state. Bright (orange) contours represent positive (right) axial velocity. Dark (blue) contours represent negative (left) axial velocity. The darkest and brightest contours represent -0.02 and +0.02 m/s respectively.

The axial (z) velocities are an order of magnitude lower than the downhill (x) velocities. In order to visualize the axial flow of the particles in the banded state, we overlaid an image of the banded state at t=4765 s with a color contour, shown in figure 4.7. Dark (blue) contours represent negative (left-hand) axial velocity and bright (orange/yellow) contours represent positive (right-hand), axial velocity. The brightest and darkest contour lines represent numbers near +0.02 m/s and -0.02

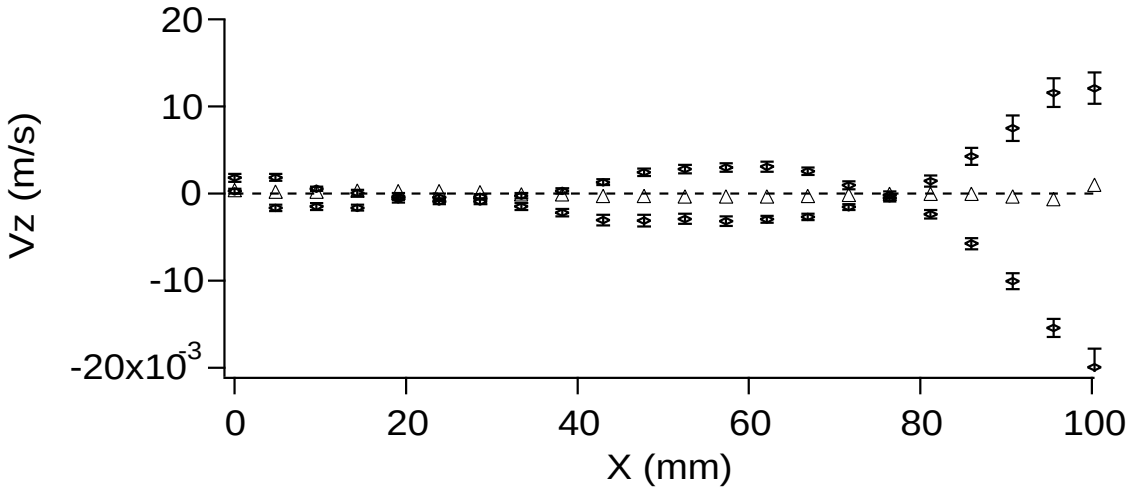

Figure 4.8: The axial velocity, v_z, as a function of x averaged over sections 60 pixels by 20 pixels to the left and right of the small particle band. The triangles represent the initial v_z averaged over the entire image.

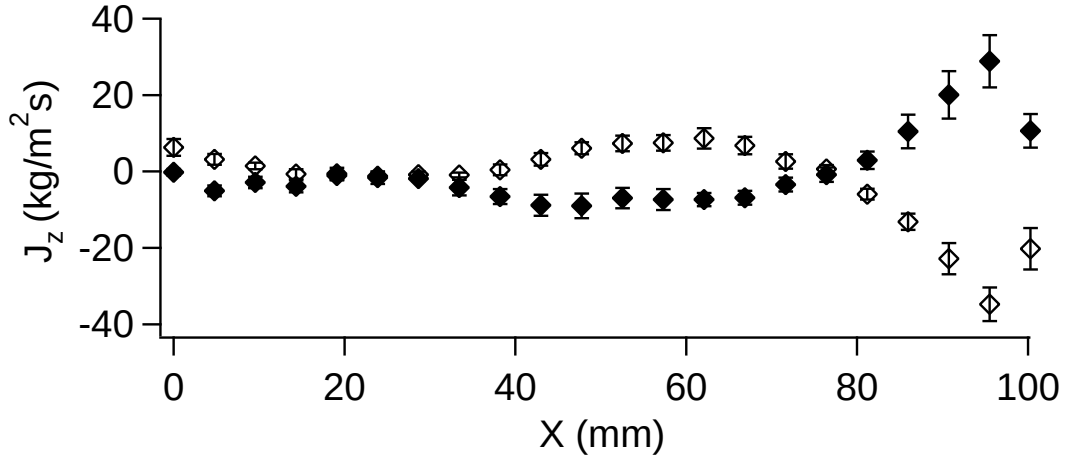

Figure 4.9: The axial current, j_z, calculated from $j_z = (Nm_i v_x/\Delta x)/Area$, as a function of x. The current was averaged over sections 20 pixels by 20 pixels to the left (hollow circles) and right (solid circles) of the small particle band.

m/s respectively. A plot of the drift at the left and the right edges of the band is shown in figure 4.8. We averaged over an area 60 pixels wide (3 sections) in z at the visible edge of the each band.

The most prominent feature in the axial velocity is the in and out axial flow at the edges of the band of small particles. If we look at the left edge of the band, we see a small positive (right-hand) velocity at the start of the flow, a larger positive velocity in the mid range x positions, and a very large negative (left-hand) velocity at the end of the flow. The opposite is seen at the other edge of the band so that there is an axial velocity into the band at the middle of the surface flow and a large axial velocity out of the band at the very bottom. At the top of the flow, there is a slight axial flow of particles into the small particle band, but this is small compared to the axial flows at the middle and bottom.

The current $d\rho/dt$ can be calculated:

$$j_z = \frac{Nmv_z}{Adx} \tag{4.1}$$

where j_z is the density current, N is the number of particles, m is the 2-D mass of a given type of particle, and the area, A, is $\Delta z \Delta x$. The resulting density current j_z is plotted in figure 4.9 at the left and the right edges of the small particle band. The current is similar to the axial velocities as expected. Although the currents look symmetric around their middle, the flux is skewed in the negative direction and there is a net outward flux (see table 4.1). There may also be axial flow underneath the top surface layer but we expect that it will decrease quickly as a function of depth

Table 4.1: Total Fluxes

Total flux ($kg/(m^2s)$):	
Left edge	-47.6
Right edge	-4.2
Total	-51.8
Mean	-2.35

under the top surface (as the downhill velocity decreases as well).

One source of systematic error in the drift could be the slight decrease in the dynamic angle of repose (2 degrees) of the small particle bands. Because this means that the camera will see the top of the small particle band as slightly farther away and the bottom of the band as slightly closer, this could cause a slight outward drift all the way down the flow–for a band right in the center of the camera view. The magnitude of the apparent drift from a small change in surface angle can be approximated from: $v_z \approx v_x tan^{-1}(-L * \frac{r}{(r+Rsin\theta)^2} sin\theta)$ where L is the width of the band, R is the radius of the drum, r is the distance from the camera to the band, and θ is the offset angle. For r = 0.5 m, L = 5 cm, θ = 2 degrees, and R = 5 cm, this equals $(0.002)v_x$, and so $v_z \approx 0.0004$ m/s. The maximum magnitude of the drift velocity that we see is around 0.02 m/s, much more than this slight error. Furthermore, the bands are not exactly centered in the field of view of the camera, and off-center bands still show the same drift pattern.

In figure 4.10 we plot the drift at the left edge of the band as a function of rotation rate for 3 slices in x (top, middle, bottom). Within the error bars, the z velocity does not appear to change significantly with increasing rotation rate. This

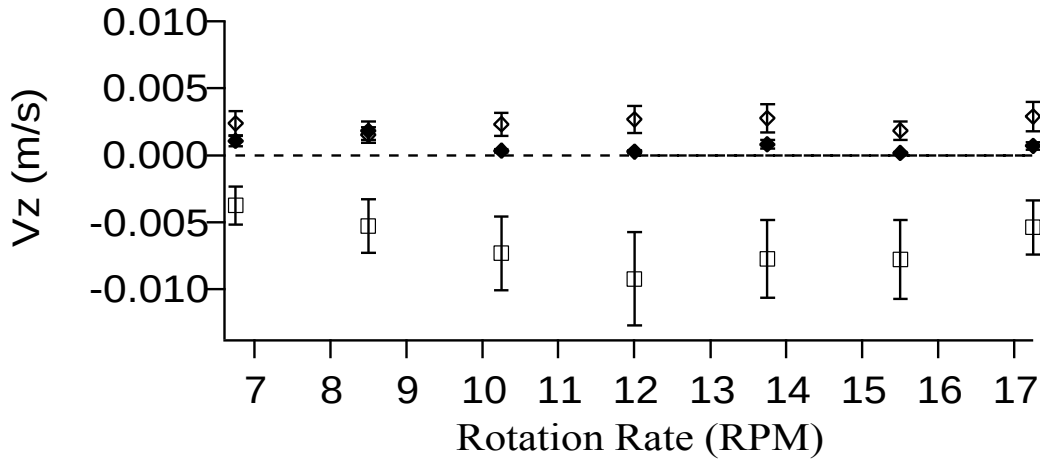

Figure 4.10: v_z averaged at the left side of the small particle band, as a function of rotation rate. v_z is shown averaged over the top third, the middle third, and the bottom third of the downhill flow.

is surprising since the x velocity increases significantly with increasing rotation rate, and we might have expected the z velocity to increase as well. Hajra et al. [87] showed that the radial diffusivity increased at a rate much slower than linear with rotation rate. So the relatively constant axial velocity might not mean a significant decrease in the segregation. For one thing, the higher velocity will mean that the flowing layer samples deeper into the radial core.

In our mixture, the radial segregation tended to get weaker with higher rotation rate. As we have seen in chapter 2, strong radial segregation tends to oppose axial segregation. As the radial segregation gets weaker due to increased rotation rate, the axial banding will not require as strong surface currents.

4.4 Granular Temperature

An effective granular temperature is often defined from the fluctuations in the velocity [24, 88]. The granular temperature has the form $T_g = \langle v^2 \rangle - \langle v \rangle^2$. Notice that temperature normally has units of $\frac{1}{2}mv^2$, but the granular temperature is defined without the mass. Experimental studies [89] and simulations [90] have shown that there is no equipartition of energy between large and small grains in a range of driven granular systems. Instead the nature of energy sharing is complex and depends on how the system is excited. Therefore one must assume that particles of different kinetic energy interact in a flow, and that the differences in kinetic energy depend on the system properties.

The velocity fluctuations, or the squared standard deviations in the velocity, still can provide interesting insight into the dynamics of the flowing properties. This assumes that the actual velocity fluctuations can be distinguished from the error in our particle tracking. The group of Michel Louge [91] outlined a nice discussion of the errors in determining the granular temperature. They discussed two relevant sources of measurement error that might contribute to the temperature: errors in tracking the particle centers due to finite pixel size and the error due to collisions occurring between frames.

The additional fluctuation due to particle tracking error is given by:

$$\frac{2}{3}\Delta_p^2 * (pF)^2 \tag{4.2}$$

where Δ_p is the uncertainty in the particle center in terms of pixels, p is the size of a pixel and F is the rate at which images are taken. For nearest pixel accuracy, Δ_p

would be 1/2.

The accuracy of our particle tracking will depend on the size and nature of our particles. The particle tracking program can achieve subpixel accuracy by averaging over an entire circular spot (with Gaussian intensity distribution) and fixing the center. For spots that are too small or that are not circular, the accuracy will go down. The code is officially rated for an accuracy of up to 0.1 pixels. This is only true for particles that are larger than 5 pixels in diameter. Lower than this, the accuracy significantly decreases. The accuracy is difficult to estimate. If we put it somewhere in-between, we might get an accuracy of 1/4th of a pixel and a Δ_p of 1/8. Our frame rate, F is 1000 frames/s and our pixel size p in this experiment is about .24 mm/pix. This gives a velocity fluctuation contribution from error in the tracking of 0.0006 m^2/s^2. If instead the Δ_p is 1/4 then we get fluctuations of .0024 m^2/s^2.

The average number of collisions a particle experiences between successive images is

$$n_{coll} = f_{coll}/F \tag{4.3}$$

where F is the frame rate as defined before and f_{coll} is the frequency of collisions. Assuming that f_{coll} is less than F, then a decrease in the temperature can be derived: $\Delta T = \frac{n_{coll}}{3} T$.

In order to estimate the time between collisions and other causes of our velocity fluctuations, we plot the velocities as a function of time for a few representative particle tracks in figure 4.11. The top graph represents the z velocities, the middle

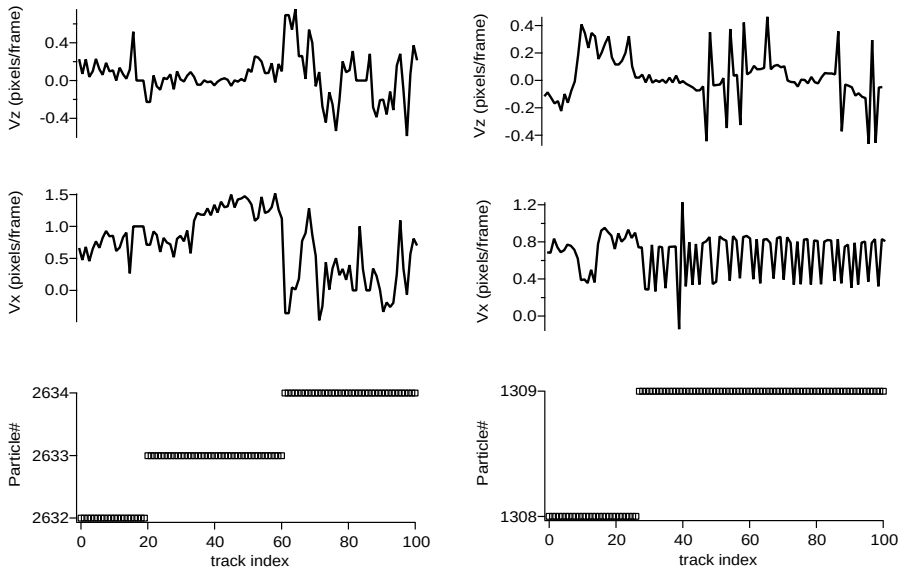

Figure 4.11: Sample particle tracks for 2 sets of 100 track indices. The top plots show v_z, the middle plots show v_x, and the bottom plots show the corresponding track numbers. The array indices are evenly gridded in time. Each set of particle tracks shows multiple particles, and the particle identification number is shown in the bottom plot.

graph is the x velocities, and the bottom graph is the particle number being plotted. The velocities generally do not change drastically in one time step but instead tend to change every 2-15 time steps. Only the smallest fluctuations shown should come from the pixilated nature of the image, although this depends on the particle spot size and shape.

In figure 4.12 we show contour plots of the axial velocity fluctuations of the banded state. The bright contours represent areas of high temperature. In figure 4.13 we plot the z velocity fluctuations (T_z) for the large and small particles at different times. The filled symbols and the crosses represent the small particles, and the empty symbols and the X's represent the large particles. We notice that the fluctuations are on the order of 0.002 m^2/s^2 which is larger than the best possible accuracy but significantly lower than nearest pixel resolution. At the very least, these plots mean that we must be getting at least 1/2 ($\Delta_p = 1/4$) pixel resolution.

Some very distinct features are noticeable in the plots. Generally the smaller particles have higher fluctuations. In the small particle band, the fluctuations of the small particles are much lower, except at the very bottom of the small particle band where the fluctuations are very high. There is a clear asymmetry in the fluctuations at the top and the bottom of the small particle band. We also notice a lot of systematic looking error in the fluctuations of the large particles, ie. the large particles fluctuations show no consistent patterns.

Even if we assume that the contribution from particle tracking errors to the fluctuations is high, 0.001 m^2/s^2, and that it varies significantly over the mixture, there are still some things that we are able to glean from the temperature. First, the

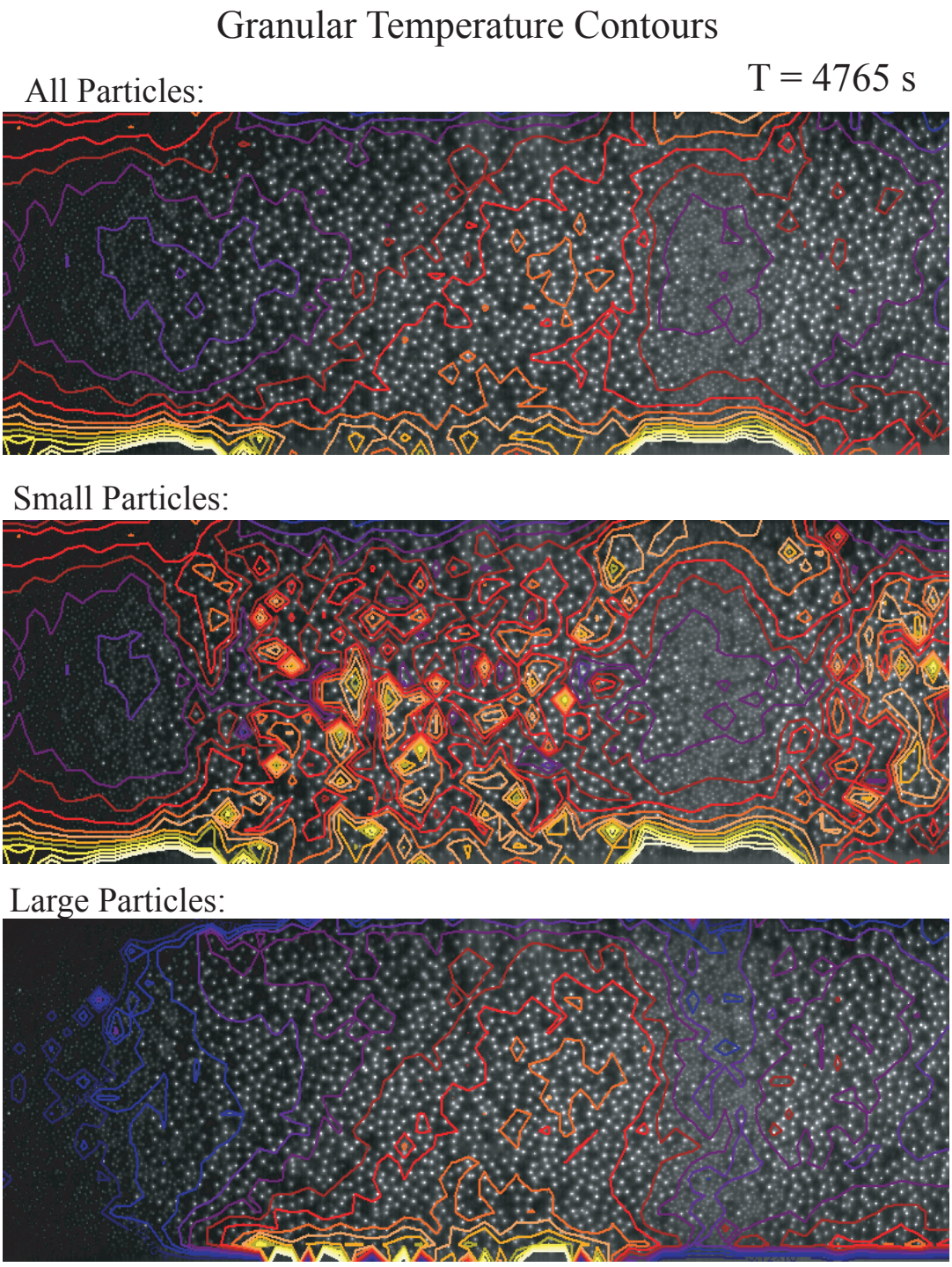

Figure 4.12: Color contour plots of the axial (z) velocity fluctuations. Bright (yellow) contours represent high fluctuations, and dark (purple) contours represent low fluctuations. The contour lines represent a range from 0 to 0.005 m^2/s^2.

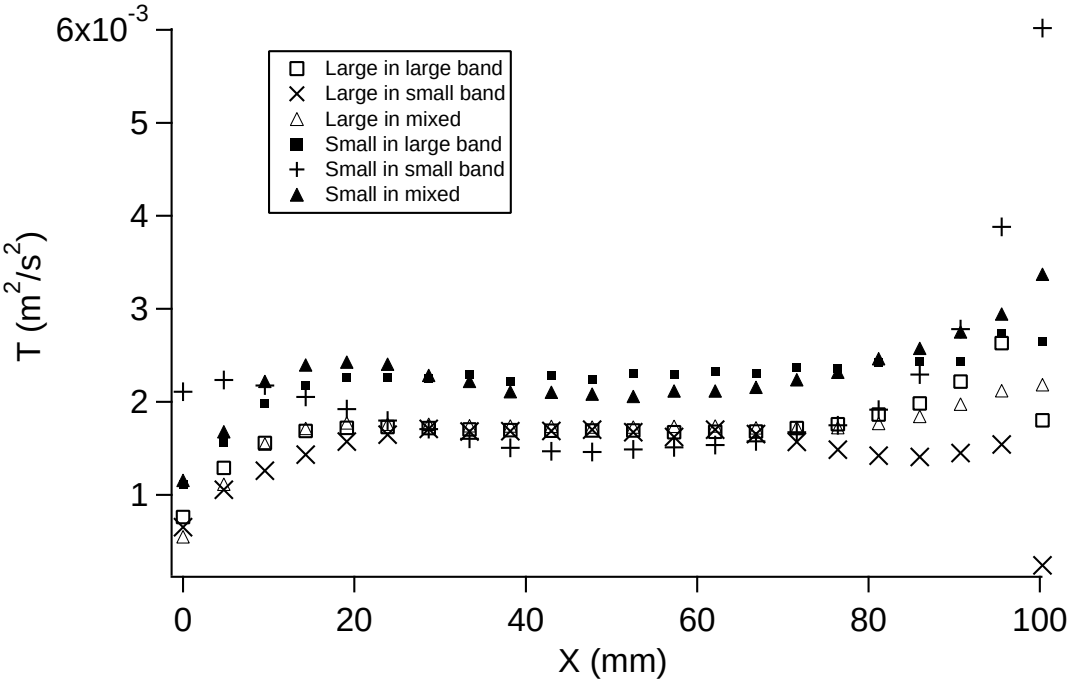

Figure 4.13: The axial (z) velocity fluctuations as a function of x. Fluctuations are plotted for small particles in a small particle band (crosses), large particle in a small particle band (x's), small particles in large particle bands (hollow squares), large particles in large particle bands (solid squares), small particles in the initial mixed state (hollow triangles), and large particles in the initial mixed state (solid triangles). Small particles in large particle bands and large particles in small particle bands will have large errors due to misclassification.

fluctuations are clearly much higher at the bottom of the small particle band. This is most likely an indication of true increase in temperature due to collisions that are needed to slow down the flow (deceleration). At the top, the accelerating particle are likely to see the same or fewer collisions as the mixture stretches since particles can accelerate due to gravity alone, without the need for collisions (or receive energy from neighbors).

Second, there a distinct drop in the fluctuations for small particles over the small particle band. It is impossible to determine whether this is an indication of true temperature difference or just due to the differences in particle tracking or collision frequency of the different particle types. Or it may be that the particles in the small particle band collide much more often. This would raise n_{coll} and lower the temperature.

4.5 Concentration

An important parameter in the model by T. Elperin as well as in our proposed model is the distribution in the concentration of particles. Using the data from our experiment on binary mixtures as viewed from the side (see figure 2.2), we measured the number concentration of the small particles versus radial position. Because the bottom of the mixture was not imaged, we measured across a horizontal slice near the beginning of the bulk rotation and calculated r, the distance from the drum center, from $r = \sqrt{h^2 + x^2}$, where h is the vertical (y) distance from the center of the drum and is a constant in this analysis. The error in distinguishing between

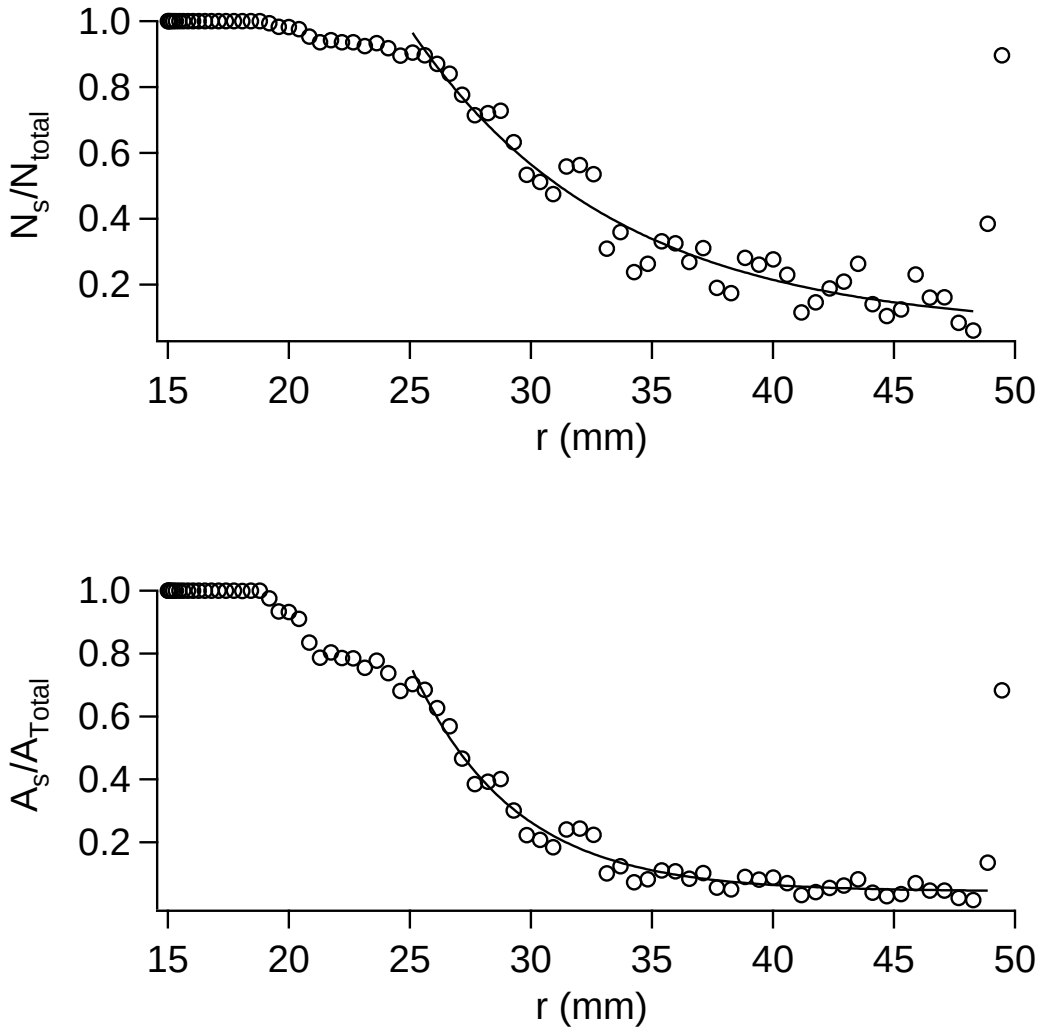

Figure 4.14: Top: Number concentration (in the bulk) of small particles as a function of distance from the radial center of drum. Bottom: Concentration by area of small particles as a function of distance from the radial center of the drum. Exponential fits (solid lines) have been applied to both data sets. This is data for a 50% filling binary mixture of 1/16" and 1/8" steel beads rotated at 7 RPM (See figure 4.1).

large and small particles was significantly less from the side than from the top because the zoom was higher. For the bright area of the image we are measuring, the misclassification was well under 2% (See appendix 2).

We plot the concentration of small particles as a function of r in figure 4.14. The first plot shows the number of small particles over the total number of particles and the second shows the mass concentration (this was found by using the cross sectional area of a single particle: A_{small}/A_{total}). The particles are nearly constant for the first 12 mm (about 8 particle diameters) and then show an exponential drop off (as seen in other experiments [36]). At the very end, there is a spike in the number of particles, but this is largely because we are encountering the wall of the drum which is being tracked as small particles.

We fit the decreasing area of concentration to an exponential (solid line). The exponential fit to the concentration (A_{small}/A_{total}) gave a characteristic length, $\lambda = 4.21$ mm, and a vertical offset of $C_0 = 0.043$. The amplitude was $e^{\alpha r_0} = 272$, giving the edge of the core (where $c_s \approx 1$), $r_0 = 24.2$ mm.

Looking now at the mixture from above, we plot the number of small particles for the small particle band in the process of forming at t = 720 s in figure 4.15. At the top and bottom of the mixture, large particles tend to get tracked as small particles as they are rotating up into the mixture and therefore appear fainter. There is also some mistracking in the (5%) in the rest of the mixture, and this will cause observed differences between large and small particles to be damped by about 10% [84]. Despite this, we see a distinct increase in the number of small particles in the middle of the free surface. This is consistent with the arguments given in

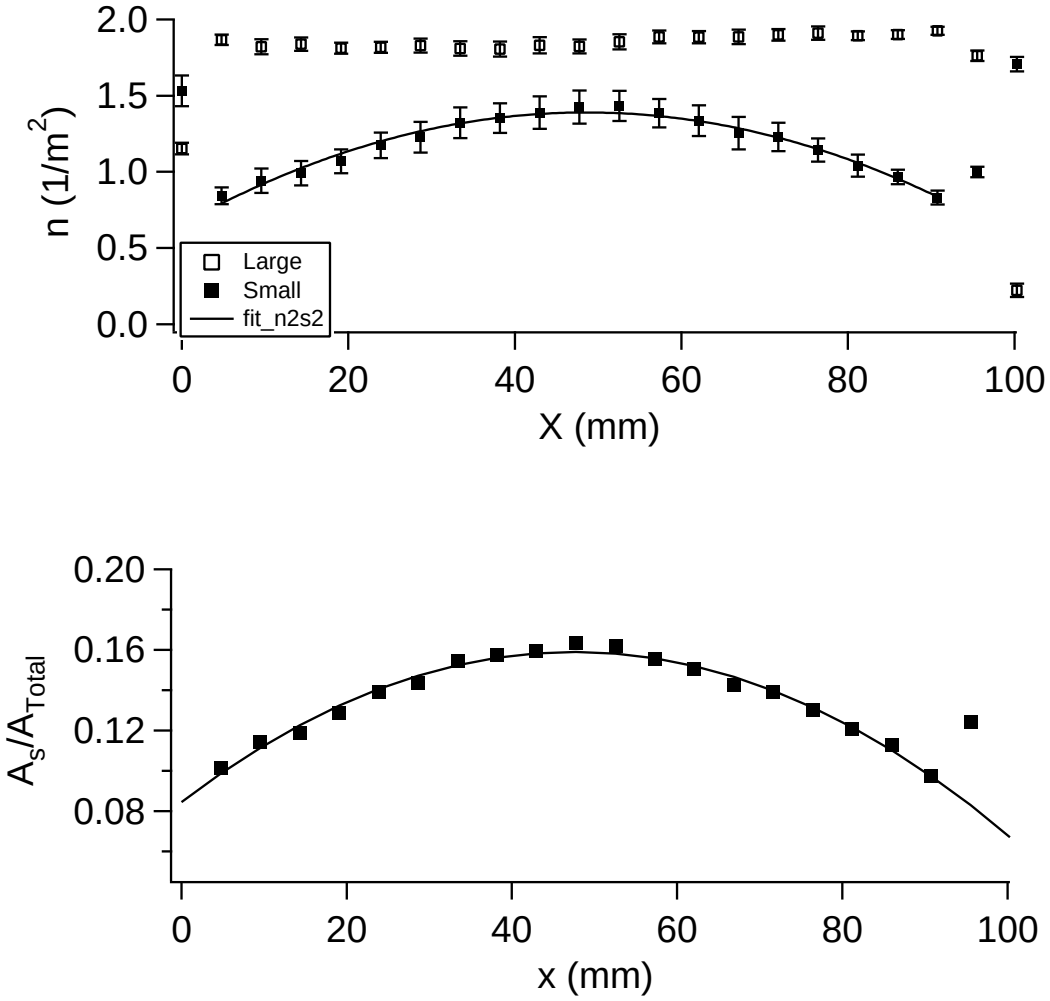

Figure 4.15: Top: The number of small (solid squares) and large particles (hollow squares) versus x as seen by the camera on the top surface at run 7 (720 s). A 2nd degree polynomial has been fit to the data (solid line). Bottom: The concentration of small particles, $\frac{N_s/4}{N_s/4+N_L}$, as seen on the top surface with the corresponding polynomial fit.

chapter 2 based on conservation of mass. The number of particles fit well to a 2nd degree polynomial.

4.6 Discussion

We are now in a position to test each model with our results. In every model the bands form due to the growth of initially small concentration differences. Almost all models assume that the flow happens entirely in a thin surface layer and drift in the direction of steepest descent proportional to the gradient of the surface height (h) with respect to z, $j_z \propto \partial_z h$. Often an undefined or bulk backflow which is equal for each particle type is assumed as well. Often, the models assume that the velocities of the different particle types are different, even at the same point in the flow. Small particles would then be flowing past larger particles at a given point in the flow.

The models give predictions for the dynamics as follows:

- Savage [71]: Required a difference in the lateral mobility of the particles and a higher angle of flow one particle type. He also required that there be a difference in the height of the two surfaces all the way down the flow.

- Das Gupta [51]: Did not require a difference in angle, but required an increase in height for the small particle band all the way down the flow. Required a higher mobility of small particles at all points in the flow.

- O. Zik [70]: Required a difference in the angle of flow and shape of the flow between the two particle types. Also required a difference in mobility of the

particles that, in the model, was due to their difference in monodisperse dynamic angle of repose.

- Aranson [7]: Claimed that the dynamic angle of repose could be out of phase with the concentration of the mixture. Particles flow in the direction of steepest descent. Required a difference in mobility of the particles which, in the model, was due to differences in the static angles of repose.

- Elperin [74]: Allowed homogeneous flow of large and small particles with differences in concentration at different x positions. This allows for the dynamics of the radial core to be incorporated in his model. Required an "s" shape free surface and flow of particles out of a small particle band at the top and into the small particle band at the bottom with an asymmetry between the in and out flow.

- Newey and Losert: We do not assume drift proportional to $\partial_z h$ and allow for homogeneous flow. We require that there are more small particles at mid x positions. We also require drift into small particle bands in the middle of the flow and out of small particle bands at the top or bottom. The driving force for drift is the differences in flow velocity between large and small particle bands. The radial core would be incorporated in a model through the dependence of concentration of particles on x-y position.

The profiles we saw in chapter 3 did not give any increase in the average height for either particle type and were reasonably symmetric at the top and bottom. Thus,

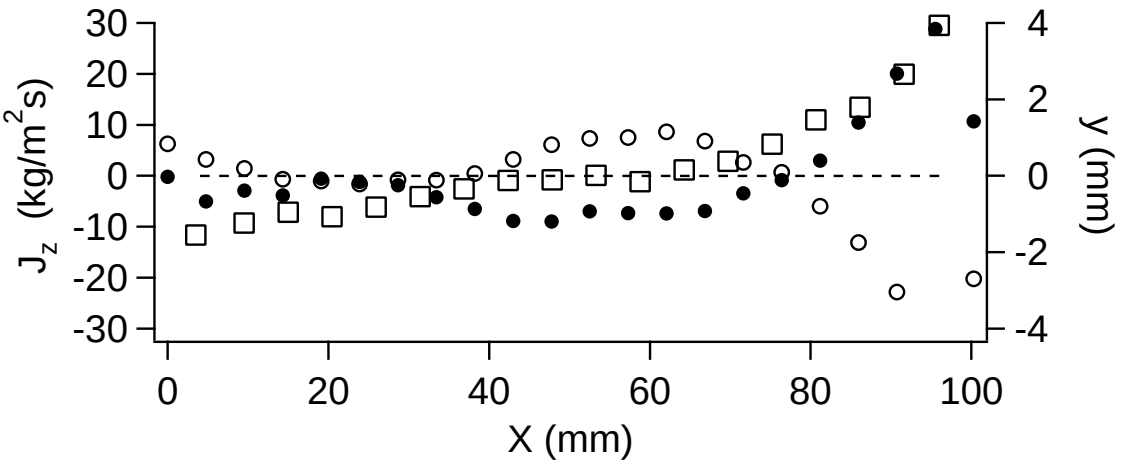

Figure 4.16: The height difference of the surface obtained from the laser line experiments described in chapter 3, $\Delta_z h$, plotted alongside the axial current at the left and right of the band. The height difference is simply the difference between the height at the center of the small particle band and the height a few particle diameters into the large particle band. An approximation to the gradient might be calculated from $\Delta h/\Delta x$.

the assumptions of Das Gupta and Savage are immediately violated as both require a raised free surface for one particle type.

We compare our measurements to the hypothesis that the axial current is proportional to the direction of steepest descent: $j_z \propto \partial_z h$. In chapter 3, we observed that at 12 RPM, the small particle bands have a shallower angle than the large particle bands. This gives a direction of steepest descent towards small particle bands at the top and away from small particle bands at the bottom.

In figure 4.16 we have plotted the difference in the heights at the middle of a small particle band and in a large particle band (from the profiles in figure 3.3). We have plotted the currents, j_z, to the left and right of the small particle band. Note these are not taken from the same band, but from two different experiments with a

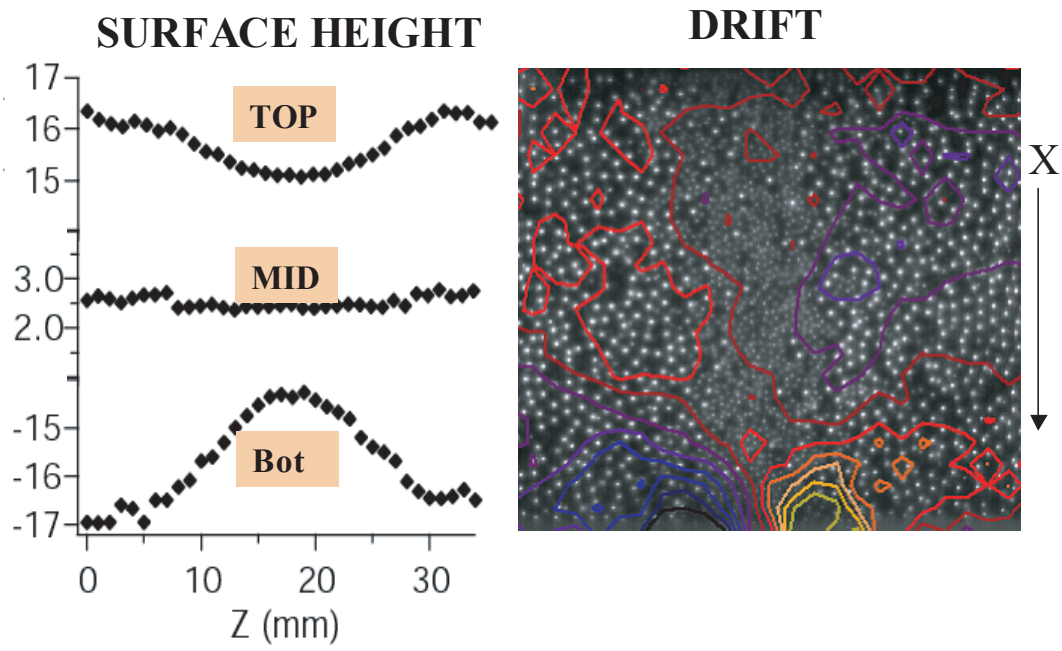

Figure 4.17: Left: The height of the surface at the top, middle, and bottom of the downhill flow. Right: The drift contour plot shown earlier (see figure 4.8).

binary mixture of 50% small particles at the same rotation rate. Similarly, we have plotted height differences and the axial velocity contour together in figure 4.17.

The axial current is in the same direction as steepest descent at the top and the bottom. On the other hand, in the middle of the flow where there is inward drift, there is little z height gradient. Obviously a model assuming drift proportional to axial height gradients cannot give this middle drift. It might be possible to incorporate it into some of the models as the correcting backflow.

We also find that as far as we are able to measure, the particles flow homogeneously. That is, a small particle and a large particle at a given 3-D position in the flow will have the same x velocities. We were unable to compare z velocities.

Our results fit in some ways with the model of Elperin and Vikhansky, as we do have an asymmetric axial flow at the start and end of the downhill flow, and a higher concentration of small particles in the middle. On the other hand, they also did not account for the middle of the flowing layer. Slight corrections might be made to their terms to allow for an inward middle flow, giving a more physically correct description.

The ideas that we formulated at the end of chapter 2 were based on all of our available data plus insights from the literature. The differences in x position of the net flow of particles and the differences in x position of the number of small particles near the free surface, as seen in our experiments, give a driving force for segregation. Particles flow into the small particle band in the middle–the region where more small particles are near the free surface–and out of the small particle band at the ends–the region where the top surface consists mostly of large particles.

This gives a net flow of small particles into small particle bands and large particles into large particle bands.

Chapter 5

TERNARY PATTERNS

5.1 Polydisperse Mixture Background

To expand upon our work, we also studied the long term dynamics of the band formation. Binary mixtures have been studied extensively in the literature. The number of variables that it is possible to vary with mixtures in a rotating drum is vast. One can vary the rotation rate, the drum filling fraction, the percentage of each component, the polydispersity, the type of particles, and more. The effect of many of these on band formation have been investigated in the literature for different mixtures. We expand upon the literature by studying the effect of increasing the polydispersity on the pattern formation in a system of different sized glass beads.

Ternary and mixtures of more particle sizes have special utility, as they can give information that would not otherwise be available. The existence of a middle particle type can help to tell the order and sequence of band formation. More polydisperse systems are also more like real geological situations, which tend to involve a large range of sizes. Parts of this work recently appeared in Europhysics Letters [47].

5.2 Experimental Setup

Two drums were used: For the initial experiments, a short, 38 cm long, 10 cm diameter drum was used, which was later replaced by a 67 cm long, 10 cm diameter drum (the same one used in the high speed and laser line experiments). Both drums were made of transparent perspex with transparent perspex endplates. We will focus on the mixtures in the longer drum here. The drum was half filled with particles and was rotated at 10-30 RPM. Most of the experiments reported on here will be for rotation rates of 30 RPM. The experiment used a high resolution color CCD camera placed to image the top surface of the granular material. In addition, we imaged the sample through the transparent sideplates to investigate radial segregation.

For the majority of the experiments, we used colored glass beads, with various sizes between 0.2 mm and 8 mm. Although the beads were made to be similarly spherical and smooth, the smaller beads (1 mm and below) tended to be more rough and less spherical. In some cases we also used ceramic or steel balls of around 1 mm. For the main ternary results that we focus on here, we used blue/green 0.5 mm beads, 1.0 mm gold beads, and 2.0 mm red beads.

5.3 Basic Axial Band Formation

Using an equal percentage of 1 (gold) and 2 mm (red) diameter glass beads, we confirmed that a binary mixture of our particles formed axial bands as expected for the rotation rates studied here. We observed radial segregation, with the small particles on the bottom of the flowing layer, after only a few rotations of the drum.

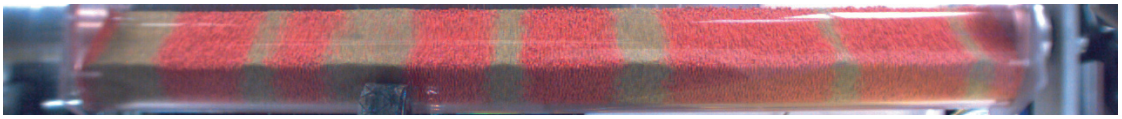

Figure 5.1: Banding in a binary mixture of 1.0-1.25 mm (gold) and 2.0-2.25 mm (red) glass beads. This experiment was run with equal concentrations of small and large particles with a 50% filling fraction rotated at 30 RPM. This image was taken after 257 seconds of rotation.

We observed the typical pattern of alternating bands, with the larger 2 mm glass beads next to the wall. A picture from this experiment is shown in figure 5.1. The bands near the endwalls formed early on in the process, although not necessarily first, and the bands formed away from the endwalls in no particular order. The bands in this binary mixture coarsened over time as expected. Binary mixtures did not show any traveling bands or oscillatory behavior.

5.4 Band Within Band Formation

The focus of this chapter is on ternary mixtures of particles in a rotating drum. It has been observed in other studies that ternary [51] and continuous distribution [49] mixtures segregate in order of size (small to intermediate to large). We expand upon these studies, looking at different filling fractions and particle sizes and types, and find new and interesting phenomena in polydisperse mixtures.

The richest patterns and dynamical instabilities were obtained from mixtures of three particle types. We used three sizes of colored glass beads, 0.5-0.75 mm (green/blue), 1-1.25 mm (gold), and 2-2.25 mm (red). The percentage of each

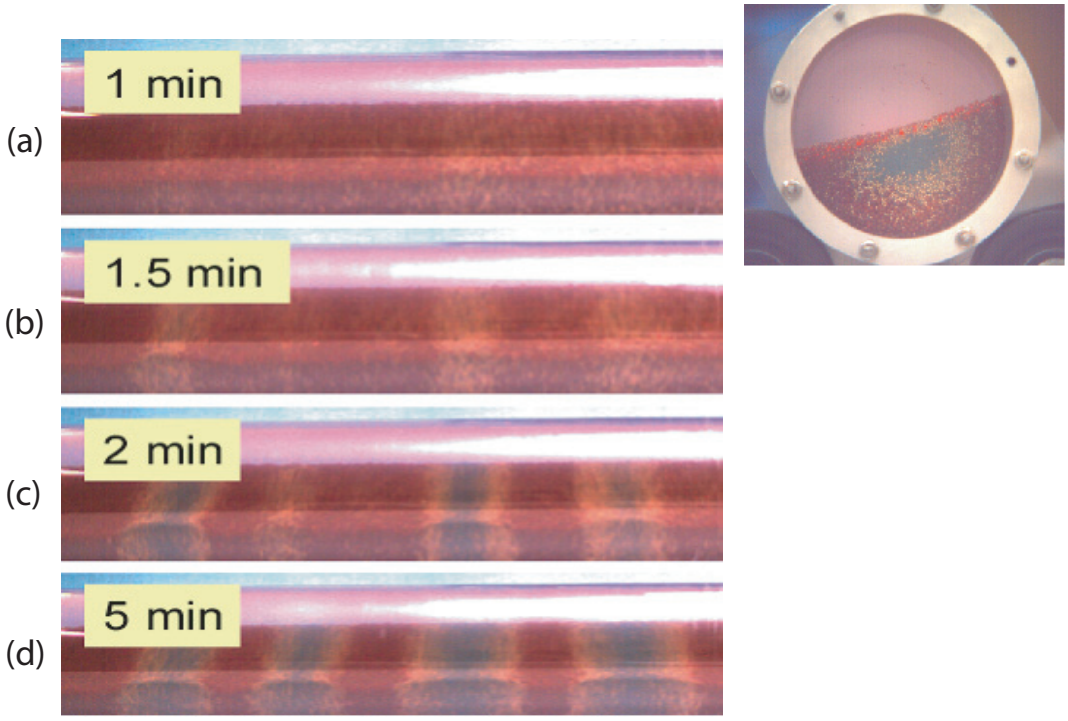

Figure 5.2: An image sequence for a mixture of 40% 0.5-0.7 mm (green/blue), 33% 1.0-1.25 mm (gold), and 27% 2.0-2.25 mm (red) (50% filling fraction) rotated at 30 RPM. The upper right image shows the view from the side of the radial core for a different run with the same mixture.

particle size in the drum was varied. The drum was rotated at 30 rpm for periods of several hours.

Figure 5.2 shows radial segregation and the axial band formation process. Similar to binary mixtures, we found radial segregation after only a few rotations with the small particles in the center surrounded by the medium particles, with the large particles on the outside. This radial segregation can be seen at the endwalls as shown in the inset to figure 5.2.

After radial segregation, but before axial segregation, the largest (red) particles

predominate on the externally visible cylindrical surface of the tube. After about one minute of rotation axial bands begin to form, starting with bands of the medium sized particles. Within another minute, the smallest particles form bands inside the bands of medium sized particles. Bands within bands like this form across the entire tube until, after 5 minutes, there is a roughly evenly spaced array of bands within bands.

As seen in experiments on binary mixtures, the axial pattern coarsens with time (i.e., bands merge to form wider bands), sometimes on very long timescales of hours or days. Generally we did not run the experiment long enough to observe the final pattern, but when we let it run for long periods of time (of order days), we observed a final state with a single band within band pattern.

We were also able to visually confirm that the radial segregation extends throughout the entire tube before and after band formation for both small and medium particles (see the bottom of figure 5.4). We wet the glass particles with anti-static spray and rotated the tube until band formation was observed. We then stopped the drum rotation and allowed the mixture to come to rest. The interstitial fluid created liquid bridges between the particles. In the case of 0.5 mm and some 1.0 mm particles, these liquid bridges were strong enough to hold the particles together so that they retained their bulk patterns. The larger particles were too heavy and flowed more freely. This allowed us to see the extent and form of the radial core. It clearly extended beyond the bands, and small particles could be found at all axial positions (even if there were two few to clump together), indicating the presence of a radial core in the banded state, similar to the results found using MRI for binary

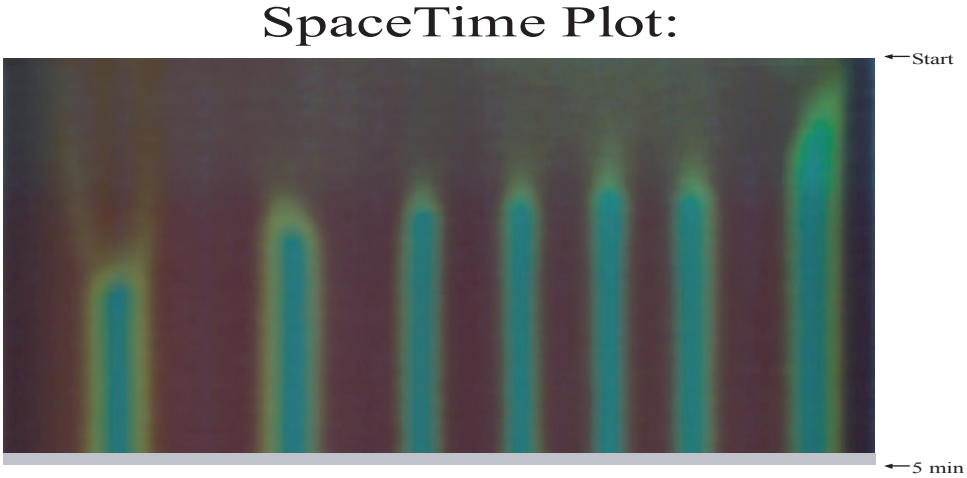

Figure 5.3: A spacetime plot showing the initial band formation for a mixture of 27% 0.5-0.7 mm (green/blue), 33% 1.0-1.25 mm (gold), and 40% 2.0-2.25 mm (red) rotated at 30 RPM (50% filling fraction). The vertical axis represents 5 minutes of rotation.

mixtures.

To visualize the evolution of the banding pattern over long time periods, we create spacetime plots. A space-time plot is made by representing the entire pattern at each time step in a single horizontal line. At each z position in the drum, a vertical average is taken. This gives a horizontal line of pixels representing an the horizontal pattern of the image at each time. These horizontal lines are stacked so that the first is at the top and times proceeds downward.

In figure 5.3, we display a space-time plot of the initial band formation in a ternary mixture of 0.5, 1.0, and 2.0 mm beads. Images were taken every 1.7 seconds and the entire image represents about 5 minutes of rotation. Looking closely at this image we notice a couple of features. First, we can see the characteristic band-in-band formation. At the beginning (top) of every band within band, we see a yellow

peak representing the initial medium particle band. This is followed by a small particle band forming inside it. Once formed these bands appear to be very stable on the short time periods we are observing here.

In the band on the far left we notice faint coarsening that happens even before the appearance of small particles. You can see two faint yellow trails (medium bands) that combine together as the small particles appear. It is interesting that the area where the medium particles first form is not always the same as the center of the band within band. The size of the medium particle bands on each side of a small particle band is also not always the same. When the medium particle band forms initially to one side of where a small particle band will form, then that side will tend to have a large band of medium particles.

The explanation for the observed band within band formation can be described by a simple schematic (see figure 5.4). The pattern of band formation (bands-in-bands) is consistent with the connection we have made in our model (see chapter 2) between radial and axial segregation [33, 32]. We will discuss the dynamics of bands within bands in the context of our model further below. For mixtures of four or fewer particle sizes, the axial segregation pattern and the sequence in which the bands appear can be described as shown schematically, in a cross-section parallel to the free surface, in Figure 5.4(a)-(d). After a few rotations, radial segregation extends throughout the entire tube (Figure 5.4a). An instability of this axially uniform state begins to expand outward (Figure 5.4b) until the outermost edge of the core, made up of medium sized particles, reaches the cylindrical wall of the tube (Figure 5.4c). As viewed from the outside of the tube, this would be a band of

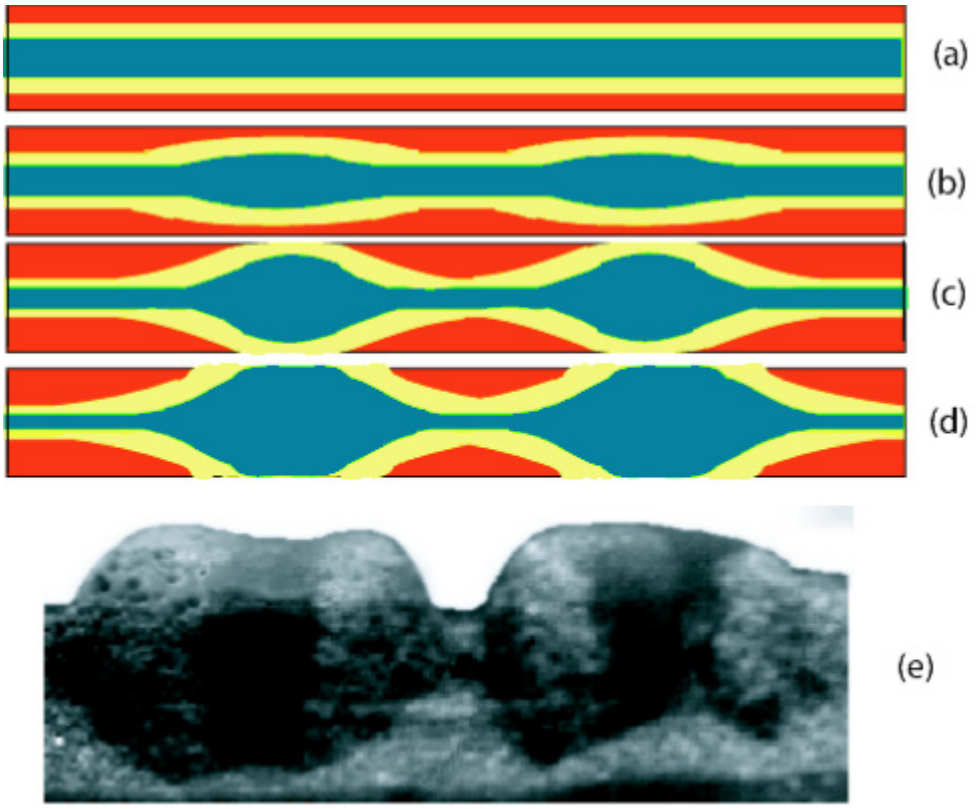

Figure 5.4: (a)-(d) Schematic of the band formation process shown in a cross-section parallel to the free surface. (e) An actual image of the inner core of small particles using wet glass particles. When the drum rotation was stopped, the interstitial fluid created liquid bridges between the particles. In the case of 0.5 mm and some 1.0 mm particles, these liquid bridges were strong enough to hold the particles together so that they retained their bulk patterns.

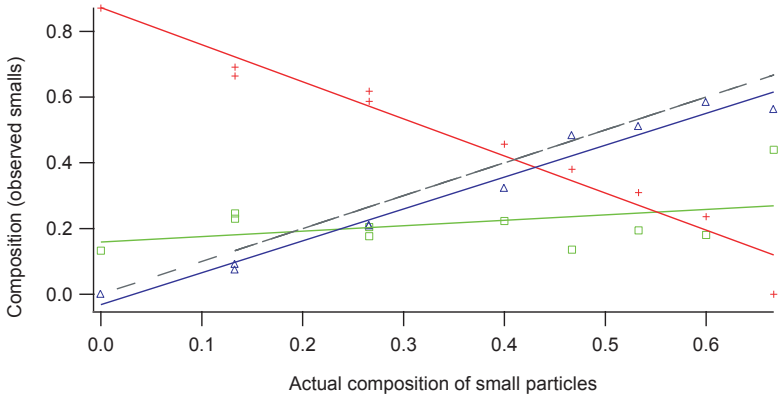

Figure 5.5: Total bandwidth of each particle type vs. input composition of small particles. Bandwidth of 2mm particles (red crosses), 1mm particles (green squares) and 0.5 mm particles (blue triangles). Each data set is fit to a line. They are plotted with the slope one line (black dashed line) which represents the total concentration of small particles in the mixture. Note that the total bandwidth of small particles, or the total amount of small particles in bands, is less than the number of particles in the mixture, indicating the presence of a radial core of small particles.

medium sized particles (Figure 5.2b). The inner core continues to expand until the smallest particles reach the surface (Figure 5.4d) thus forming the band within band structure visible at the surface (Figure 5.2c,d).

Although this accurately describes the sequence and patterns that are created, there is a lot of variety in how this pattern might look in real life. There is competition between the radial segregation of small and medium, and of medium and large. Different ratios of these particle sizes can lead to interesting dynamics as we shall see below.

We varied the composition percentage of the large and small particles while holding the composition of the medium particles the same. We studied the banded state as a function of the composition percentage of small particles. We shall see

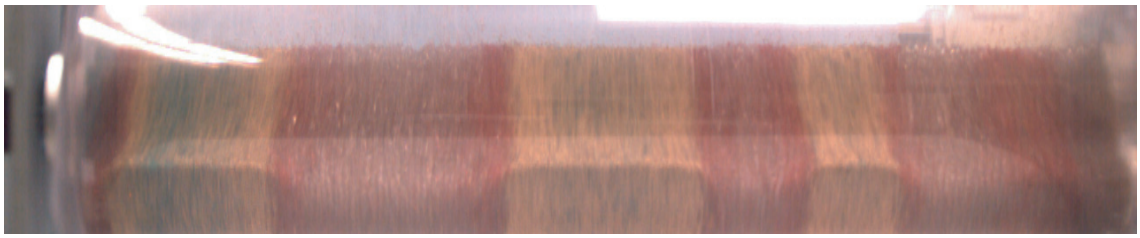

Figure 5.6: Band formation in an equal mixture of 4 particle sizes: 0.5 mm (green/blue), 1.0 mm (gold), 2.0 mm (red) and 4.0 mm (clear) glass beads. The filling fraction was 50% and the drum rotation rate was 30 RPM.

in the next section that some of the richest patterns happen when the composition of the small particles is high. We have plotted in figure 5.5 the total width of all the bands of each particle type (averaged over time after the bands had formed) vs. composition percentage of the small particles. We added the widths of each band in the steady state for each pattern at each composition. Linear fits have been applied to these plots.

When the composition of small particles is low, the large particles predominate on the surface (due to radial segregation). As composition increases, the bands of largest particles decrease in total width, and the smallest particles increase in total width. The medium particles retain a roughly constant total width over the whole range. We have plotted the slope one line, or the line representing the total amount of small particles in the mixture. We find that the data representing the total amount of small particles in bands is below this line. This is consistent with our observation that many small particles are still in an inner core.

We also mixed four particle types with clear 4 mm particles added in equal

volume to the mixture (still total 50% filling fraction). We found them to also segregate both radially and axially. The axial segregation pattern again showed a band within band formation starting with the largest particles and going to the smallest. The banding here is not as distinct as for ternary mixtures and the order of band formation was not easily observable.

We tested mixtures of five and six different particle sizes by adding 8 mm clear (five) and 0.2 mm (six) beads to the mixtures. This gives a ratio of 64:1 between the largest and smallest particle diameters. These mixtures of five and six different particle sizes quickly segregate radially, but do not segregate axially at all for the large range of rotation rates we have investigated (from intermittent avalanching to centrifugally dominated regimes). To determine whether axial segregation is too slow to be observed, we seeded mixtures with an initial band of the smallest particles (one sixth of the total mixture) and observed the evolution of that band. The band gradually disappeared after roughly 200 rotations for a large range of rotation speeds (between 10 and 110 rpm), indicating that axial segregation is suppressed for mixtures of five or more particle types in our system.

The scaling of Morris [50] predicts a cutoff of particle to drum diameter ratio for binary mixtures: $\overline{d}/D < .025$. Here, $\overline{d}$ refers to the average size between the two particle types and D is the drum diameter. In other words, $\overline{d}/D$ must be less than .025 or bands will not form. In our mixture of six particle sizes, the particle to drum diameter ratios of our beads, d/D, were 0.002 (0.2 mm), 0.005 (0.5 mm), 0.010 (1 mm), 0.020 (2 mm), 0.040 (4 mm), and 0.080 (8 mm).

The ratio, $\overline{d}/D < .025$, for the 8 and 4 mm, is .060 (well over the critical

ratio),and the average for the 4 and 2 mm beads is .030 (just barely over the critical ratio). This suggests that binary mixtures of 2 and 4 mm beads may or may not form bands, and binary mixtures of 4 mm and 8 mm beads definitely would not. Considering mixtures of four, five, and six of these particle types, we see that $\overline{d}/D <$ 40 for the 4 mm beads with all the lower diameter bead sizes is near or below 0.025, while $\overline{d}/D < 40$ for the 8 mm beads with the lower diameter beads is above 0.025. It was only in the mixtures of five or six particle types that these 8 mm beads were introduced and these beads did not band. Therefore these results are consistent with this earlier prediction.

The beads underneath the 8 mm particles may still form bands that were not visible but it is more likely, because they are more confined, that they will not be easily able to form bands if the topmost layer does not. Another reason for the lack of segregation in the five and six particle size mixtures is that as the total number of particles goes down for each particle type, there will be more interaction between non-"nearest-neighbor" particle sizes. For example, there would be fewer 4 mm beads between 2 and 8 mm beads and therefore more interaction between 2 and 8 mm beads. As we saw in chapter 2, we would expect this to increase the mixing that opposes axial segregation.

5.5 Ternary Oscillations

When we increased the concentration of small particles in a mixture of three particle types, we observed fascinating oscillations in some of the band positions

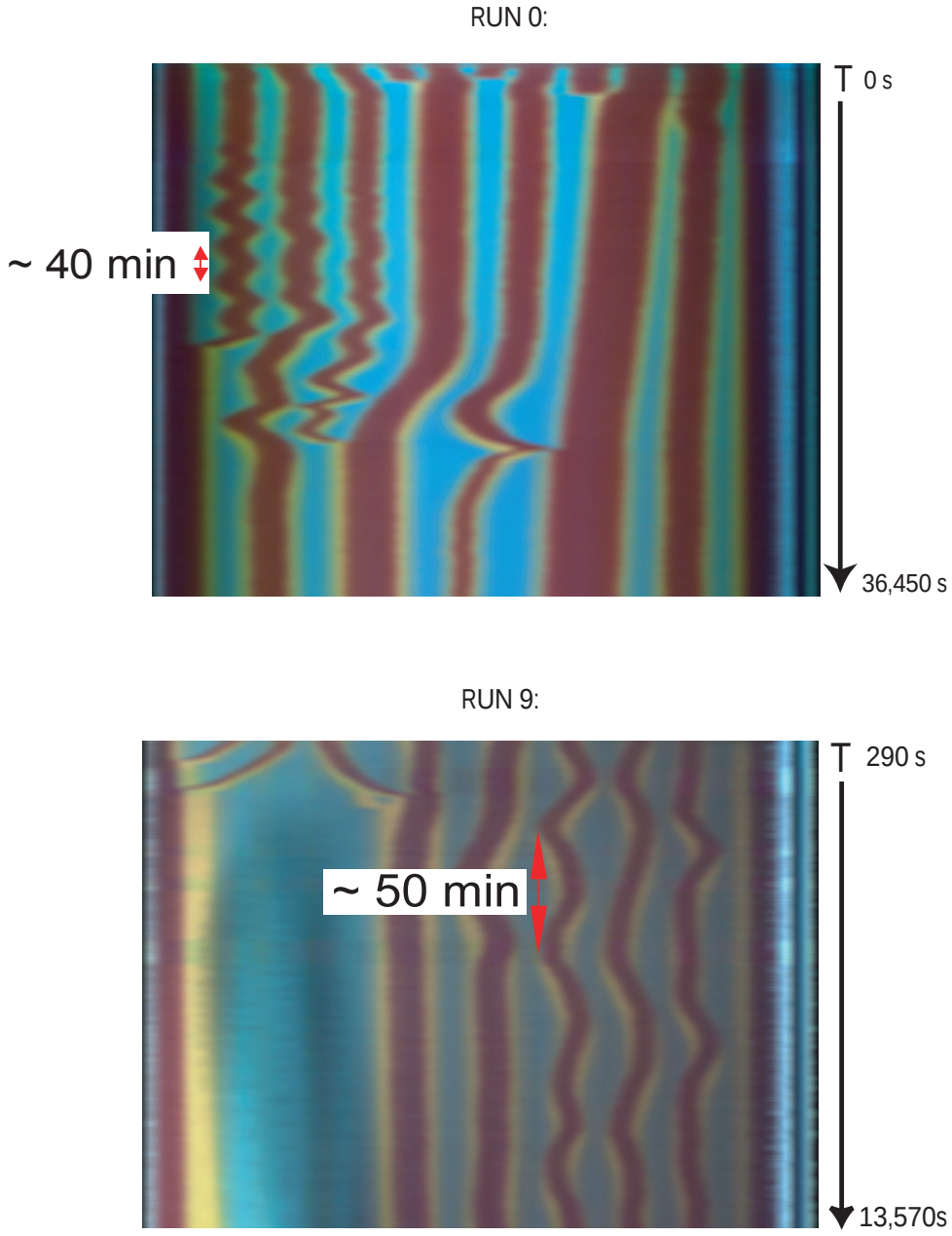

Figure 5.7: On top: Space-time plot of oscillations in a ternary mixture of 0.5 mm (blue/green), 1.0 mm (gold), and 2.0 mm (red) particles. This mixture has a high concentration of small particles (40% small, 33% medium, and 27% large particles). On bottom: A space-time plot of oscillations in a mixture with an even higher concentration of small particles (53% small, 33% medium, and 13% large particles). Both experiments had a rotation rate of 30 RPM.

and widths over time. Figure 5.7a shows a space-time plot of a mixture with excess small particles (40% small particles, 33% medium, and 27% large particles). The mixture initially coarsens (at the very top of the space-time plot) and quickly goes into oscillations of the axial band positions in locations where the bands are closest. The bands on the left of the figure oscillate with a period of about 40 minutes, before coarsening to increase the width and spacing of the bands. As the oscillations end and the band coarsens, some very striking patterns occur: we see one of the large bands move to the right and connect with another large band, but then instead of combining, it reverses direction and moves back near its previous position. It almost appears as if it is 'bouncing' off the other large particle band.

These semi-stable oscillations and this 'bouncing' pattern were first reported on in the literature by Newey et al. [47]. Similar oscillations and patterns occurred in almost every experiment that we ran with above 33% concentration of small particles. In figure 5.7b we show another example of oscillations, this time with higher time resolution, and without the distinct 'reflecting' event. This one is interesting in that some of the bands oscillate with a period that is exactly 1.5 times the predominant period of oscillation. The shortest period here is about 1 hour.

In figure 5.8, we have plotted the band positions and widths for one of the oscillating bands from figure 5.7a. The band width for the large particles (red) is unchanged with time while the width of small (blue/green) and medium (gold) particle bands oscillates with time. The observed change in width of bands of small particles requires influx and outflux of particles. This is consistent with our observation that an inner core of small and medium sized particles remains within

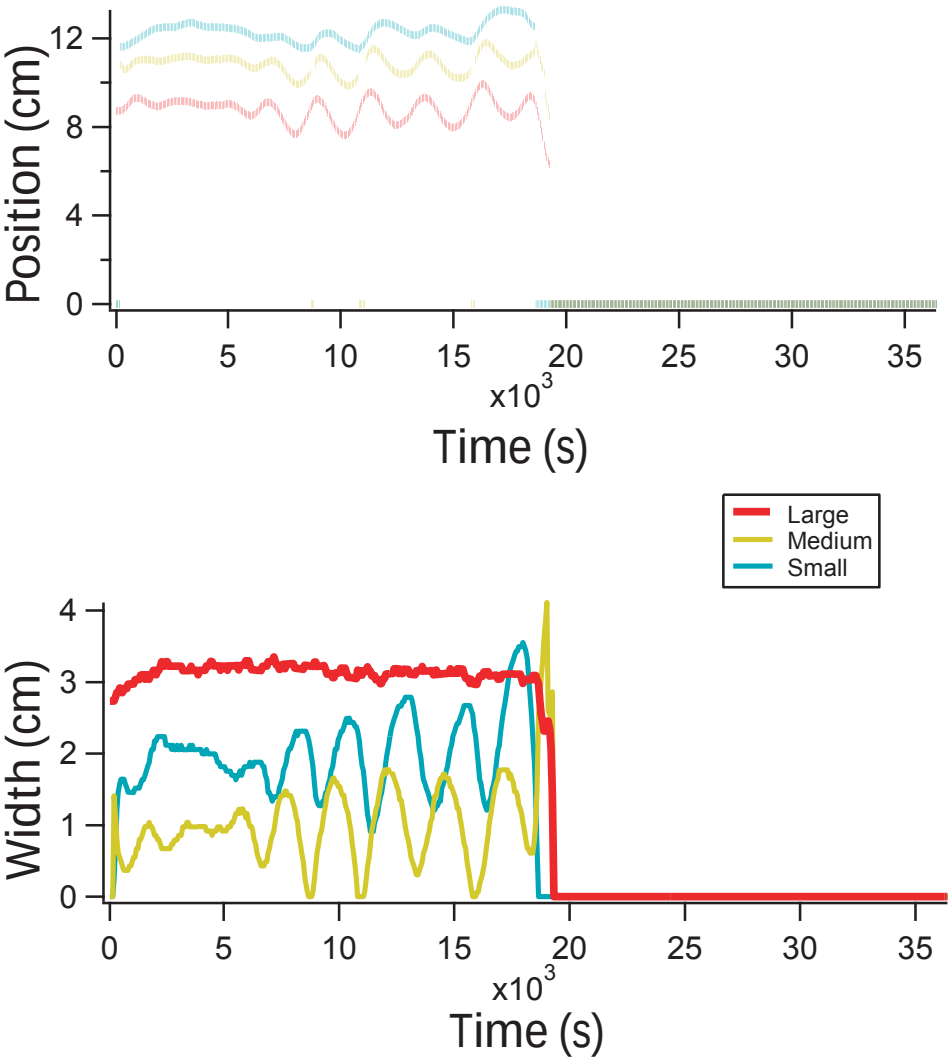

Figure 5.8: The positions and widths versus time of the small (blue/green), medium (gold), and large (red) particle bands.

bands of larger particles (Fig. 5.4). The presence of an inner core near the small and large particle bands means that new material can be easily obtained from the surrounding mixture. Transport of material between bands of large particles, on the other hand, is inhibited.

It is interesting to note that the widths of the small and medium particles oscillate out of phase (by about $\pi/2$ radians). The center positions of the small particles are also out of phase with the center positions of the other two particle types. This suggests out of phase coupling between the interactions of the large and medium and the large and small particles, which we discuss in more detail below.

To ascertain the sinusoidal form of the oscillations, we fit the center positions of the large particle band to a sine function in figure 5.9. On top we have the real data as well as the fitted sine wave. The curve fits well to a sine wave although the center position shifts in the data. On the bottom we have plotted the fourier spectrum of the wave. We see a distinct peak, at about the fitted frequency of the oscillating data.

We calculated the fourier spectrum for all of the bands in experiments where oscillations were observed. We extracted the frequency and list the frequencies for the different bands and runs in table 5.1. The amplitude appears to vary significantly from run to run, but the period is, for the most part, between 2000 s and 3000 s (40 and 60 minutes). Rarely a few larger periods appear, which are 1.5 times higher than the others.

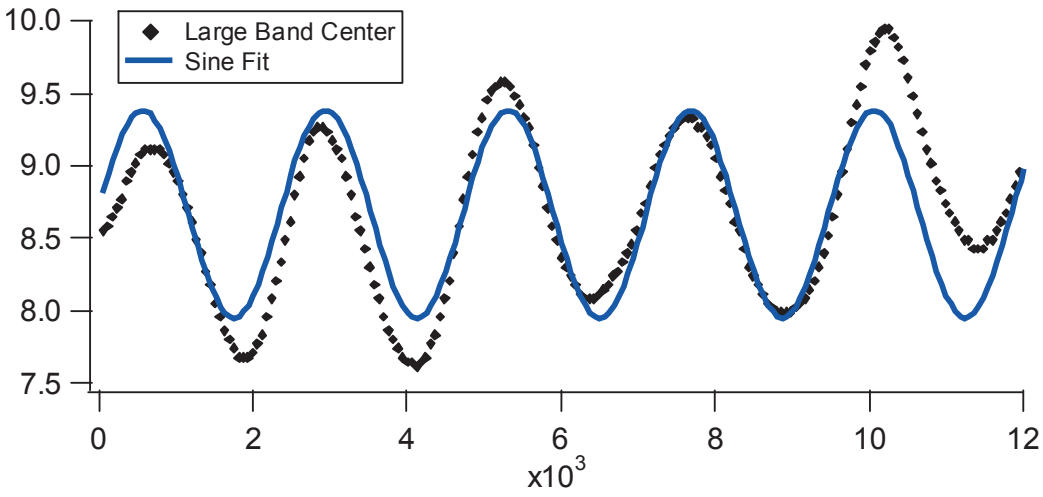

A = .71523 ± 0.0285

f = 0.000419 ± 1.76e-06

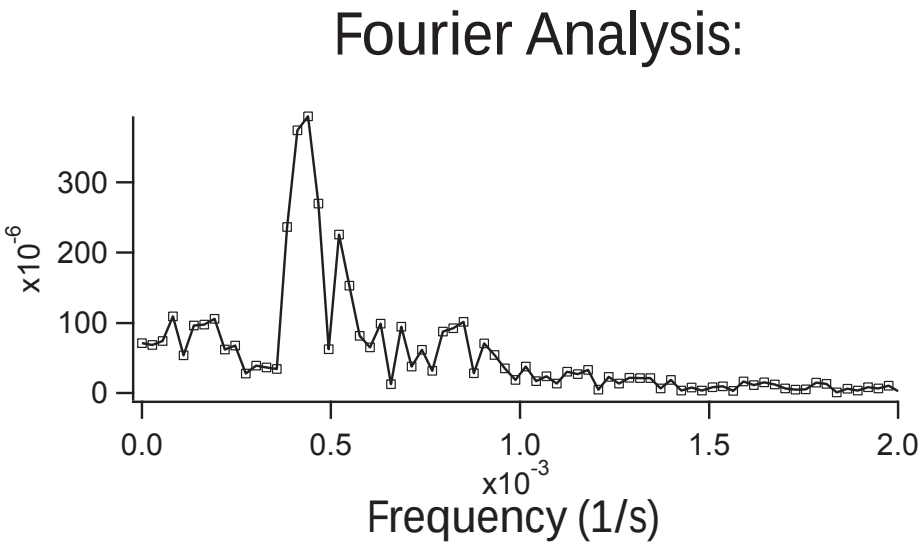

Figure 5.9: On top: A sine fit to an oscillating band from run 0. Fourier spectrum of the band center position during the time of oscillation.

Table 5.1: Oscillating Bands

run	size (mm)	band	frequency (1/s)	period (s)	amplitude (cm)
0	0.5	16	0.000439	2278.127	0.65
0	0.5	17	0.000384	2604.467	0.7
0	0.5	18	0.000410	2439.024	0.3
0	2.0	03	0.000439	2278.112	1.6
0	2.0	04	0.000384	2604.167	0.5
0	2.0	06	0.000455	2200.000	0.8
6	2.0	00	0.000365	2739.726	1.0
9	2.0	05	0.000333	3000.000	2.2
9	2.0	06	0.000300	3333.333	2.5
9	2.0	07	0.000225	4444.444	3.0
9	2.0	08	0.000225	4444.444	3.0
9	2.0	08	0.000375	2666.667	3.0
12	2.0	08	0.000475	2105.263	2.0
12	2.0	08	0.00058	1724.138	2.0
14	2.0	10	0.0002	5000	2
14	2.0	11	0.0004	2500	2

5.6 Traveling Bands

In addition to oscillating bands, we also see traveling band patterns. A space-time plot of two runs that exhibited this phenomena is shown in figure 5.10. The bands follow a fascinating menorah-like pattern, branching away from the middle of the pattern. In the first run, all of the small particles on the right end up in the middle, leaving only large and medium particles on the right. In the second run there are still small particle bands on the right. In the second run, we also see one of the bands exhibit a brief oscillation after the branching has been completed. As we make observations and consider this interesting pattern, we note that most of the observations apply to the oscillating bands as well. It may be that traveling

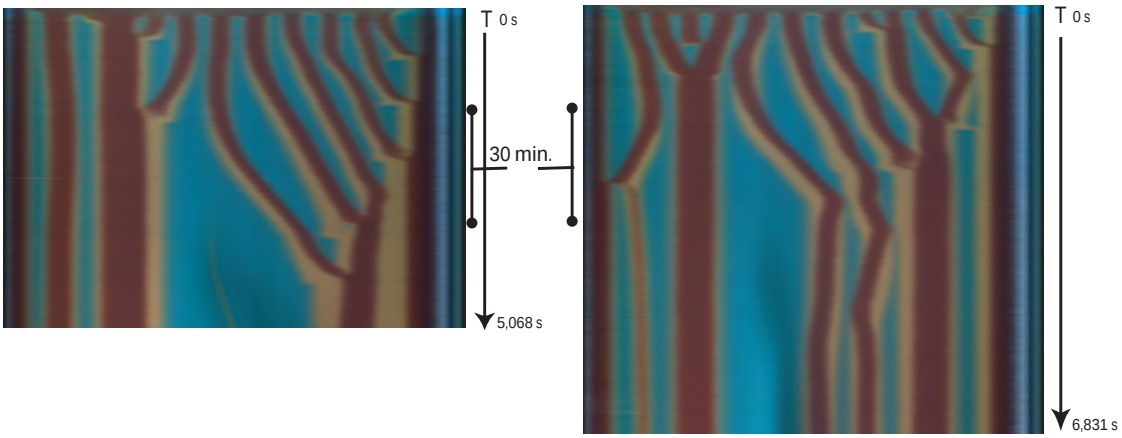

Figure 5.10: Two spacetime plots showing a distinct traveling wave pattern. The images are taken from a run with 53% small, 33% medium, and 14% large particles (left image) and 47% small, 33% medium, and 20% large particles (right image). Filling fraction is 50% and the rotation rate is 20 RPM.

waves result when all the bands move in the same direction and oscillating bands result when the bands 'want' to move in opposite directions.

The direction of the movement of the *particles* is not always the same as the direction of the movement of the *bands*. Looking in figure 5.10, we see that while the large, medium, and small particle bands may be moving to the right, the small particles are moving to the left (because the area of small particles is getting larger in the middle). The sideways velocities of the traveling bands also appear to increase right before they combine with other bands.

Another interesting observation is the movement of a small particle band is accompanied by an asymmetry in size of the medium particle bands on each side of the small particle band. The small particle bands almost always move away from the side where there are fewer (or no) medium particles. This is true for the oscillations

in figure 5.7 as well. This means that segregation is occurring on one side of the band, while on the other the particles are mixing and diffusing.

5.7 Discussion

These oscillations can be understood in a couple of ways. A simple diffusion term can never give oscillations, but two coupled equations could. When working with a mixture of three particles types, one particle type can always be eliminated by the relation: $c_1 + c_2 + c_3 = 1$, where c_i is the concentration of particle type i. In a review article still in developement, Aranson proposed using $C_A = c_1 - c_2$ and $C_B = c_2 - c_3$, in a coupled system of diffusion equations like those given for binary mixtures (see equation 2.4).

$$\partial_t C_A = D_A \partial_z^2 C_A + \mu_A \partial_z^2 C_B \tag{5.1}$$

$$\partial_t C_B = D_B \partial_z^2 C_B + \mu_B \partial_z^2 C_A \tag{5.2}$$

If μ_A and μ_B have opposite signs (i.e. the oscillations of the two equations are out of phase) then this gives the observed oscillations.

Looking carefully at our oscillating spacetime plots (figure 5.7) and at figure 5.8 we see that the particles do oscillate out of phase in space and time. An easy verification of the oscillations in time can be made by taking a vertical line down one of our oscillating space time plots at the edge of an oscillating band (see figure 5.11. The concentration as a function of time goes from small to large to medium to small

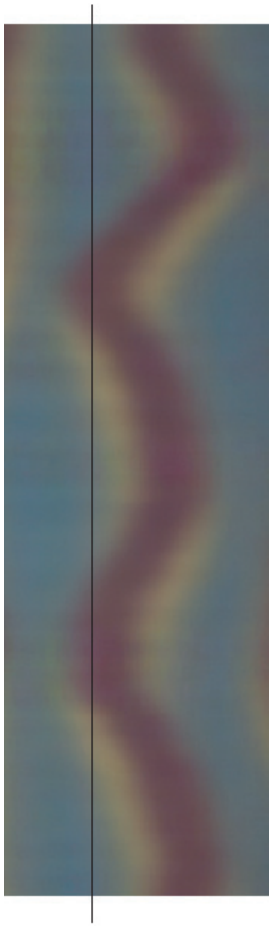

Figure 5.11: A zoomed in section from the leftmost oscillating band in figure 5.7a. If we follow the solid line downward, we can see oscillations in time that are 120 degrees out of phase: we go through a small band, then through a large band, then through a medium band, and then through a small band again, etc.

again. If each of these are sine waves and the visible particles represent peaks in the sine waves, then each of the concentrations are oscillating 120 degrees out of phase.

We now compare to our model, using c_1 and c_2 as C_A and C_B for convenience. A similar result could be worked out with other models by replacing v_x with the dynamic angle of repose θ. In equation 2.12, we gave a simplified equation for the concentration:

$$J_{tot} = -D\partial c_z + \beta_2 \partial c_z F(c) \tag{5.3}$$

where $F(c) = C_{mid} - C_{bot}$. For a three particle system, we assume the downhill velocity, v_x to depend on the sum of the concentrations, $c_1 + c_2$. The diffusive mixing will be different for different particle size ratios (see chapter 2), ie. D_{small} mixed with medium particles will be different than D_{small} mixed with large. Radial segregation is not complete and the top surface flow will consist of mixtures of large, medium, and small particles. The diffusion coefficients for each particle type will be dependent on the concentrations of the other particles. We label the diffusion coefficient for small particle $D_1(c_1, c_2)$ and the diffusion coefficient for medium particles $D2(c_1, c_2)$.

The axial current will be dependent on the gradient in the velocity which is dependent on $c_1 + c_2$. F(c) will depend mainly on the concentration of the particle type in question.

$$J_1 = (\beta_1 \partial_z c_1 + \beta_2 \partial_z c_2) F(c_1) - D_1(c_1, c_2)\partial_z c_1 \tag{5.4}$$

$$J_2 = (\beta_1 \partial_z c_1 + \beta_2 \partial_z c_2) F(c_2) - D_2(c_1, c_2)\partial_z c_2 \tag{5.5}$$

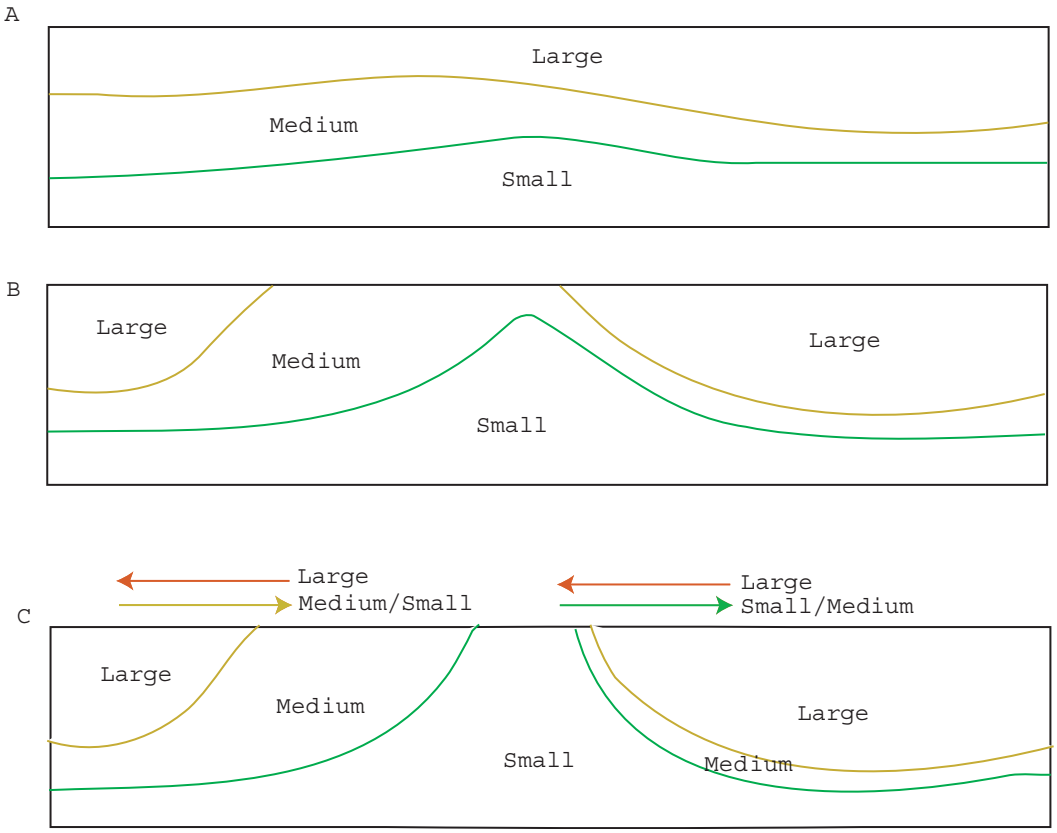

Figure 5.12: Image sequence for band formation with uneven particle concentrations on either side of the band.

Taking $\partial_t c = \partial_x J$, and rearranging terms, we get:

$$\partial_t c_1 = \beta_1 \partial_z^2 c_1 F(c1) - D_1(c1, c2)\partial_z^2 c_1 + \beta_2 \partial_z^2 c_2 F(c1) \tag{5.6}$$

$$\partial_t c_2 = \beta_2 \partial_z^2 c_2 F(c2) - D_2(c1, c2)\partial_z^2 c_2 + \beta_1 \partial_z^2 c_1 F(c1) \tag{5.7}$$

Here we have coupling interaction in two places: in the diffusion coefficients $D_{1,2}$ and in the last term in each equation. These equations allow oscillations in space and time assuming the oscillations of c_1 and c_2 are out of phase.

In figure 5.12, we have provided a schematic of how traveling waves might occur. The large and medium particles have a 2:1 size ratio, the medium and small have 2:1 size ratio, but the large and small particles have a size ratio of 4:1. In other words, the radial segregation and diffusion mixing will be stronger for interfaces between large and small particles with 4:1 size ratio.

If the medium particle band was small on one side of a small particle band, there would be more interaction between small and large particles and the particles might diffuse on that side while segregating on the other, causing movement of the small particle band away from the small medium particle band. If there are fewer medium particles near one side of a small particle band, then there will be more interaction between the small particles and the neighboring large particles. This will cause the diffusion to be higher on this side of the band. If this diffusion is higher than the segregation, strength then the band might move. Mixing on the right side of the band means that small particles will move right and large particles will move left. Segregation on the left side of the band would mean that small particles were also moving right and large left there. This would give a net movement of small particles to the right but of the small particle *band* to the left.

Oscillations may occur with more complicated interactions between the three particle types. One thought is that oscillations may occur when two bands are traveling in opposite directions, as the core will grow when the bands get close together. This may stop the movement of the band, and if there was a difference in the core between particle types, cause the bands to reverse direction .

Chapter 6

CONCLUSIONS

In this work we have presented a series of new and interesting experimental results on the banded state of granular particles in a rotating drum. We studied the basic surface characteristics of the band formation through high speed imaging and laser line deflections. Our results are applicable for a range of conditions and materials in the rotating drum, and are generally consistent with earlier experimental data. Our data provides a more complete picture than earlier studies. Based on our observations we discuss two flow processes that are important for understanding the physical mechanisms that lead to axial segregation and present evidence that one hypothetical process that is used in several models of axial segregation may not always be correct. In summary, our results our:

1.) We find that the particles follow an interesting axial velocity pattern: In the high speed middle of the flow, particles drift towards small particle bands. In the decelerating bottom of the flow, particles tend to flow away from small particle bands.

2.) We find that particles in small particle bands actually flow downhill faster than particles in large particle bands. This creates an interesting shear flow as you traverse the band in the axial direction: The small particles shear past the large particles. We present evidence that natural asymmetries in a granular flow lead to

the axial pattern given above being caused by this difference in downhill velocity. One piece of evidence is the increased velocity fluctuations at the bottom of the flow in the small particle band. This leads to outward flow from small to large particle bands at the bottom of the flow.

3.) We measure the surface height of the banded state in the rotated drum. We test current models for axial segregation that assume that gravity forces particles to move in the direction of steepest descent. We find that though there are surface height differences that can explain some of the axial velocities, height differences are insufficient to drive the axial flow that we experimentally observed.

These results paint quite an unexpected picture of the motion of particles flowing in the drum. With our natural eyes we can discern little except fast downhill flow on the surface of the drum, and yet, the particles flow sideways, in and out, as they move down the hill. These results don't fit with the more intuitive understanding that has been presented previously. Most of the models in the literature explain the band formation through axial surface flows driven by gravity in the direction of steepest descent. As shown above, our results only partially match up with these models. Instead, a better driving force for axial flow might be the differences between the downhill flow velocities of the large and small particle bands.

Regardless of the driving force, a similar mathematical form for the axial segregation of the particles can be determined: The segregation is described using a diffusion equation with a negative diffusion coefficient, similar to Spinodal decomposition. This naturally suggests that an investigation of this common description might be useful.

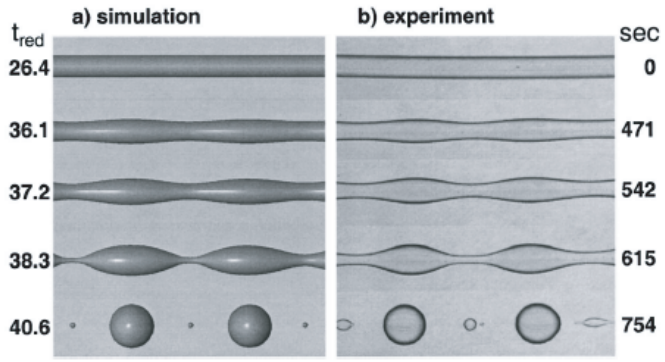

Figure 6.1: Example of fluid thread breakup from Douglas et al. [54]. Pictures are shown for experiment (right) and simulation (left).

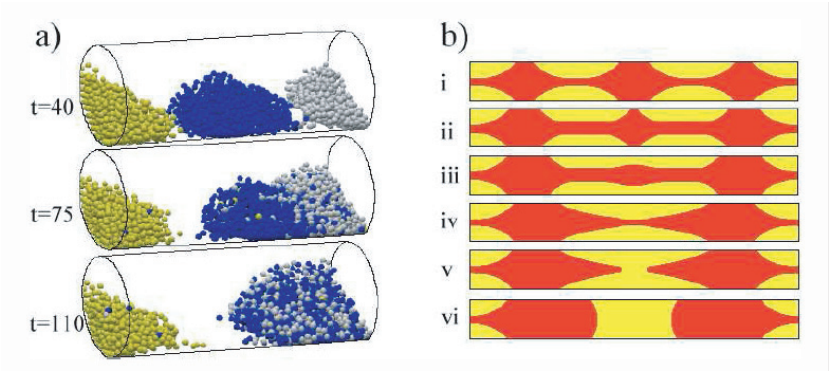

Figure 6.2: On the left: Simulation results of the large beads in run C. The color of each grain is chosen according to the position after a short time. On the right: Schematic cross sections showing a typical merging event [44].

We can make comparisons with phase separation, which is found in a variety of systems such as non-mixing fluids, thin films, and alloys. Jack Douglas' group [54]has done extensive work on phase separation of two fluids in confined geometries. In figure 6.1, we show the segregation of two fluids in a cylindrical tube. Inspecting the figure, we see clear similarities to band formation in a rotating drum. Like band formation in a rotating drum, the fluid's initial state is a segregated core of one fluid type surrounded by the other fluid type. This core breaks up into bands much like in a rotating drum. In figure 6.2, we show a very similar picture from simulations of a rotating drum from work done by Taberlet et al. [44]. We have outlined experimental evidence that points to similar behavior as well in chapter 5. Sometimes, oscillatory instabilities are also seen exactly like those in our ternary mixture of particles in the rotating drum.

The evolution of the concentration field during phase separation is often modeled using the Cahn Hilliard equation.

$$\frac{\partial C}{\partial t} = M_c[\nabla^2 f'(C) - \epsilon \nabla^4 C] \tag{6.1}$$

where C is the concentration, M is the mobility, and f is the free energy. The Cahn Hilliard equation gives the change in the concentration based on the derivatives of the free energy. It often results in a diffusion equation like the equations describing segregation that we have examined in chapters 2 and 4. This suggests that reasonable comparisons might be made with our experiment and phase separation theory.

When Cahn Hilliard is used leading to segregation, the process is often called Spinodal decomposition. Spinodal decomposition happens when there is a downward curvature in the free energy leading towards segregation. Then, small fluctuations in the concentration decrease the free energy and those concentration differences grow. The decreasing free energy due to segregation is offset by a cost caused by the boundary between the two phases. This can lead to a specific wavelength formed by initial phase separation process (see to the work of Khan et al. on drums).

One problem with this kind of analysis arises because axial segregation is not a movement from an unsegregated state to a segregated state, but instead the system goes from one segregated state to another. If a free energy were defined the axially segregated state might have a lower free energy than the radially segregated state. Mixtures that segregated axially would have lower free energies in the axially segregated state and mixtures that did not would have higher free energies. The free energy could be lower for two reasons: the segregation is stronger in the axially segregated state, or the surface area of the boundary between the two phases is lower. The second reason is similar to experiments done on the breakup of fluids in mixtures (see above). In those cases, the fluid thread breaks up into droplets when the surface area of the droplets are less than the surface area of the core.

One basic necessity for this kind of analysis is the ability to define a free energy. Problems arise in granular materials as it is very difficult to define a free energy. There is no free energy in a flowing granular material since the system is not in thermal equilibrium. Instead it is constantly driven and dissipates energy. Some think that such a system would choose a state of minimization of energy dissipation

rates, rather than minimization of free energy. So the question is not what is the energy, the question is what other function could be used instead of energy.

One way to define the interface penalty is to look at the shear velocity. If we minimize dissipation, part of the interface penalty could come from a velocity shear. The higher the shear, the more energy is dissipated, particularly between different particle types. Even though there is shear on the surface between the large and the small particle bands, it is significantly less than the shear in the radially segregated state between particle type. It is intuitive that a system of similar type particles might dissipate less energy everywhere in the flow as well, particularly if one particle type wanted to flow faster than the other.

Regardless, one would of course have to choose a minimization function that is smaller in the axially segregated state. This brings us back to the basic question of how to model the band formation (ie. what function to choose).

We have, in the previous chapters, presented the foundation for a model to describe granular pattern formation in a rotating drum through completely novel physics. This foundation is conceptual in nature, and could have similar form to many of the models currently out there. It is possible that those models could be modified to take into account the physics demonstrated in this thesis without too much trouble. Associating this work with that in phase separation might then be a logical next step.

The focus of this thesis is not on the prediction, or even the modelling of this pattern formation. Rather, it is on understanding the science of why these fascinating patterns form. Predictions can be made using various simulations, but

this was not our focus. Instead we illuminated some key ideas on why the granular patterns formed.

Our results are consistent with scaling studies done on granular mixtures, as outlined in chapter 2. As observed by Khakhar et al. [56] and Ottino et al. [24], our velocities are inversely related to the square root of the particle diameter. Our proposed mechanisms are consistent with the lense like flow profile observed by Ottino et al. [24] and the density profiles observed by Rajchenbach [60].

An important observation made in chapter 2 is that, because the velocity decreases linearly as a function of depth below the surface, the velocities below the surface can be inferred from the velocities on the surface. Therefore, we have related the axial segregation process to the radial core. The velocity of the particles depends on the size of the radial core. An asymmetry in the drift drives band formation through a basic asymmetry in the physical processes in granular flows. Since we assume the drift happens near the surface, the strength of the axial segregation is determined by how strong the radial segregation is. Weaker radial segregation allows more small particles to be near the surface and to participate in the axial flow. While some radial segregation is required for this process, very strong radial segregation tends to weaken axial segregation.

Though we have investigated a wide variety of experimental conditions, many further checks remain to be done. Our proposed mechanism allows for concrete predictions that can be checked experimentally. The processes that we looked at here are not just important for the rotating drum but may also play a significant role in other experiments on flowing granular mixtures.

Appendix A

RELATING FLOW CONCENTRATION TO CORE SIZE

A.1 Derivation

A.) Define the top layer as the amount of material 'visible' to the camera, or it could be the amount of massing in a normal packing in a certain distance d:

$$\sigma_0 d = \frac{M_{cam}}{\Delta x} \tag{A.1}$$

$$\sigma_0 d = \sigma(x, y) l \tag{A.2}$$

B.) Flux balance: The mass flow of particles through the top layer must be the same as the amount rotated back by the drum. The amount rotated through a distance l on the surface will equal the amount rotated back by the drum according to mass flux balance:

$$\int_R^R 1\sigma_0 \omega r dr = \sigma l v_x = \sigma_0 dv_x \tag{A.3}$$

$$\sigma_0 \omega / 2(R^2 - R_1^2) = sigma_0 dV_x \tag{A.4}$$

$$R_1^2 = R^2 - \frac{2dv_x}{\omega} \tag{A.5}$$

This equation for any vertical line perpendicular to the flowing surface through the drum mass.

$$c_s = e^{\alpha r - \alpha r1} \tag{A.6}$$

Where r1 is the distance at which the core is no longer concentration one and begins to decay.

$$C_s = \frac{\int_{R1}^{R} r c_s dr}{\int_{R1}^{R} r dr} \tag{A.7}$$

$$\frac{e^{-\alpha r1} + \alpha R}{2\alpha R}(1 - \frac{1}{\alpha R} - \frac{e^{-\alpha r1} + \alpha R_c}{2\alpha R_c}(1 - \frac{1}{\alpha R_c}) \tag{A.8}$$

if $\alpha = -1/\lambda$, and K is the $1/(\lambda/R)$ then

$$e^{kr1/R}(\frac{e^{-k}}{-2k}(1 + 1/k) - \frac{e^{-k\frac{R}{R_c}}}{-2K\frac{R}{R_c}}(1 + 1/K\frac{R}{R_c})) \tag{A.9}$$

$$\frac{1}{-2k}(1 + 1/k)e^{kr1/R}(e^{-k} - \frac{R}{Rc}e^{-k\frac{R}{R_c}}) \tag{A.10}$$

Appendix B

PARTICLE TRACKING DETAILS

B.1 Particle Tracking

The mixture of glass or steel beads is illuminated with a single bright lamp so that each particle on the surface of the flow reflects a single bright spot. These bright spots can be identified and tracked using software developed by Grier and Crocker in IDL. First the software processes the images so that only the bright spots remain. Then the bright spots are identified and the particles are connected in time. After that velocities are computed from the displacements in the particle tracks.

The processing has a few simple parts to it. The images are 8-bit gray scale, and the brightness of each pixel is represented by a value from 0 to 255. It is necessary to know the approximate size of the bright spots that we want to track in the image. A bandpass filter of this size is applied to remove noise and pick out the spots. The image is also thresholded–all pixels with a value (brightness) less than the threshold value are removed.

In figure B.1a we have plotted a small blowup section of the original image and the result of the image processing is shown in figure B.1b. The mixture shown is a binary mixture of steel beads in an initial mixed state with small and large particles on the flowing surface. The program picks out the obvious bright spots shown in figure B.1b as individual particles. The next step is done by connecting the particle

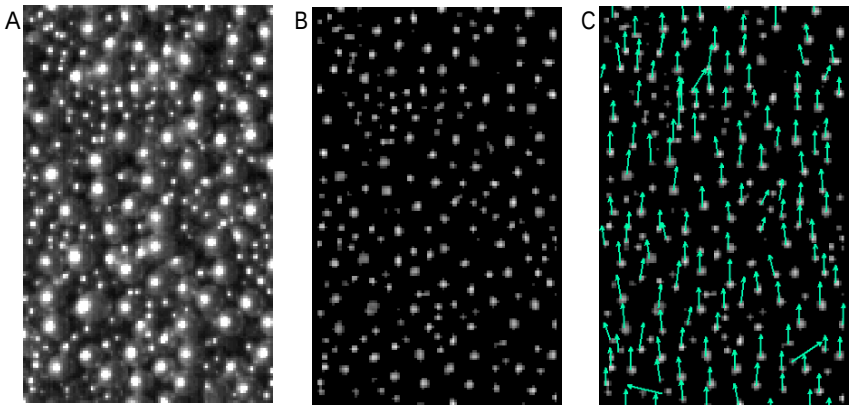

Figure B.1: An image sequence showing the image processing and particle tracking. A. The original image, B. Processed image, C. Processed image with arrows representing tracked particle velocities (the velocities are magnified for the purpose of demonstration).

positions over time. The algorithm connects the particles by comparing each image in sequence and connecting particles based on displacement. It is necessary that the particles do not move more than the minimum distance between particles, otherwise the tracking code will not work. Parameters are entered for the minimum separation between particles (to prevent tracking the same particle twice) and the maximum radius of the particles.

The particle tracking code is very powerful. It continues to track particles even if they disappear and come back on the same trajectory a short while later. Parameters can also be entered for the maximum distance a particle can move to be counted, the minimum number of frames a particle must stay in order to be tracked, and a reference offset velocity for all of the particles.

The particle tracking code returns values for the position, intensity, ellipticity, and velocity of the particles. In fig. B.1c is an overlay of the velocities (multiplied

by a factor of 7 for visibility) on the processed image(fig. B.1b). We see that the particle tracking does a reasonably good job of tracking the particles. There are many sources of error: Some particles do not stay on the surface long enough to be tracked; Sometimes the code misidentifies the same particle as a different particle at a later time and so the particle may not stay long enough to be tracked; Sometimes particles are large enough that they have multiple reflections and get tracked as two particles. It varies for different material types and sizes. In general steel beads are tracked the most accurately, and large transparent glass beads are the least accurate.

Regardless, for all particle types, the number of particles is in the millions and averages can be calculated very accurately despite the errors.

B.2 Distinguishing Between Large and Small Particles

One of the variable that the particle tracking code calculates is the integrated intensity (ie. brightness and size) of the bright spot. Different size particles give off different size spots. The particles can then be distinguished by size. Unfortunately, due to the particle tracking algorithm, we can only track and therefore distinguish particles with about a 2:1 size ratio. Because the code requires the particle size as an input, as the size ratio goes to 2:1 and beyond, the particle tracking becomes less and less accurate and then impossible.

Of course there is some overlap in the brightness, and some small particles will be tracked as large and some large particles will be tracked as small. Therefore if we are comparing some quantity (like average velocity) of the two, this will tend to

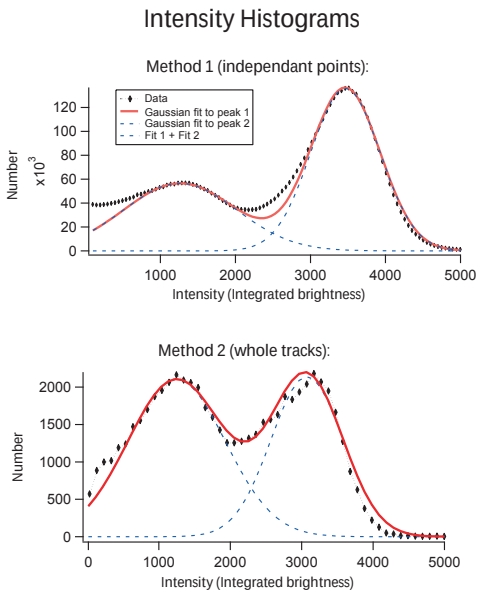

Figure B.2: Intensity distributions for particles in individual images (top) and for averages of a single particle track (bottom). Gaussian's were fit to each plot and are plotted as well.

make it look like the difference between the two is less than it is.

There are two different methods by which particles can be identified. The first is to simply classify particles based on brightness at each time step. With this method, a particle identified as a large particle in one from might be identified as a large particle in a later frame. Particles are identified in each frame independent of the other frames. The other method is to average the intensity of a tracked particle over its entire lifetime and then to use this intensity to classify the particles. This method might seem more effective but there are some problems with it.

We try 2 ways to estimate the error in classification: a. plot the Gaussian of the intensity for the two methods of distinguishing particles and determine the overlap and b. to look by eye and make a rough estimate of the percentage of

particles that are misclassified.In figure B.2, we show the intensity histograms for the two methods of identifying particles. In both cases, there is overlap. In table B.1 we list the error in the tracking for the histogram of method 1, for the histogram in method 2, and by eye analysis of data classified with method 1, as well by eye analysis of radial data classified with method 1.

There are some immediately noticeable problems or causes of systematic error in the classification. First is that at the top and bottom of the image, the particles stop flowing and drop under the surface. There are also reflections of the particles at these places. Here we tend to track a lot of small particles that don't exist. Either we track large particles as small (there brightness is lower because they are dropping below the surface) or reflections of large particles as small particles. All of these are for binary mixtures of 1/16" and 1/8" steel beads.

The method where we average the intensity over a whole particle track before classifying actually magnifies this problem. The average is pulled down enough by the particles spending a lot of times at the edges, that large particles that are only tracked near the edges tend to be tracked as small. This means this error penetrates farther from the edges of the drum.

Arthur Lewbel [84], a respected economist, worked out the error in comparing two variables due to misclassification of one or both of them. If two measured variables are classified as small or large (for example) and then they are compared, the misclassification will cause the observed difference between the two to be lower than the true difference. In an extreme example, if more than 50% of the particles classified as small are actually large, than the observed difference between the two

Table B.1: Misclassification: For the by eye, we looked at 1/10th near the edge banded state and calculated

	Method 1	Method 2	by eye	radial by eye
N_{small}	2.03248×10^6	34298.7	201	558
N_{large}	3.18062×10^6	26597.8	274	249
N_{total}	5.2131×10^6	60896.5	474	807
$n_s = N_{smallaslarge}$	107789	2143.43	9	7
$n_L = N_{largeassmall}$	58192.2	1662.52	13	10
Extra	243642	1126.48	5	NM
# Not Tracked	NA	NA	39	22
b_0	0.053	0.062	0.045	0.0125
b_1	0.018	0.063	0.047	0.0402

particles will give an answer opposite in sign to the truth (assuming there is a difference).

If b_0 is the probability of misclassifying small particles as large and b_1 is the probability of misclassifying large particles as small and r is the number of small particles, m is the percentage underestimation when subtracting $F_s - F_L$, where F is a quantity that varies with particle type:

$$m = (\frac{1}{1 - b_1 - b_0})(1 - \frac{(1 - b_1)b_0}{r} - \frac{(1 - b_0)b_1}{1 - r}) \tag{B.1}$$

BIBLIOGRAPHY

[1] Troy Shinbrot and Fernando J. Muzzio. Nonequilibrium patterns in granular mixing ang segregation. *Physics Today*, page 25, 2000.

[2] Hernan A. Makse, Shlomo Havlin, Peter R. King, and H. Eugene Stanley. Spontaneous stratification in granular mixtures. *Nature*, 386:379, 1997.

[3] Loic Vanel, Daniel Howell, D. Clark, R.P. Behringer, and Eric Clement. Memories in sand: Experimental tests of construction history on stress distributions under sandpiles. *Phys. Rev. E*, 60(5):R5040–3, 1999.

[4] J.B.Knight, H.M.Jaeger, and S.R.Nagel. Vibration-induced size separation in granular media: the convection connection. *Phys. Rev. E*, 70:3728, 1993.

[5] J. Duran and A. Reisinger. *Sands, Powders, and Grains: An Introduction to the Physics of Granular Materials*. Springer-Verlag New York, Inc., November 1999.

[6] E.C. Rericha, C. Bizon, M.D. Shattuck, and H.L. Swinney. Shocks in supersonic sand. *Physical Review Letters*, 88:014302/1–4, 2002.

[7] I.S. Aranson and L.S. Tsimring. Dynamics of axial separation in long rotating drums. *Phys. Rev. Lett.*, 82:1975, 1999.

[8] M. Toiya, J. Stambaugh, and W. Losert. Transient and oscillatory granular shear flow. *Phys. Rev. Lett.*, 83:088001–1, 2004.

[9] B. Utter and R.P. Behringer. Transients in sheared granular matter. *Euro. Phys. J. E*, 14:373–380, 2004.

[10] S. J. Friedmann, G. Kwon, and W. Losert. Granular memory and its effect on the triggering and distribution of rock-avalanche events. *J. Geophys. Res.*, 108(B8):2380, 2003.

[11] A. Rosato, K.J. Strandburg, F. Prinz, and R.H. Swendsen. Why the brazil nuts are on top: size segregation of particulate matter by shaking. *Phys. Rev. Lett.*, 58(10):1038–40, 1987.

[12] T. Poeschel and H.J. Herrmann. Size segregation and convection. *Europhys. Lett.*, 29(2):123–8, 1995.

[13] J. Braun. Segregation of granular media by diffusion and convection. *Phys. Rev. E*, 64(1):011307/1–7, 2001.

[14] Loic Vanel, Daniel Howell, D. Clark, R.P. Behringer, and Eric Clement. Periodic, aperiodic, and transient patterns in vibrated granular layers. *Physica A*, 249:1–9, 1998.

[15] J. Galanis, D. Harris, D. Sackett, W. Losert, and R. Nossal. Spontaneous patterning of confined granular rods. *Preprint*, 2006.

[16] J. Stambaugh, K. Van Workum, J.F. Douglas, and W. Losert. Polymerization transitions in two-dimensional systems of dipolar spheres. *Physical Review E*, 72:031301, 2005.

[17] Brad White. avalanche, year unknown. This is an electronic document. Date of publication: [unavailable]. Dateretrieved: July, 2006. Date last modified: [unavailable].

[18] J. C. Yarnold. Analysis and implications of large martian and terrestrial slides. *Ph.D. thesis, Cal. Inst. of Technol., Pasadena*, page 451 pp., 1991.

[19] J. C. Yarnold. Rock-avalanche characteristics in dry climates and the effect of flow into lakes: Insights from the mid-tertiary sedimentary breccias near artillery peak, arizona. *Geol. Soc. Am. Bull.*, 105:345360, 1993.

[20] S. J. Friedmann. Rock avalanches of the miocene shadow valley basin, eastern mojave desert, california: Processes and problems. *J. Sediment. Res., Sect A.*, 67:792 804, 1997.

[21] Groupement De Recherche Milieux Divises. On dense granular flows. *Eur. Phys. J. E*, 14:341–365, 2004.

[22] H.A. Makse and H. Hlalat, 1997. This is an electronic document. Date of publication: [unavailable]. Dateretrieved: July, 2006. Date last modified: [unavailable].

[23] L. Vahl and W.G. Kingma. *Chem. Eng. Sci.*, 1:253, 1952.

[24] J. M. Ottino and D. V. Khakhar. Scaling of granular flow processes: from surface flows to design rules. *AIChE J.*, 48:2157, 2002.

[25] Kiam Choo, T.C.A. Molteno, and S. W. Morris. Traveling granular segregation patterns in a long drum mixer. *Phys. Rev. Lett.*, 79:2975, 1997.

[26] K.M. Hill and J. Kakalios. Reversible axial segregation of binary mixtures of granular materials. *Phys. Rev. E*, 49:3610, 1994.

[27] Gerald H. Ristow. *Pattern formation in granular materials.* Springer-Verlag, New York, USA, 2000.

[28] J. Rajchenbach. Flow in powders: from discrete avalanches to continuous regime. *Phys. Rev. Lett.*, 65:2221, 1990.

[29] H. M. Jaeger, C.H. Lie, and S.R.J. Nagel. Relaxation at the angle of repose. *Phys. Rev. Lett.*, 68:40, 1989.

[30] G. Felix and N. Thomas. Evidence of two effects in the size segregation process in dry granular media. *Phys. Rev. E*, 70:051307, 2004.

[31] D.V. Khakhar, A.V. Orpe, and S.K. Hajra. Segregation of granular materials in rotating cylinders. *Physica A*, 318:129–136, 2003.

[32] A.R. Rogers and J.A. Clements. The examination of segregation of granular materials tumbling mixer. *Powder Technology*, 5:167–178, 1971-1972.

[33] K.M. Hill, A. Caprihan, and J. Kakalios. Bulk segregation in rotated granular material measured by magnetic resonance imaging. *Phys. Rev. Lett.*, 78:50, 1997.

[34] D. Hirshfeld and D. C. Rapaport. Evidence of two effects in the size segregation process in dry granular media. *Phys. Rev. E*, 56:2012, 1997.

[35] F. Cantelaube and D. Bideau. Radial segregation in a 2d drum: An experimental analysis. *Europhys. Lett.*, 30:133–138, 1995.

[36] E. Clement, J. Rajchenbach, and J. Duran. Mixing of a granular material in a bidimensional rotating drum. *Europhys. Lett.*, 30:7–12, 1995.

[37] J. J. McCarthy, T. Shinbrot, G. Metcalfe, J. Eduardo Wolf, and Julio M. Ottino. Mixing of granular materials in slowly rotated containers. *AIChE J.*, 42:3351, 1996.

[38] J.Kakalios. This is an electronic document. Date of publication: [unavailable]. Dateretrieved: July, 2006. Date last modified: [unavailable].

[39] Y. Oyama. *Bull. Inst. Phys. Chem. Res. Jpn. Rep.*, 18:600–639, 1939. In Japanese.

[40] Y. Oyama. Studies on mixing of solids: Mixing [in a]...binary system of two [particle] sizes by ball mill motion. *Sci. Papers Inst. Phys. Chem. Research (Tokyo)*, 37:951, 1940. In English.

[41] Boris Levitan. Long-time limit of rotation segregation of granular media. *Physical Review E*, 58:2061, 1998.

[42] Vidar Frette and Joel Stavans. Avalanche-mediated transport in a rotated granular mixture. *Phys. Rev. E*, 56:6981, 1997.

[43] R. Chicharro, R. Peralta-Fabi, and R. M. Velasco. *Powders and Grains*, page 479, 1997.

[44] N. Taberlet, W. Losert, and Patrick Richard. Understanding the dynamics of segregation bands of simulated granular material in a rotating drum. *Europhys. Lett.*, 68:522–528, 2004.

[45] Kiam Choo, M.W. Baker, T.C.A. Molteno, and S. W. Morris. Dynamicsofgranularsegregationpatternsinalongdrummixer. *Phys. Rev. E*, 58:6115, 1998.

[46] H. Caps, R. Michel, N. Lecocq, and N. Vandewalle. Transverse flow and mixing of granular materials in a rotating drum. *Physica A*, 326:313–321, 2003.

[47] M. Newey, S. Van der Meer, J. Ozik, E. Ott, and W. Losert. Band-in-band segregation of multidisperse granular mixtures. *Europhys. Lett.*, 66:205, 2004.

[48] M.B. Donald and B. Roseman. Mixing and de-mixing of solid particles, part 1: Mechanisms in a horizontal drum mixer. *British Chemical Engineering*, 7(10):749 – 753, 1962.

[49] Masami Nakagawa. Axial segregation of granular flows in a horizontal rotating cylinder. *Chem. Eng. Sci.*, 49:2540–2544, 1994.

[50] Christopher R. J. Charles, Zeina S. Khan, and Stephen W. Morris. Pattern scaling in the axial segregation of granular materials in a rotating tube. *Preprint.*

[51] S. Das Gupta, D.V. Khakhar, and S.K. Bhatia. *Chem. Eng. Sci.*, 46:1513, 1991.

[52] T.S. Krasnopol'skaya, G. J. F. van Heijst, J. H. Voskamp, and S. A. Trigger. Similarities of patterns in fluid and granulated flow inside a horizontally rotating cylinder. *Int. Appl. Mech.*, 37:929, 2001.

[53] M. Tirumkudulu, Anubhav Tripathi, and Andreas Acrivos. Particle segregation in monodisperse sheard suspensions. *Physics of Fluids*, 11:507, 1999.

[54] John G. Hagedorn, Nicos S. Martys, and Jack F. Douglas. Breakup of a fluid thread in a confined geometry: droplet-plug transition, perturbation sensitivity, and kinetic stabilization with confinement. *Phys. Rev. E*, 69:056312, 2004.

[55] Masami Nakagawa. Non-invasive measurements of granular flows by magnetic resonance imaging. *Experiments in Fluids*, 16:54–60, 1993.

[56] A.V. Orpe and D.V. Khakhar. Scaling relations for granular flow in quasi-two-dimensional rotating cylinders. *Phys. Rev. E*, 64:031302, 2001.

[57] A. Alexander, T. Shinbrot, and F. J. Muzzio. Scaling surface velocities in rotating cylinders as a function of vessel radius, rotation rate, and particle size. *Powder Tech.*, 126:174–190, 2002.

[58] C.S. Campbell. Rapid granular flows. *Annu. Rev. Fluid Mech.*, 22:57, 1990.

[59] H. J. Hermann. On the thermodynamics of granular media. *J. Phys. II*, 3:427, 1993.

[60] J. Rajchenbach, E. Clement, and J. Duran. Experiments in model granular media: a study of gravity flows. *Fractal Aspects of Materials. Symposium*, pages 525–8, 1995.

[61] G.H. Ristow. Dynamics of granular materials in a rotating drum. *Europ hys. Lett.*, 34:263–268, 1996.

[62] D. Bonamy, F. Daviaud, and L. Laurent. Experimental study of granular surface flows via a fast camera. *Physics of Fluids*, 14:1666–73, 2002.

[63] Nicholas A. Pohlman, Julio M. Ottino, and Richard M. Lueptow. Boundary flow in granular tumblers. *Preprint.*

[64] Y.L. Ding, R. Forster, J.P.K. Seville, and D.J. Parker. Segregation of granular flow in the transverse plane of a rolling mode rotating drum. *International Journal of Multiphase Flow*, 28:635–663, 2002.

[65] D.V. Khakhar, J.J. McCarthy, Troy Shinbrot, and J. M. Ottino. Transverse flow and mixing of granular materials in a rotating drum. *Phys. Fluids*, 9:31, 1997.

[66] B. Roseman and M.B. Donald. Mixing and de-mixing of solid particles, part 2: Effects of varying the operating conditions of a horizontal drum mixer. *British Chemical Engineering*, 7:823 – 827, 1962.

[67] Christian M. Dury, Gerald H. Ristow, Jamie L. Moss, and Masiami Nakagawa. Boundary effects on the angle of repose in rotating cylinders. *Physical Review E*, 57(4):4491–4497, April 1998.

[68] R. T. Fowler and W. B. Chodziesner. The influence of variables upon the angle of friction of granular materials. *Chem. Eng. Sci.*, 10:157, 1959.

[69] J. Bridgewater, N.W. Sharpt, and D. C. Stocker. Particle mixing by percolation. *Trans. Inst. Chem.*, 47:T114, 1969.

[70] O. Zik, Dov Levine, S.G. Lipson, S.Shtrikman, and J. Stavans. Rotationally induced segregation of granular materials. *Phys. Rev. Lett.*, 73:644, 1994.

[71] Stuart B. Savage. Radial mixing of granular materials in a rotating cylinder: experimental determination of particle self-diffusivity. page 255, 1993.

[72] Z. S. Khan, W. A. Tokaruk, and S. W. Morris. Oscillatory granular segregation in a long drum mixer. *Europhys. Lett.*, 66:212–218, 2004.

[73] Z. S. Khan and S. W. Morris. Subdiffusive axial transport of granular materials in a long drum mixer. *Phys. Rev. Lett.*, 94:048002, 2005.

[74] T. Elperin and A. Vikhansky. Mechanism of the onset of axial segregation in a rotating cylindrical drum filled with binary granular mixtures. *Phys. Rev. E*, 60:1946, 1999.

[75] M. Newey and W. Losert. Understanding axial band formation in a rotating drum through particle tracking of the banded state. *Preprint.*

[76] Saikat Chakraborty, Prabhu R. Nott, and J. Ravi Prakash. Analysis of radial segregation of granular mixtures in a rotating drum. *Eur. Phys. J. E*, 1:265–273, 2000.

[77] G.S. Riley and G.R. Mann. Effects of particle shape on angles of repose and bulk densisties of a granular solid. *Mat. Res. Bull.*, 7:163–170, 1972.

[78] A.C. Santomaso, Y.L. Ding, J.R. Lickiss, and D.W. York. Investigation of the granular behaviour in a rotating drum operated over a wide range of rotational speed. *Mat. Res. Bull.*, 7:163–170, 1972.

[79] K. M. Hill, J. Kakalios, K. Yamane, Y. Tsuji, and A. Caprihan. Dynamic angle of repose as a function of mixture concentration. *Unpublished*.

[80] K. Yamane, M. Nakagawa, S. A. Altobelli, T. Tanaka, and Y. Tsuji. Steady particulate flows in a horizontal rotating cylinder. *Physics of fluids*, 10:1419, 1998.

[81] R. Khosropour, E. Valachovic, and B. Lincoln. Investigation of the granular behaviour in a rotating drum operated over a wide range of rotational speed. *Phys. Rev. E*, 62:807, 2000.

[82] N. Taberlet, M. Newey, P. Richard, and W. Losert. On axial segregation in a tumbler: an experimental and numerical study. *J. Stat. Mech.*, P07013:1–17, 2006.

[83] W. Losert, M. Newey, N. Taberlet, and P. Richard. Segregation transients in a tumbler flow. *Powders and Grains*, 2:845, 2005.

[84] Arthur Lewbel. Estimation of average treatment effects with misclassification. *Preprint*.

[85] T. Elperin and A. Vikhansky. Granular flow in a rotating cylindrical drum. *Europhys. Lett.*, 42:619–623, 1998.

[86] Rapaport. Simulational studies of axial granular segregation in a rotating cylinder. *Phys. Rev. E*, 65:061306, 2002.

[87] Suman K. Hajra and D. V. Khakhar. Radial mixing of granular materials in a rotating cylinder: Experimental determination of particle self-diffusivity. *Physics of fluids*, 17:013101, 2005.

[88] J. Casas-Vazquez and D. Jou. Temperature in non-equilibrium states: a review of open problems and current proposals. *Rep. Prog. Phys.*, 66:1937–2023, 2003.

[89] W. Losert, D. G. W. Cooper, J. Delour, A. Kudrolli, and J. P. Gollub. Velocity statistics in vibrated granular media. *Chaos*, 9:682, 1999.

[90] J. E. Galvin, S. R. Dahl, and C. M. Hrenya. On the role of non-equipartition in the dynamics of rapidly flowing granular mixtures. *J. of Fluid Mech.*, 528:207–232, 2005.

[91] H. Xu, A. Reeves, and M. Louge. Measurement errors in the mean and fluctuation velocities of spherical grains from a computer analysis of digital images. *Rev. of Sci. Instr.*, 75:811, 2004.